The Evaluation of Using in-Fibre Bragg Grating Sensors Within a Periodontal Ligament Space for Strain Measurement

by

Kathryn Pamela Houg

A thesis submitted in partial fulfillment of the requirements for the degree of

Master of Science

Department of Mechanical Engineering
University of Alberta

Abstract

The Periodontal Ligament (PDL) is a soft connective tissue that anchors the tooth to the surrounding alveolar bone, forming a tooth-PDL-bone complex (TPBC). The PDL demonstrates nonlinear, viscoelastic, anisotropic, and heterogeneous mechanical material properties that facilitate in protection and adaptation of the TPBC against external loads. The PDL will act as a shock absorber to protect the TPBC against high magnitude loads, such as mastication. The TPBC can adapt in response to long-term low magnitude load conditions, such as those applied through orthodontic appliances, as the stress/strain state within the PDL can trigger a cellular biological response leading to alveolar bone remodelling and, subsequently, tooth movement. Determining the PDL's mechanical material properties and its stress/strain response to applied loading is critical to understanding its behaviour and biological implications. Due to the small and varying geometry, direct mechanical measurements from an intact PDL are limited. An in-fibre Bragg grating (FBG) sensor is a small and flexible sensor that can be placed within the PDL space of an intact TPBC and measure repeatable strains. The repeatability of sensor measures within a single TPBC has been demonstrated in previous works. However, the repeatability, sensitivity, reproducibility, and verification of measurements has yet to be evaluated.

The objectives of this work were to first define an apically directed, quasi-static, displacement-controlled experimental protocol to obtain force, displacement, and FBG strain measurements from an intact TPBC. Second, a cross-verification between FBG strain measures obtained using the defined experimental protocol and a finite element model was used to determine the relationship between FBG and finite element strain measurements.

A rigorous investigation of the repeatability, sensitivity and reproducibility of output FBG strains from within the PDL space and reaction force measurements was completed. It was concluded that: the experimental protocol was repeatable within, but not across, TPBCs; the output measures were highly sensitive to experimental protocol input parameters; and the force and strain measures were reproducible when replacing an FBG within a TPBC. Using the defined experimental protocol, a cross-verification between strain magnitudes from a representative finite element model and FBG strain measurements suggested a one-to-one comparison was not appropriate. However, a statistically significant linear relationship was found for the change in strain induced by varying tooth displacement between experimental and finite element model outputs, suggesting the FBG is capable of predicting a change in the PDL strain.

The results of this thesis showed that the FBG could be replaced within a TPBC and measure a representative change in strain with varying tooth displacements. Therefore, the proposed FBG method has potential applications within *in vivo* studies where the mechanical properties of an intact PDL are to be monitored over time, eliminating the need to sacrifice specimens to isolate the PDL for mechanical measurement. This could be implemented to advance literature focused on treatment protocols within a diseased or injured PDL or for optimization of orthodontic treatments.

Preface

This thesis is original work completed by Kathryn Houg. Contents of this thesis have not been previously published. However, Chapter 3 of this thesis has been submitted to the Journal of Mechanical Behavior of Biomedical Materials for review. The author of this thesis was responsible for the design of the experimental protocol, data collection, data analysis, and composition of the manuscript.

Acknowledgments

I would first like to acknowledge my supervisors, Drs. Dan Romanyk and Christopher Dennison, for their continuous guidance, support, and expertise. I am profoundly grateful for the hours of work they dedicated to my growth as a researcher, professional, and individual. They challenged me to work through problems on my own while passing on their knowledge through invaluable critique and discussion.

I would like to thank Dr. Tracy Popowics, whose positivity and knowledge was vital to the completion of this research. Thank you, Dr. Michael Doschak, for contributing time in working with me to analyze the µCT scan data.

To the amazing past and present members of the Romanyk Lab and the Biomedical Instrumentation Lab, thank you for the laughs and collaboration. It has truly been an honour to work alongside you.

Finally, I would like to acknowledge my friends and family for their support and encouragement. I truly couldn't have done it without you. Thank you to my parents and grandparents for their unconditional love and determination to care about "the small thing between your teeth". Thank you to Brendan for being my sounding board and making me laugh through my trials and tribulations.

Table of Contents

List of Tables

List of Figures

List of Nomenclature and Acronyms

ARMS	Adjusted Root Mean Square
FBG	In-Fibre Bragg Grating
FE	Finite Element
LPM2	Left Second Premolar
LPM3	Left Third Premolar
n_{eff}	Effective refractive index of the in-fibre Bragg grating core
PC	Preconditioning
PDL	Periodontal Ligament
P_{ij}	Pockels coefficients
PM	Premolar
PM2	Second Premolar
PM3	Third Premolar
RPM2	Right Second Premolar
RPM3	Right Third Premolar
SDM	Standardized Deviation in Medians
S_ε	In-fire Bragg grating strain sensitivity (1.21 pm/με)
TPBC	Tooth- Periodontal Ligament-Bone Complex
ε_z	Axial strain along in-Fibre Bragg Grating
Λ	Grating pitch
λ_B	Bragg wavelength
μCT	Microcomputed Tomography
με	Micro strain
ν	Poisson's ratio

Chapter 1: Introduction

This chapter introduces the importance of investigating the mechanical output of the periodontal ligament and introduces a potential fibre optic sensing method for mechanical strain measurements. This chapter will also outline thesis objectives, organization, and contributions.

1 Thesis Motivation

Dental care is a significant component of Canada's health spending. In 2019, it was projected that $450 per capita, approximately $16.9 billion, would be spent on dental care [1]. There are nine recognized branches of dentistry in Canada, including public health dentistry, endodontics, oral and maxillofacial surgery, oral medicine and pathology, oral and maxillofacial radiology, pediatric dentistry, prosthodontics, periodontics, and orthodontics. To some degree, each specialty deals with the health and treatment of the dental tissue [2]. Orthodontics focuses on the correction of misaligned teeth and malocclusions. Misaligned teeth and malocclusion can cause psychological challenges and difficulties with oral function, in addition to leaving the individual at higher risk for trauma, periodontal disease, or tooth decay [3]. A key aspect of orthodontics is maintaining the health of the periodontal ligament (PDL) and utilizing its biological properties to aid in permanent tooth movement. Periodontics focuses on the diagnostics and treatment of ailments affecting the periodontium, including the gum tissue and PDL [4]. In 2009-2010, 47.2% of adults 30 years or older in the United States were reported to have some degree of inflammatory disease of the PDL (periodontitis) [5].

The PDL is a soft connective tissue that fills the space between the tooth and the alveolar bone, forming the tooth-PDL-bone complex (TPBC) (Figure 1). The PDL provides support, proprioception, nutrition, and protection against occlusal forces for the surrounding bone [4]. The altered stress/strain state of the PDL can trigger a cellular biological response in the alveolar bone, leading to tooth movement. Specifically, bone resorption in areas of compression and bone formation in areas of tension [3], [4], [6]. This phenomenon stabilizes tooth position that can be altered by daily pressures induced by speech, swallowing, the tongue, and the lips. It is also utilized in orthodontics to correct misalignments [3].

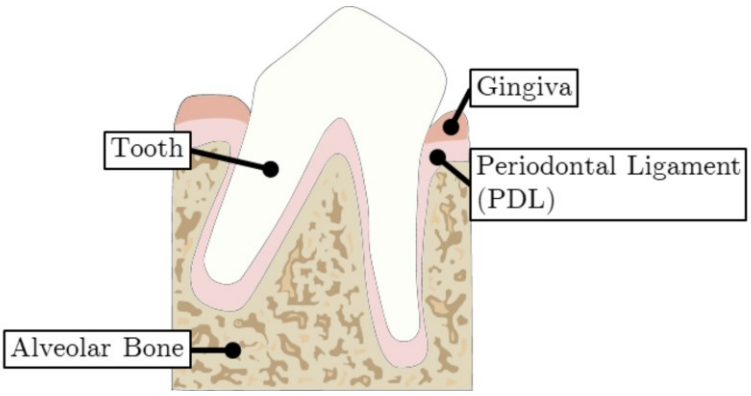

Figure 1 Cross-section of a multirooted tooth indicating the tooth-PDL-bone complex

Injury and disease of the PDL can affect the mechanical properties and, ultimately, the functionality [3], [4], [7]–[10]. Periodontitis leads to the destruction of the PDL and, if allowed to progress, bone and tooth loss [4], [9]. Traumatic injury to the PDL is painful, expensive to repair, and can lead to further damage to the tooth due to the disruption of the neurovascular networks [10]. Monitoring the mechanical properties of a PDL that is affected by disease or injury can be used to track regeneration and repair within the PDL; this information could then be utilized in the development of better treatment protocols [7]. Orthodontic treatments may be optimized through the characterization of PDL mechanical properties [11]. For instance, force levels must be large enough to initiate tooth movement in a timely manner but low enough to minimize side effects such as root resorption and damage to the PDL tissue [3], [11], [12]. Understanding the PDL mechanical properties would allow for improved design of appliances and treatments that would produce an optimal range of stress/strain in the tissue leading to physiological tooth movement.

Extensive research has been published characterizing the mechanical properties and response of the PDL. Direct mechanical measurement of the PDL from an intact TPBC are limited as the small and intricate size is highly three dimensional and located between hard tooth and bone structures, preventing the placement of conventional strain sensors [6], [13], [14]. Previous work completed at the University of Alberta implemented an in-fibre Bragg grating (FBG) sensing method to obtain strain measurements from within the PDL space of an intact swine TPBC [15]. FBGs are flexible silica sensors with a diameter of 0.125 mm and a gauge length of 1 mm, making them a potential candidate to fit within the PDL space and measure strain. Additionally, FBG

sensors have noted benefits over conventional strain sensors and measurement techniques for biomechanical applications such as biocompatibility, high sensitivity, and immunity to electromagnetic interference [16]–[19]. A feasibility and repeatability analysis of the output FBG strain measures has previously been reported within swine premolars [15], [20]. This work was novel as it was the first time mechanical strain measurements from an intact PDL space have been reported.

2 Thesis Objectives

The objectives of this thesis were to expand upon previous work presented by Romanyk *et al.* [15] on the use of FBG sensors within an intact PDL space. The first objective was to design a displacement-controlled experimental protocol to obtain force, displacement, and FBG strain measurements from an intact TPBC. A rigorous investigation of the repeatability of the output measures, sensitivity of the output measures to experimental input parameters, and reproducibility of the output measures was conducted to fully define the experimental protocol. The second objective implemented a cross-verification between FBG strain measures obtained using the previously outlined experimental protocol and a representative finite element (FE) model to determine the relationship between FBG and FE strain measurements.

3 Thesis Organization

This thesis is composed of five chapters. Chapter 2 includes a review of the anatomy and physiology of the PDL, previously applied testing protocols used to study the mechanical properties of the PDL, FBG working principles, and a summary of previous works using FBG sensors within an intact TPBC.

Chapter 3 outlines the experimental design to evaluate the repeatability, sensitivity to experimental input parameters, and reproducibility of the strain and force output measurements made during mechanical testing of an intact TPBC. This chapter is a re-formatted manuscript titled "Experimental repeatability, sensitivity, and reproducibility of force and strain measurements from within the periodontal ligament space during *ex vivo* swine tooth loading" that has been submitted for review to the Journal of Mechanical Behaviour of Biomedical Materials in November 2020. The first author of this manuscript is also the author of this thesis.

Chapter 4 implements the experimental protocol defined in Chapter 3 to determine the relationship between FBG and FE outputs with respect to both strain magnitudes and changes in strain caused by varying tooth displacements. This chapter is a re-formatted manuscript titled "Using an in-fibre Bragg grating sensor to measure strain within the periodontal ligament space in an intact swine premolar", that has been prepared for submission to a peer-reviewed forum at a later date upon publication of the manuscript presented in Chapter 3. The first author of this manuscript is also the author of this thesis.

Chapter 5 details thesis conclusions, contributions, and suggested future works.

Appendix A includes relevant sections of MATLAB code used for data analysis. Appendix B outlines the preliminary FE model setup, including a mesh convergence analysis, verification of the PDL width, and material property selection.

4 Thesis Contributions

To the author's knowledge, FBG sensors are the first sensors that have been implemented to obtain direct mechanical measurements from within the PDL space of an intact TPBC. Direct mechanical measurements would allow for a more comprehensive definition of the PDL's mechanical response and improved validation of relevant FE models. This thesis advanced previous works using FBG sensors within the PDL by introducing and demonstrating the repeatability of force output measurements [15]. As there are no known similar sensing methods to compare output FBG strains to, the output force measurements allowed for comparison of the presented experimental results to other studies and FE models. It has been suggested that inconsistencies within and between experimental protocols could contribute to the wide range of PDL mechanical properties that are reported [13]. This work confirmed that experimental inconsistencies affect output measures and demonstrated the importance of objective *a priori* definition by quantifying the sensitivity of force and strain output measures to confounding input variables associated with the experimental protocol.

This work demonstrated the feasibility of practical applications of the FBG sensing technique for *in vivo* studies. It was shown that an FBG can be replaced within a TPBC and can measure a representative change in strain from within the PDL space. This would allow for temporal

monitoring of PDL mechanical properties without having to sacrifice specimens at each time point for dissection and isolation of the PDL. Applications could include improved validation of FE models, advanced characterization of the progression of inflammation and disease, and definition of regeneration and repair within the PDL following injury or surgery.

Chapter 2: Background

This chapter provides an overview of relevant periodontal ligament anatomy and previous methods for mechanical testing of the periodontal ligament. This chapter details in-fibre Bragg grating sensors and the previous application of the sensing method on which this work was based.

1 Anatomy and Nomenclature

The human oral cavity, made up of an upper and lower dental arch, is associated with the respiratory system, digestive system, and speech. Teeth are housed within each dental arch in a tooth socket or alveolus [4], [21]. Alveolar bone makes up the upper and lower dental arches known as the maxilla and mandible, respectively [21], [22]. There is a thin layer of compact bone surrounding the alveolus that is perforated to connect the periodontium to bone marrow canals [22]. The maxilla's and mandible's outer layers are composed of dense, cortical bone. Spongy, trabecular bone is found between the alveolus and the dense outer layer [4], [21], [22]. When referring to the direction associated with dental arches, mesial refers to the anterior direction, distal toward the posterior direction, lingual toward the tongue, and buccal toward the cheek [23](Figure 2).

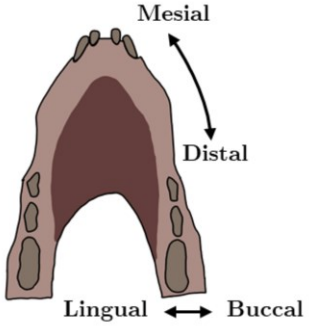

Figure 2 Superior-down view of representative swine mandible indicating the relevant dental directions

The tooth consists of a crown and a root (Figure 3), where the cusp refers to the top of the crown, and the root apex refers to the bottom portion of the root. The superficial portion of the crown is

a hard tissue known as enamel, and the outer portion of the root is cementum. There is a pulp cavity within the tooth that contains blood and lymph vessels. The pulp cavity is surrounded by dentin [23]. Gingiva (gum tissue) surrounds each tooth and attaches to the adjacent alveolar bone [4], [21]. The tissues involved in anchoring the tooth to the bone are referred to as the periodontium and include the cementum, the periodontal ligament (PDL), the alveolar bone, and portions of the gingiva [22], [23]. The PDL provides physical attachment between the cementum and the alveolar bone and the gingiva provides support by creating a seal around the tooth [22].

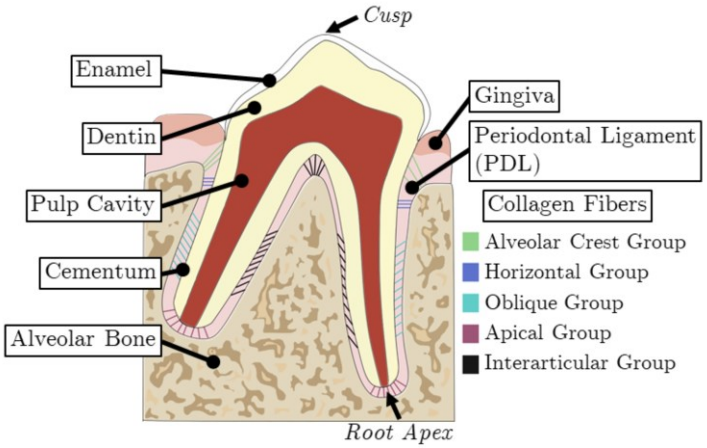

Figure 3 Cross-section of a multirooted tooth highlighting relevant dental structures

1.1 The Periodontal Ligament

The PDL provides physical attachment, support, protection, and proprioception within the tooth-PDL-bone complex (TPBC) [3], [4], [24], [25]. It is a soft connective tissue with a varying thickness that ranges from 0.15 mm to 0.38 mm along the root of a healthy human [26]. Parallel collagen fibre bundles, or principal fibres, make up approximately 53% to 74% of the PDL's volume [27], [28]. The terminal ends of the fibre bundles that are embedded into the cementum and alveolar bone for attachment are known as Sharpy's fibres [4], [24], [29]. Principal fibres are mainly composed of type I, type III and type V collagen [4], [30], with other non-fibrillar collagen types such as type IV, VI, XIII, and XIV less prominently present in the PDL [4], [24], [31]. Type I, type III, and type V collagens provide structure, connectivity, and tensile strength within the PDL [31]. The principal fibre bundles form a hammock-like structure to protect the tooth and

resist tooth displacement during normal function such as mastication, bruxism, speech, and swallowing [3], [4], [25], [30]. Based on orientation and location, the principal fibres are organized into six groups (Figure 3)[3], [4], [25], [30]: the transseptial group (not pictured) extends between the cementum of adjacent teeth; the alveolar crest group run at an angle from a superior portion of the tooth downward to the alveolar crest; the horizontal group are perpendicular to the tooth and the alveolar bone; the oblique group run at an angle toward the root apex; the apical group is perpendicular to the cementum and alveolar bone at the root apex; and, the interradicular fibres run at an angle towards the root apex within the furcation areas of multirooted teeth. In general, the oblique fibre group resists the majority of the vertical displacement, and the alveolar crest group resists the majority of lateral tooth displacement [4], [32]. Vascular elements, making up 1% to 2% of the PDL, provide nutrition within the TPBC [4], [27]. Some elastic proteins are found within the PDL, which are believed to help regulate blood flow. Nerves within the PDL transmit sensory information within the TPBC such as tactile, pressure, and pain sensations [4], [30]. Fibroblasts, the main cell type found in the PDL, form the collagen fibres [4], [24]. Lymphocytes, macrophages, mast cells, and neutrophil cells aid in the healing process (i.e., regeneration and repair) of the PDL after injury or disease [4]. Other cells, such as epithelial cells and cementoblasts, which are responsible for the formation of cementum, are also found in the PDL [4], [24]. The principal fibres, blood vessels, nerves, and other cells are all suspended in an extracellular matrix known as the ground substance [4].

The tooth is subjected to applied mechanical loads through natural applications (e.g., pressures from the lips and tongue) and external applications (e.g., orthodontic appliances and habits such as thumb sucking) [3]. The PDL is responsible for absorbing and distributing these forces to the surrounding alveolar bone, acting as a shock absorber [3], [4], [24]. Three simplified cases can describe the PDL's mechanical response to typical loading regimes: rapid intermittent load application ($>\tilde{}10$ N for $<\tilde{}1$ second [3], [12]); long-term high magnitude load application ($>\tilde{}10$ N for $>\tilde{}1$ second to days [3], [12]); and long-term low magnitude load application ($<\tilde{}1$ N to 10 N for $>\tilde{}1$ second to days [3], [12], [33], [34]). The PDL will act as an incompressible fluid during rapid load application that is maintained for less than approximately 1 second [3], [4], [12]. The force applied to the tooth will be distributed to the surrounding alveolar bone and will result

in low magnitude mechanical loading of the bone [3]. Incompressibility within the PDL allows the TPBC to resist short term large magnitude loading application, such as mastication (>~10 N to 500 N for < ~1 second [3]). When a load is held for longer than 1 second, the PDL's extracellular fluid will begin to seep out into the surrounding marrow spaces in the alveolar bone [4], allowing the tooth to move within the alveolus [3], [4], [12]. When long term loads are too large, portions of the PDL will be significantly compressed between the tooth and alveolar bone, pinching the blood supply and nerves. This significant compression can lead to necrosis in the tissues within a few hours [3], [12]. It is hard to quantify a threshold for what is considered a load that is too large as it is dependent on tooth shape and PDL thickness. However, orthodontic loads of approximately 3 N have been shown to cause more adverse effects, such as root resorption, as compared to loads closer in range to 0.5 N [34], [35]. If the load magnitude is low enough, such as loads typically applied during orthodontic treatment (~1 N to 10 N [3], [33], [34]), compression and tension within the PDL will not obscure blood supply and will trigger a cellular biological response of bone remodelling causing permanent tooth movement within a matter of days. Specifically, areas of compression within the PDL will lead to bone resorption, and tension areas will lead to bone formation [3], [12]. Thus, tooth movement can be understood as a PDL-induced phenomenon resulting from externally applied mechanical loads [3]. Characterizing the PDL's mechanical properties is vital to understanding and optimizing the response of the TPBC to mechanical loads [3], [6].

2 Mechanical Testing of the Periodontal Ligament

The nature of tooth movement and, subsequently, the PDL's mechanical properties have been the subject of many studies [6], [13], [14], [27], [28]. The mechanical properties of the PDL have been reported as anisotropic [36], [37], nonlinear [36], [38], viscoelastic [39], [40], and heterogeneous [28], [41]. The properties are not only dependant on time and location, but also on the tooth shape and size [6]. The PDL is small, and significant damage to the principal fibres will affect the mechanical properties; therefore, studying the mechanical properties is challenging and is not as simple as placing a strain sensor within the PDL space. As a result, experimental protocols in the literature are diverse, and a range of Young's moduli and Poisson's ratios have been reported from 0.01 MPa to 1750 MPa and 0.30 to 0.49, respectively [13]. In general, the PDL's mechanical

properties have been studied experimentally by isolating the PDL outside of the TPBC (*in vitro*) and using an intact TPBC (*ex vivo* or *in vivo*) (Figure 4). Complementary numerical models have been derived using data from both methods with varying degrees of complexity [6], [13], [14]. Recently, two extensive literature reviews summarizing analytical and experimental studies regarding the mechanical response of the PDL were published [13], [14]. Fill *et al.* highlighted the variation in experimental procedures [13] and numerical models [14], suggesting this attributed to the wide range of reported mechanical properties. It was also suggested that each tooth's PDL has a unique mechanical behaviour, and an all-encompassing mechanical model may not be possible or appropriate [13]. Nevertheless, advances are continually made with more complex models and experimental techniques to define and understand the mechanical response of the PDL.

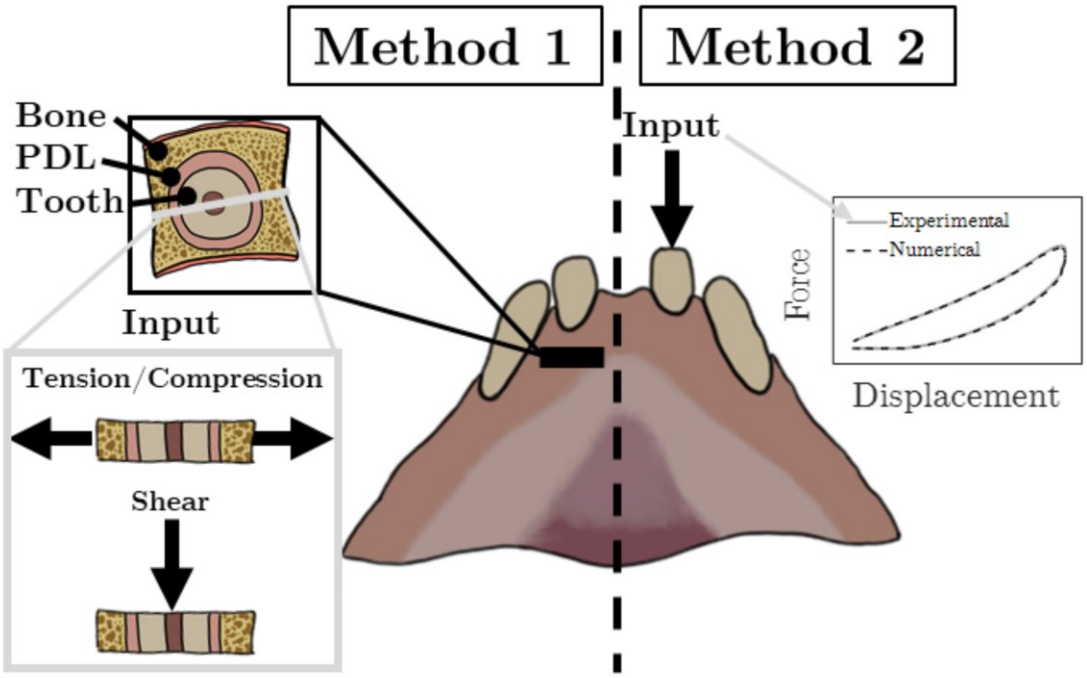

Figure 4 Simplified illustration of two general testing protocols for the PDL's mechanical properties, including: Method 1, a mechanical load applied to an isolated PDL section and; Method 2, mechanical load applied to an intact TPBC

2.1 Isolated Periodontal Ligament Section

Atkinson and Ralph [42] were the first to mechanically test an isolated section of the PDL. The PDL and bone were removed from around a tooth, with the exception of a small portion of PDL and bone that was left intact midway along the root. The experiment involved pulling the intact portion of bone away from the tooth at the approximate angle of the PDL until it ruptured. This method was later improved, decreasing the size of the isolated PDL section to approximately 1 mm thick transverse cross-sections to limit the effect of the curved geometry of the tooth and PDL on the output measurements [38]. This became a popular method of testing the PDL mechanical properties by subjecting the PDL to tension, compression, and shear loading regimes (Figure 4). As the cross-sectional area of the PDL can be determined, the stress/strain state of the PDL can then be calculated from the output force/displacement data. Early experiments strained the isolated PDL sections until rupture to calculate the PDL's ultimate tensile strain [28], [38], [42]. Eventually, the entirety of the stress/strain curve was evaluated to define the PDL's mechanical properties [37]. Using quasi-static ramp-like loading regimes, toe and linear regions in the stress/strain output demonstrated the nonlinear properties of the PDL [36]. Viscoelastic properties were observed through stress relaxation, hysteresis, and the dependence of the mechanical output on loading rate [40], [43]. Dynamic or cyclic loading regimes applied to an isolated section of the PDL have demonstrated the nonlinear viscoelastic response of the PDL through varying frequencies and loading amplitudes [44]–[49]. Isolated PDL sections have also been used to highlight the uniqueness of the PDL, such as the difference in mechanical outputs observed between species [50], ages [36], [51], locations along the root [36], [37], and loading directions [36], [41].

Using the known cross-sectional area and, therefore, calculated stress/strain profile from the PDL section, many analytical models have been derived to describe the PDL's various mechanical properties. Toms *et al.* [52] were the first to quantify the viscoelastic behaviour of the PDL, fitting a quasi-linear viscoelastic model to data collected from human isolated PDL sections. Other viscoelastic models [47]–[49], [51], [53], [54] and hyper-viscoelastic models [55]–[58] have since been derived. The response of isolated PDL sections has been extended to three dimensional FE analysis using models such as hyperelastic [59] and poro-hyperelastic [60], [61].

Experimental methods beyond uniaxial testing of isolated PDL sections have been used to determine PDL mechanical properties. Nanoindentation techniques have been implemented and used to define viscoelastic [62], hyperelastic [63], hyper-viscoelastic [64], and poroelastic [65] models. Qian *et al.* [66] sectioned a swine premolar TPBC along the long axis of the tooth and used digital image correlation during intrusively directed tests to measure the strain field through the periodontium. A complementary FE study fit a hyperelastic and bilinear elastic model during loading and a Maxell-based viscoelastic model during the stress relaxation period.

Isolating the PDL is beneficial in that the direct mechanical response of the PDL can be measured, and the stress/strain profile can be calculated. More control over the boundary conditions, loading regime, and geometry allow a uniaxial stress/strain state to be induced within the PDL, which is required to determine quantitative material properties [40]. This is advantageous over testing an intact TPBC, as the PDL within an intact TPBC will be in tension and compression instantaneously when loaded and has a complex geometry, which limits the ability to calculate a known stress/strain state [40]. However, to achieve a uniaxial stress/strain state in an isolated PDL section, simplification of the anisotropic properties and typical *in vivo* loading patterns is required. Simplifications of the system will lead to fundamental changes in material properties from an *in vivo* PDL. Specifically, removal from, and damage to, the three-dimensional principal fibre support structure and removal from the circulatory system, which replenishes fluids in the PDL, will alter the material properties and limit the output from an isolated PDL section [4], [40].

2.2 Intact Tooth-PDL-Bone Complex

Testing an intact TPBC is useful to understand the mechanics of tooth movement and allows for the application of more physically relevant loading patterns, as opposed to uniaxial testing of isolated PDL sections. However, the PDL geometry is irregular, and therefore, the stress/strain relationship can not be directly calculated from this method. Instead, FE modelling techniques have been implemented to estimate the stress/strain relationship in the PDL. In general, the PDL's material properties are adjusted until the force/displacement output of the FE model matches the experimental output. Alternatively, previously developed analytical models are implemented within an FE model and compared to the experimental output. Both *ex vivo* and *in*

vivo intact TPBCs have been studied using this combined experimental/numerical method [11], [39], [67]–[76].

Early studies used *in vivo* testing to characterize tooth movement under different loading conditions and directions [27]. As experimental methods and transducers to measure tooth displacement became more sophisticated, so to did the characterization of the PDL's mechanical response [77]. Spring-damper viscoelastic models were used to describe the force/displacement output of *in vivo Macaca irus* monkey [78], [79] and human tooth displacement [80]. More recently, van Driel *et al.* [39] applied a mesial/distal load to Beagle dogs' second premolars and monitored the force/displacement output over 5 hours. A poroelastic FE model for the PDL and alveolar bone was fit to the force/displacement data. The results highlighted the importance of the PDL's viscoelastic material property in response to long term loading. Chen *et al.* [11] created an FE model of a dental arch in which the PDL was simulated as a hyperelastic material. The surrounding alveolar bone geometry would update and re-mesh in response to hydrostatic pressures calculated in the PDL in order to numerically simulate bone remodelling during orthodontic treatment. The FE results of tooth movement were compared against clinical data from dental impressions taken over 12 weeks, during which time a constant force of 0.5 N was applied through an orthodontic appliance. In addition to clinical data, intraoral loading devices have been designed to obtain force/displacement output data from *in vivo* human subjects. For example, Keilig *et al.* [74] designed a high-resolution intraoral loading device capable of applying numerous loading rates. Bilinear elastic FE models were fit to the experimental data obtained from the intraoral loading device for each of the different loading rates.

In vivo testing allows for a more complete definition of the PDL's mechanical response to applied loading. The fluid phase, loading conditions, and boundary conditions would be more physically representative, as the fluids will be able to move in and out of the PDL naturally, and the TPBC geometry is not altered. However, direct mechanical measurements from the PDL are challenging, and the complementary numerical models are reliant on user-defined assumptions, geometries, and material properties. Further, as no direct measurements of an intact PDL have been reported, validation of the FE models for PDL material response presented in literature is limited [14]. Significant ethical limitations also arise when working with *in vivo* specimens, such

as the range of potential magnitudes of applied loading, the control of the input loading vector, sample size, and availability of high-resolution imaging to create accurate FE geometries. The use of *ex vivo* intact TPBCs addresses some of these limitations. When *ex vivo*, intact TPBCs are used, more sophisticated control of the loading regime (i.e., direction, magnitude, and loading rate), boundary conditions, and crown displacement tracking can be implemented and used as inputs to a corresponding FE model [67]. *Ex vivo* samples can be scanned using microcomputed tomography (μCT) to define the complex geometry of the PDL. This is valuable as many variables can affect the PDL's material properties, including the species [50], the nature of loading [13], [36], and the geometry of the tooth and PDL [75], [81]–[83]. However, as with *in vivo* testing, the PDL's stress/strain state cannot be measured and relies on numerical models.

The first *ex vivo* studies were used to determine the extraction force required to remove a tooth from its alveolus to estimate the ultimate tensile strength of the PDL [28]. With the development of FE models in the 1970s, the use of *ex vivo* experimental/numerical combined methods have been implemented to define the material properties of the PDL with varying complexity [14]. A linear elastic PDL model was defined by Andersen *et al.* [67], where the corresponding crown displacement data was collected from human molars and premolars using strain gauges. Bilinear elastic PDL models were defined by various authors where the corresponding crown displacement data were collected from: human incisors using a laser sensing system [70]; swine premolars using a three-dimensional optical method [72]; and swine premolars using a laser diode based optoelectronic measurement system [68], [76]. Hyperelastic PDL models have also been defined were the corresponding swine crown displacement data were collected from a laser diode based optoelectronic measurement system [69], a linear variable differential transformer [84], and a universal testing machine [75]. Chang *et al.* [73] tracked tooth movement using μCT images during loading and implemented a previously derived hyperelastic FE model. A high correlation between experimental and FE displacements was reported (R^2=0.9799). Although great strides have been made in defining the PDL's material properties using FE analysis in conjunction with experiments, comparing the force/displacement outputs does not allow for as strong of a validation of the FE models as being able to experimentally measure the strain from an intact TPBC.

3 In-fibre Bragg grating sensors

In-Fibre Bragg grating sensors (FBGs) are small, flexible, germanium-doped silica sensors. Originally developed as selective data filters for the optical telecom industry, Bragg gratings can be configured as strain and temperature transducers [85], [86]. FBG sensors are advantageous, particularly in biomechanical applications, due to their small size, biocompatibility, high sensitivity, chemical inertness, immunity to electromagnetic interference, and multiplexing capabilities [16]–[19]. The fibre acts as a waveguide for a broad spectrum of light that is passed through the inner core. A cladding surrounds the core with a higher refractive index to guide light. A Bragg grating is written into the core through periodic changes in refractive index and acts as a reflection filter, selectively reflecting a narrow wavelength back along the fibre (Figure 5) [17], [85]–[87].

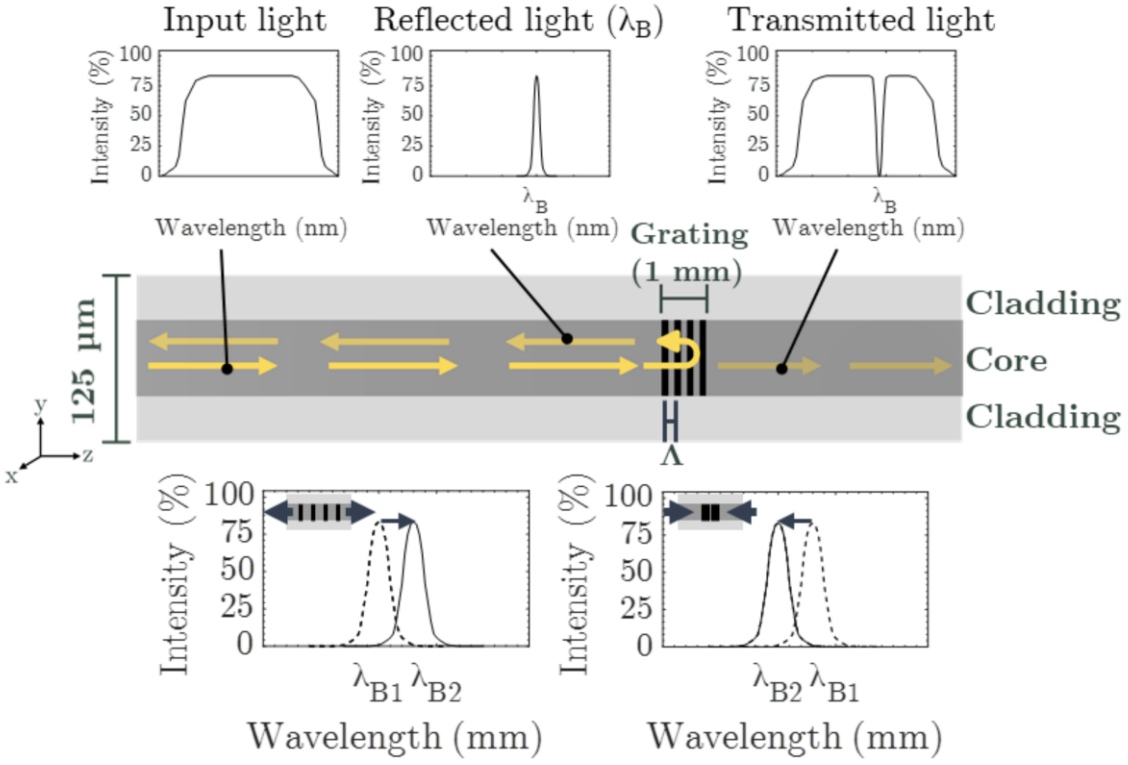

Figure 5 Cross-section of an FBG with a visual representation of the working principles and key elements including a visualization of the increase in wavelength observed when the FBG is stretched and the decrease when the FBG is compressed

3.1 Working Principles

The basic principle behind FBG sensors is monitoring a shift in wavelength that is reflected at the Bragg grating, known as the Bragg wavelength, λ_B [17]. The Bragg wavelength is controlled by the spacing between each grating, or pitch (Λ), and the effective refractive index of the fibre core (n_{eff}) (Equation (1)) [17]–[19], [87].

$$\lambda_B = 2n_{eff}\Lambda \quad (1)$$

Physical strains to the FBG will change the grating pitch and, due to strain-optic effects, will change the effective refractive index. Tension will increase, and compression will decrease the Bragg wavelength (Figure 5) [17], [87]. Similarly, changes in temperature will result in thermal expansion or contraction of the grating pitch and, due to thermo-optic effects, will change the effective refractive index [17], [87]. In this work, all experiments were preformed at room temperature; therefore, temperature was assumed constant and temperature effects were not considered. The Bragg wavelength shift, $\Delta\lambda_B$, is linearly related to axial strains, ε_z, through Equation (2), where, p_{ij} is the stress-optic tensor, and ν is the Poisson's ratio of the silica. [17], [19], [87]. The strain sensitivity is described by Equation (3), typical germanium-doped silica fibres have p_{11}=0.113, p_{12}=0.252, ν=0.16, n_{eff}=1.46, and S_ε = 1.21 pm/με [19].

$$\frac{\Delta\lambda_B}{\lambda_B} = \left[1 - \frac{{n_{eff}}^2}{2}[p_{12} + \upsilon(p_{11} + p_{12})]\right]\varepsilon_z \quad (2)$$

$$S_\varepsilon = 1 - \frac{{n_{eff}}^2}{2}[p_{12} - \nu(p_{11} + p_{12})] \quad (3)$$

3.2 Previous Relevant Work

Various applications of FBG sensors have previously been implemented within dental biomechanics. Specifically, FBG sensors have been: implanted in mouthguards to clinically measure temperature and strain changes that were calibrated to detect changes in force in patients with sleep apnea [16], [88]; secured onto mandibles to measure strains during static and impact loading [81]; [89]; used to create a sensor to measure bite force [90], [91]; and secured along a tooth and bone to measure the magnitude and location of strains during orthodontic treatment [92],

[93]. FBGs have been used within human tendons, returning comparable results to conventional strain measurement techniques during compression tests and had noted benefits including the small size, lightweight, flexibility, and corrosion resistance [94]. The feasibility of placing FBG sensors within an intact joint for measurement with limited damage or removal of biomechanically relevant structures has been shown within interverbal disks [95]–[97], knee joints [98]–[100], and hip joints [101]. The use of FBG sensors within tendons and intact joints gives promise to the use of FBGs within an intact TPBC.

Karam *et al.* [20] and Romanyk *et al.* [15] inserted an FBG sensor into the PDL space of an intact *ex vivo* swine premolar. The small and flexible FBG sensor allowed for strain measurements from within the PDL space when the tooth crown was subjected to external loading. Karam *et al.* [20] placed an FBG sensor into the PDL space of an adult swine and glued the sensor to the tooth's crown. The tooth was subjected to intrusive loads from 5 N to 100 N, and each load was maintained for 2 minutes. The feasibility of monitoring a strain response from the PDL space was reported. However, a rigorous repeatability analysis was not completed. Romanyk *et al.* [15] placed an FBG within the PDL space and completed displacement-controlled tests at varying displacement rates of 0.025 mm/s, 0.050 mm/s, and 0.100 mm/s, to displacements of 0.2 mm and 0.3 mm. Displacements were held for either 10 seconds or 5 minutes. In general, with a greater displacement, a higher peak strain was measured. A repeatability analysis showed that both peak and time series strain data from within a PDL were repeatable. The minimum coefficient of variation value was reported between 3.7% to 44.9%. When comparing the peak strain measurements between the left and right side TPBCs, three of the six comparisons had statistically significant differences, suggesting this measurement technique is not repeatable between TPBCs. This work did not include force measurement, and therefore, a repeatability analysis of the forces during tooth displacement was not included. The experimental protocol was lacking in the definition of preconditioning trials, the starting point for tooth displacement (e.g., preload), and TPBC alignment. Although it was speculated that the FBG was within the PDL space, the location was not confirmed. Finally, the FBG strain measurements were not compared to other techniques, such as FE analysis, to determine if the FBG is capable of measuring a representative physical strain within the PDL.

Chapter 3: Experimental Repeatability, Sensitivity, and Reproducibility of Force and Strain Measurements from Within the Periodontal Ligament Space During Ex Vivo Swine Tooth Loading

The following manuscript is a version of the manuscript submitted to the Journal of Mechanical Behavior of Biomedical Materials in November 2020 and is currently under review. Minor alterations have been made to help with readability and to ensure consistency within this thesis. The first author of this manuscript is also the author of this thesis.

1 Introduction

The periodontal ligament (PDL) provides support, protection, proprioception, and physical attachment between the tooth and surrounding alveolar bone (Figure 3) [3], [4], [24], [25]. It is a complex, soft, narrow connective tissue with a varying thickness ranging from 0.15 mm to 0.38 mm along the root in healthy humans [26]. The mechanical properties of the PDL have been reported as anisotropic [76], non-linear [40], [76], viscoelastic [40], [76], and heterogeneous [28]. It is essential to define the mechanical properties of the PDL to understand, characterize, and predict the response of a tooth-PDL-bone complex (TPBC) to external mechanical stimuli. The small size, complex geometry, and inhomogeneous structure of the PDL make the mechanical properties challenging to study. Further, there is no agreed-upon standardized testing protocol when studying the PDL, contributing to a large discrepancy in the reported Young's Moduli that ranges multiple orders of magnitude (0.01 to 1750 MPa [13]) [13], [76].

Fibre optic sensing techniques, specifically in-Fibre Bragg grating (FBG) sensors, have gained popularity in biomechanics due to their small size, biocompatibility, high sensitivity, chemical inertness, immunity to electromagnetic interference, and multiplexing capability [16]–[19]. Each sensor is composed of a narrow silica core surrounded by a cladding, the outer diameter measuring 0.125 mm. Permanent gratings are written into the fibre's core by way of periodic changes in the

refractive index [87]. A broad spectrum of light is passed through the core and a narrow band is reflected at the gratings, known as the Bragg wavelength [17]–[19], [87]. When the fibre is strained, there will be a physical elongation or compression of the sensor, causing a change in the spacing of the gratings and the refractive index due to strain-optic effects [17], [87]. In this work, there is assumed to be no temperature change; therefore, it is assumed that the shift in Bragg wavelength is attributed only to strain.

Karam *et al.* [20] and Romanyk *et al.* [15] have previously used FBG sensors in an *ex vivo* swine model. The sensor's small size and flexibility allow it to be placed within the TPBC and record a strain measurement from the PDL space [15], [20]. Karam *et al.* [20] demonstrated the feasibility of measuring a strain response in the PDL when the crown was displaced but lacked an in-depth investigation of the intra- and inter-TPBC repeatability. Romanyk *et al.* [15] completed a detailed repeatability analysis, demonstrating repeatability of strain measurements within a single TPBC (i.e., intra-TPBC repeatability), reporting minimum coefficients of variation ranging from 3.7% to 44.9%. When comparing left and right side TPBCs (i.e., inter-TPBC repeatability), statistically significant differences were reported in three of the six cases. Limitations of this work include the lack of force measurement during crown displacement and investigation into potential confounding variables within the experimental set up such as preconditioning, a consistent starting position for the displacement (e.g. preload), TPBC alignment, and sensor depth.

A literature review conducted by Fill *et al.* [13] identified limitations in current PDL research around best practices for characterizing its mechanical response, suggesting the need to investigate different individual factors that may contribute to the PDL mechanics. The use of preconditioning and a preload prior to displacement-controlled tests are essential to ensuring the PDL is at a similar state before each trial, warranting a more direct comparison between trials. Some plasticity is evident in *ex vivo* tissue behaviour where, after a number of cycles, the tissue reaches a preconditioned state [102]. The required number of cycles before a PDL is considered preconditioned varies widely in the literature between 5 [103] and 1000 cycles [104] for different experimental setups and loading regimes. To the author's knowledge, there is no quantitative standard for identifying when the PDL can be considered preconditioned. Due to the nonlinearity of the PDL, the starting or zero displacement position, and subsequently the absolute displacement

of the tooth, is hypothesized to affect the output force and strain measurements. The irregular shape of the tooth root allows for rotation and interaction between the root and the surrounding bone when different alignment or input displacement vectors are applied to the crown [3]. It is understood that collagen fibre orientation differs along the length of the root [4]; therefore, the depth of the sensor, and consequently the position of strain reading along the root, is hypothesized to affect the strain measurements. Due to the sizable range in the reported mechanical properties of the PDL, it has been suggested that each PDL could have its own biomechanical behavior [13]. If each PDL is unique and the strain field varies along the length of the PDL, it is necessary that the experimental setup be reproducible, yielding similar output measures when a sensor is replaced within the same TPBC. The current study evaluates the effect that specimen preconditioning, preload magnitude, TPBC alignment, and FBG sensor depth have on mechanical output measurements made during testing of a complete TPBC in order to better elucidate how variations in experimental setup may impact results.

The objectives of this work are to: (1) define an objective method to determine when the PDL is preconditioned and then determine the experimental intra-TPBC, inter-TPBC, and long-term repeatability of both force and strain output measures; (2) define the experimental sensitivity by determining the influence of the magnitude of preload, the alignment of the TPBC relative to the input displacement vector, and the sensor depth on output strain and force measurements; and (3) define experimental reproducibility of the strain and force output measures.

2 Materials and Methods

A custom-built testing stage was designed to measure the *ex vivo* strain response from within the PDL space of an intact swine TPBC using FBG sensors (Figure 6). A translating base on the testing stage allows for free movement in both the x- and z-direction to ensure a purely compressive load is applied to the TPBC in an intrusive direction (i.e., towards the root apex). An articulating base component (Thor Labs, Newton, New Jersey, USA, Model SL20/M) allows for angular adjustments of the TPBC relative to a probe. Adjustable clamps on the top plate fix either the TPBC or a custom hydration chamber to surround and fix the TPBC onto the stage. The testing stage interfaces with an Instron Electroplus E3000 material testing machine (Instron, Norwood, MA) to allow for control and measurement of displacement and force during testing.

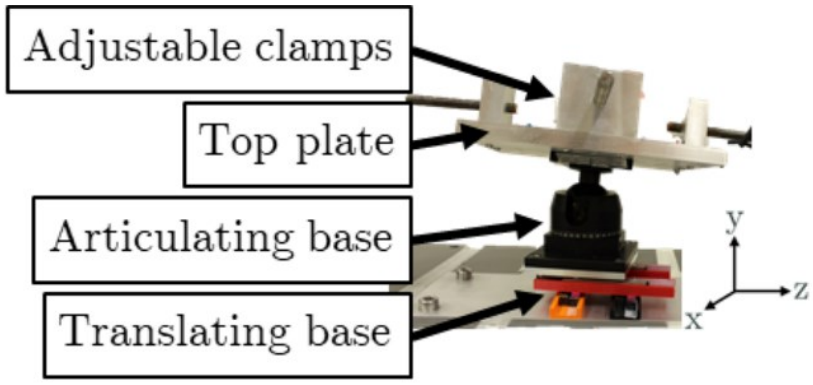

Figure 6 Experimental set up with a custom-designed testing stage that interfaces with the Instron materials testing machine

Post-mortem swine mandibles (n=11) were retrieved from 12-14 week Duroc X (Large White X Landrace) from the Surgical Medical Research Institute at the University of Alberta and stored at -24° immediately after euthanization. As the animals were used for other purposes outside of this study prior to necropsy, ethical approval for this study was granted by exemption from the University of Alberta Animal Care and Use Committee. Prior to testing, the mandibles were thawed over a 24-hour period at 0°C before two segments were sectioned from the mandible, each containing one second premolar (PM2) and one third premolar (PM3) (Figure 7). Swine were used due to their similarity in mandibular morphology and mastication patterns to humans [76], [105]. The bottom or inferior border of the mandible segments were cast in dental stone to provide a rigid base to secure the TPBC onto the testing stage. An FBG (0.125 mm major diameter, Technica SA, Beijing CN) with a 1 mm gauge length located at the approximate tip of the fibre was inserted into the PDL space on the buccal side of the premolar's (PMs) mesial root by threading it through a 27 or 27 1 ¼ gauge needle (Figure 8c). The depth of the sensor, specified below, was controlled using markings on the fibre (Figure 8b).

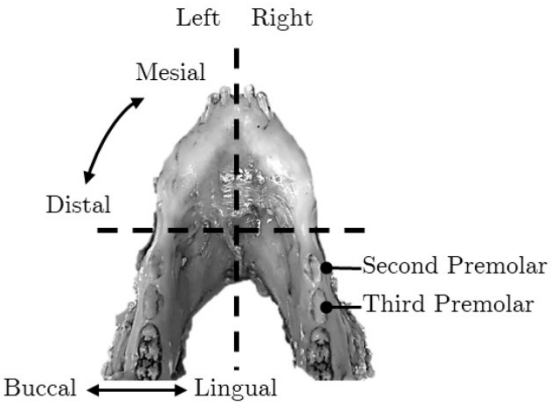

Figure 7 Swine mandible with relevant dental directions, anatomy, and dissection sectioning locations indicated

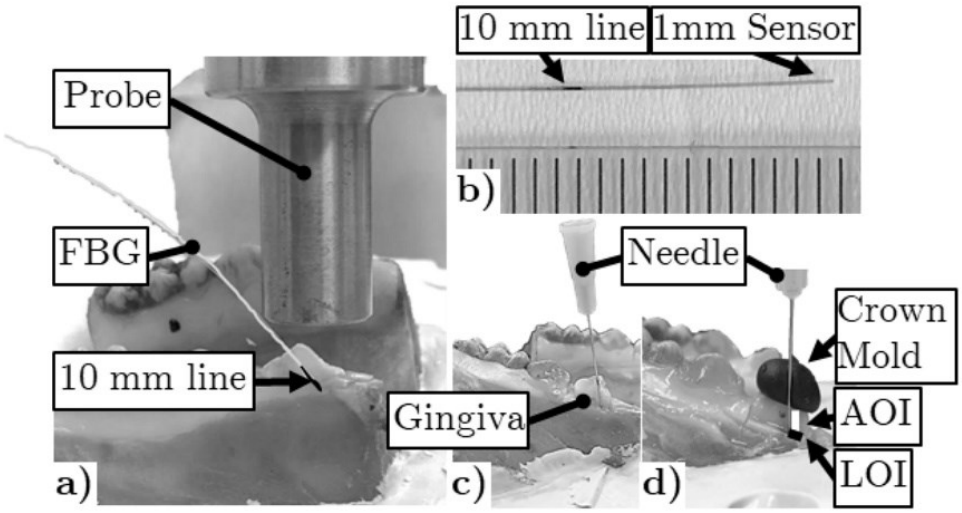

Figure 8 Representative images showing; a) an FBG placed within the PDL, with a representation of a 10 mm marking at the gingiva to control the sensor depth; b) a marking on the FBG approximately 10 mm from the sensor; c) needle placement for insertion of an FBG into the PDL space; d) setup for reproducibility tests including a crown mould to guide the needle, a representation of the angle of insertion (AOI) marking and a representation on the location of insertion (LOI) marking.

An intrusively-directed probe with a diameter of 12.7 mm (Figure 8a), was positioned at the crown cusp and brought to a specified preload to level out uneven surfaces in the system, specifically between the TPBC, dental stone, and top plate of the testing stage. All trials were displacement-controlled with a 0.05 mm/s displacement rate to a 0.2 mm displacement from the

preloaded state and held for 10 seconds before unloading. Each trial was unloaded at a displacement rate of 0.05 mm/s unless otherwise specified. Preconditioning trials were completed with identical parameters to the reported trials, and the number of preconditioning trials is specified below. Specimens were tested in a dry or hydrated environment. During hydrated experiments, the TPBC was submerged in 0.9% NaCl. The gingiva around the tooth to the level of the alveolar crest was removed and, unless otherwise stated, the TPBC was completely unloaded for approximately five minutes after each trial to increase fluid movement into the PDL between trials. Due to equipment availability, two Bragg grating interrogators were used: a SmartScan (SS) Interrogator (SmartScan Dynamic FBG Interrogator, SmartFibres Ltd., Brachnell UK), or a MicronOptics (MO) Interrogator (SM130 Optical Sensing Interrogator, Micron Optics, Atlanta, USA). Both interrogators acted as a light source as well as collected peak wavelength data, giving the same wavelength measures. The SS interrogator collected peak wavelength data at 250 Hz and was filtered using a 4th order Butterworth filter with a cutoff frequency of 50 Hz. The MO interrogator collected peak wavelength data at 200 Hz and was filtered using a 4th order Butterworth filter with a cutoff frequency of 100 Hz and a 1000th order 1D median filter. The SS interrogator was used unless otherwise specified. A gauge factor of -1.21 pm/με was used to convert the change in Bragg wavelength to a strain. A negative gauge factor was used so that compressive strains would be positive for interpretation purposes. MATLAB software (MathWorks, Natick, MA) was used to filter and convert wavelength shift to strain (Appendix A).

This study defined the experimental repeatability, sensitivity, and reproducibility of output strain and force measurements (Figure 9). The number of preconditioning trials required for the PDL to reach a preconditioned state was objectively defined using data clustering. The intra-TPBC and inter-TPBC experimental repeatability pertain to the force and strain output measures within and between TPBCs, respectively. The long-term repeatability was defined by the stability of the force and strain output measurements from a single TPBC over multiple repeated trials. Experimental sensitivity determined the influence of the magnitude of the preload, the alignment of the TPBC relative to the probe, and the depth of the sensor on the peak output measures. The experimental reproducibility was defined as the ability to replace the sensor within the same TPBC and replace the same TPBC onto the testing stage and achieve similar strain and

force output measures at various iterations. The order the work is presented in is not chronological, instead presented as such for ease of interpretation. Due to a lack of comparable studies in the literature, the experimental procedure evolved with *post-hoc* analysis. Specific procedures are further defined for each section below.

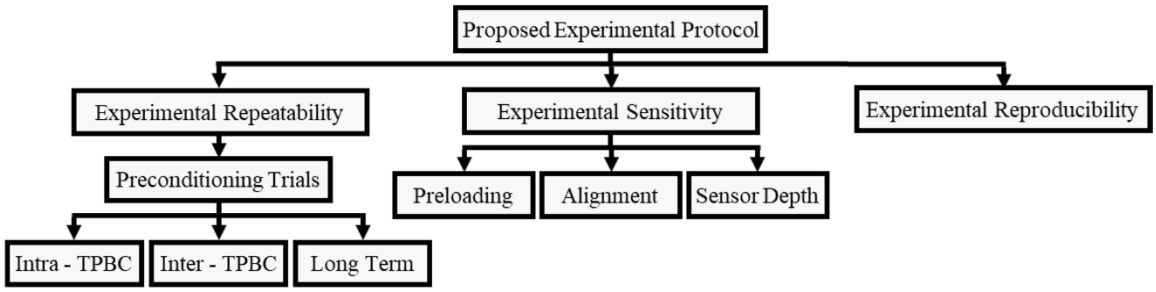

Figure 9 Flowchart indicating parameters used to define the proposed experimental procedure

2.1 Experimental Repeatability

2.1.1 Intra- and Inter- TPBC Repeatability Experimental Procedure

Four mandibles were used to determine intra- and inter-TPBC experimental repeatability, where two were tested in dry conditions, and two were tested in hydrated conditions. The hydrated mandibles were completely unloaded for approximately two and five minutes between trials, respectively. The PM2s were aligned using an alignment angle of 102°, with the alignment angle defined as the angle between the distal edge of the tooth and the input displacement vector (Figure 10a). The same stage angle was used for the respective PM3. This angle was determined through image analysis on eight PM2s. Five PM2s were pulled from three mandibles, three from the left, and two from the right side. Images were taken of the PMs buccal side using a digital single-lens reflex camera equipped with an EF-S 18-55 mm f/3.5-5.6 lens (Canon Rebel EOS t6, Tokyo, Japan). Two additional mandibles were scanned using microcomputed tomography (µCT) scans (SkyScan 1076; Bruker-MicroCT, Kontich, Belgium, current 110 µA, voltage 100 kV, voxel size of 17.2 micron), two left second premolars (LPM2) and one right second premolar (RPM2) were imaged. The approximate centerline of the mesial root was drawn and extended up through the tooth crown. The angle between the distal edge of the PM and the centerline of the root was recorded. Each measurement was repeated three times. On the µCT scans, three slices at the

approximate center of the tooth were measured. Examples of the measurements are shown in Figure 10b. Measurements from camera images were taken on IC Measure (2.0.0.161, The Imaging Source, Charlotte NC), and measurements from µCT images were taken using Avizo software (Avizo 2019.4, ThermoFisher Scientific, Waltham MA).

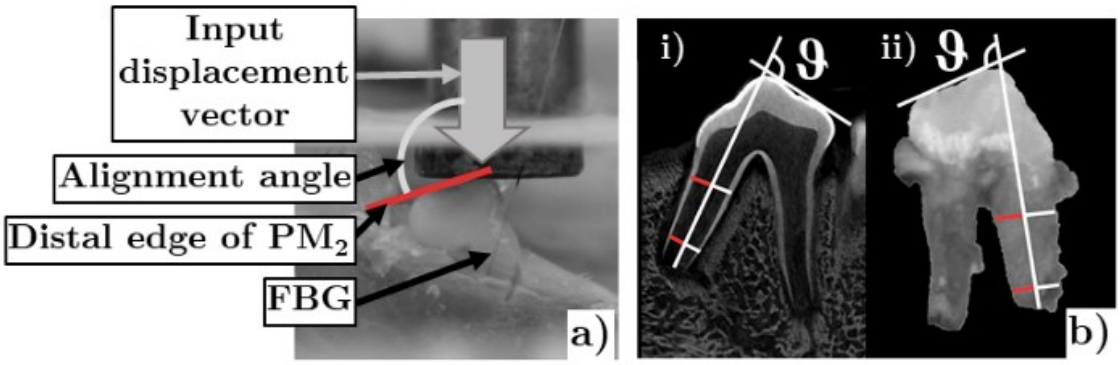

Figure 10 (a) View of the alignment of an RPM2 submerged in 0.9% NaCl with the approximate alignment angle of 102°. (b) Representation of measurements from the (i) µCT scans on an LPM2 and (ii) camera images of an RPM2, to determine the angle (ϑ) between the distal edge of the crown and the approximate axis of the mesial root.

The FBG was inserted along the same approximate angle of 102° from the distal crown edge to ensure the axial strain measured by the FBG was recorded along the displacement application direction. The depth of the sensor was controlled to be approximately 14 mm from the cusp of the crown to allow for consistency when the gingiva was removed for hydrated trials. Each tooth was preloaded to 0.5 N, and a total of 15 trials were completed on each PM. The second hydrated mandible was tested using the MO interrogator.

2.1.2 Determining the Number of Preconditioning Trials

Data clustering was used to split the force data into groups to determine if there was a detectable difference between non-preconditioned and preconditioned trials. Exploratory hierarchical data clustering was completed on MATLAB using Ward's method (Appendix A). Force data were grouped (clustered) together so that the members of each cluster followed the closest time trace output to each other [106]. Ward's method starts with n force trials distributed over n clusters. The square error between all clusters is calculated. The trials with the smallest

error were then merged into a new single cluster, leaving n-1 clusters. This process is repeated until all trials are grouped into one cluster [107]. A dendrogram was used to visualize the allocated relationship between trials and determine the appropriate number of clusters to split the data into. Once the trials were grouped, the assigned cluster numbers were then plotted against trial number to visualize if there was a chronological divide, which would indicate when the PDL was preconditioned. After a preconditioned state was identified, ten subsequent trials were used in the repeatability analysis.

2.1.3 Intra-TPBC and Inter-TPBC Repeatability Data Analysis

An Adjusted Root Mean Square (ARMS) was calculated for both strain and force on each TPBC to assess the intra-TPBC repeatability of the time series measurements (Equation (4)). The ARMS is a unitless value that can be interpreted as the quadratic mean deviation of each observed point from the median as a percentage of the time series peak measurement, where n is the total number of data points. A quadratic mean was chosen over a mean as it is more sensitive to outliers [108]. The median, 25th, and 75th percentiles were calculated to assess the intra-TPBC repeatability of the peak measurements,

$$ARMS = \frac{\sqrt{\frac{\sum_{i=1}^{n}(observed_i - median_i)^2}{n}}}{|peak|} \quad (4)$$

To assess the inter–TPBC repeatability, a Mann Whitney U test was carried out on the peak force and strain measurements from the corresponding left and right side TPBCs using MATLAB.

2.1.4 Long-Term Repeatability Experimental Procedure

The PM2s from two mandibles were used to determine the stability of force and strain output measures within a single TPBC by identifying detectable changes to the mechanical response after multiple trials. The PM2s were submerged in 0.9% NaCl during testing and aligned with an approximate alignment angle of 102°. The FBG was inserted along the same approximate angle to a sensor depth of 14 mm from the crown cusp. Each TPBC was preloaded to 0.5 N, and a total of 30 trials were completed on each PM.

2.1.5 Long-Term Repeatability Data Analysis

Exploratory hierarchical data clustering was completed on MATLAB using Ward's method to identify observable changes in the TPBC mechanical response over the 30 trials. The force time series data were grouped into three clusters to determine if there were two chronological divides. The first chronological divide would indicate a preconditioned state, and the second would indicate a change in the mechanical response, potentially due to damage or fatigue of the PDL. All trials, after the determined preconditioning, were used for the long-term repeatability analysis. An ARMS value for the strain and force time series data was calculated to assess the repeatability of the entire time series. To assess the repeatability of the peak measurements the median, 25^{th}, and 75^{th} percentiles were calculated.

2.2 Experimental Sensitivity

2.2.1 Preloading Sensitivity Experimental Procedure

To determine the effect of preload on the peak strain and force measurements, two PM2s from the same mandible were preloaded to magnitudes of 0.5 N, 1.0 N, and 3.0 N with the same sensor placement. The TPBC was aligned visually so that the crown cusp appeared to be in line with the probe. The FBG was placed to an approximate depth of 12 mm below the gingiva. Three preconditioning trials were completed with a 1.0 N preload, five trials were then completed at each preload magnitude. Each trial was immediately unloaded after the hold period. The order of the preloading conditions was varied; the left second premolar (LPM2) started with 1.0 N, 3.0 N, then 0.5 N; the right second premolar (RPM2) started with 1.0 N, 0.5 N, then 3.0 N.

2.2.2 Alignment Sensitivity Experimental Procedure

Two mandibles were used to vary the alignment of each TPBC, rotating the TPBC towards the lingual, buccal, mesial, or distal direction (Figure 7). Specifically, the LPM2s were rotated towards the lingual direction, the RPM2s were rotated toward the buccal direction, the left third premolars (LPM3s) were rotated towards the distal direction, and the right third premolars (RPM3s) were rotated toward the mesial direction. The alignment adjustments on the first mandible were approximately 5° increments, and alignment adjustments on the second mandible were approximately 10° increments. An angle of 5° was chosen to obtain baseline data,

as these were the smallest adjustments that could be made with the experimental setup. The movement angles were controlled by a custom-designed 3D printed protractor with marked 5° increments that was secured onto the articulating base. The 5° incremental adjustments were made in sequential order with the exception of the RPM2 and the LPM3, where the final adjustment was made in the opposite direction to an angle of -5° from the initial position. The order of the 10° incremental changes was randomized. The initial alignment was set so the crown cusp appeared to be in line with the probe. The FBG was placed to an approximate depth of 12 mm below the gingiva and left in the same location throughout all tests. Each trial was preloaded to approximately 3 N. Three preconditioning trials were completed at the initial alignment, and five subsequent trials were completed at each alignment angle. Each trial was unloaded immediately after the hold period.

2.2.3 Sensor Depth Sensitivity Experimental Procedure

Two PM2s from one mandible were used to assess the effect of different sensor depths on the strain and force output measures. The TPBC was aligned visually so that the cusp of the crown was in line with the probe. The depth of the FBG was varied between approximately 12 mm, 8 mm, and 4 mm below the gingiva, determined by multiple markings on the FBG. The tests were completed from the deepest position to the shallowest to avoid removing the sensor and ensuring the axial strain was measured along a similar angle. Each trial was preloaded to approximately 3 N. Three preconditioning trials were initially completed at a sensor depth of 12 mm, five subsequent trials were completed at each sensor depth. Each trial was unloaded immediately after the hold period.

2.2.4 Experimental Sensitivity Data Analysis

A rank-based alternative to a one-way repeated measures ANOVA test or Friedman test was used to find statistically significant differences in the distributions of the peak measurements within each testing condition [109]. The p-value, degrees of freedom, and test statistic were reported. A non-parametric test was chosen due to the small sample size. When the Friedman test gave a statistically significant result ($\alpha<0.05$), a Dunn pairwise comparison was conducted. The Dunn multiple comparisons rank-sum method differs from the Wilcoxon signed-rank test as it considers the data set as a whole when calculating the standard deviation of ranks [110]. The

Friedman test and Dunn pairwise analysis were conducted using SPSS software (SPSS® Statistics Premium 26, IMB®, Armonk, NY). To control the family-wise error rates the Dunn pairwise p-values were corrected using a Holms-Bonferroni adjustment [111]. The corrected p-values were calculated using MATLAB. To further define the variations between the experimental sensitivity cases, a standardized difference of medians (SDM) were calculated (Equation (5)).

$$SDM = \frac{|M_1 - M_2|}{average\ distance\ from\ the\ median} = \frac{|M_1 - M_2|}{\frac{\sum_{k=1}^{n}|y_{k,1} - M_1| + \sum_{k=1}^{n}|y_{k,2} - M_2|}{2n}} \quad (5)$$

The SDM is the difference between the median peak measurements (M_1-M_2) divided by the average of the deviation of each peak measurement from the respective median. Within Equation (5), y is the observed values, M is the calculated median, and n is the number of samples in the subset. This can be interpreted as the difference in medians as a percentage of the variation. This method was implemented to go beyond statistical and rank based differences and look explicitly at the magnitude of the median difference to provide insight into whether the differences are physically meaningful.

2.3 Experimental Reproducibility

2.3.1 Experimental Procedure

To determine the reproducibility of the strain and force measurements, four TPBCs from one mandible were tested at different positions. Each position was defined by placing the sensor into the PDL and the TPBC onto the testing stage. In between each position, the sensor was removed from the PDL, and the TPBC was removed from the testing stage, but the angular alignment of the stage was not changed. Moldable silicone-based glue (Sugru®, London, UK) was used to make an impression of the crown cusp and the angle of the insertion of the needle in order to control the FBG placement. The location and approximate insertion angle were further marked with a permanent marker on the crown (Figure 8d). The crown mould and markings were used to guide the needle and FBG placement for subsequent positions. A total of four positions were tested for each TPBC. The PM2s were tested in a hydrated state, while the PM3s were tested in a dry state. Each TPBC was aligned with an approximate alignment angle of 102°. The FBG was inserted along the same approximate angle to an approximate depth of 14 mm from the crown

cusp. Each trial was preloaded to 0.5 N. Three preconditioning trials were initially completed at the first position, and five subsequent trials were completed at each position.

2.3.2 Data Analysis

At each position, the median peak measurements and respective 25^{th} and 75^{th} percentiles were calculated. The peak measurements were compared by way of a Friedman test to determine if there were statistically significant difference between the cases ($\alpha<0.05$). If statistical significance was determined, a Dunn pairwise comparison was completed, and the Holms-Bonferroni adjusted p-values and SDM values were calculated.

3 Results

3.1 Experimental Repeatability

3.1.1 Preconditioning

Data clustering was used to objectively determine the number of preconditioning trials required for each TPBC. A visual representation of the analysis including dendrograms to determine the number of clusters required, the cluster numbers against the respective trial numbers to determine if there was a chronological divide, and the cluster time traces with all respective force time traces to visualize further the relationship for initial and preconditioned trials are shown in Figure 11. Figure 11a is an example of the typical output with two clusters from the first mandible LPM2, Figure 11b is an example where three clusters were required from the first mandible RPM2, and Figure 11c is an example where no chronological divide was evident from the fourth mandible RPM3.

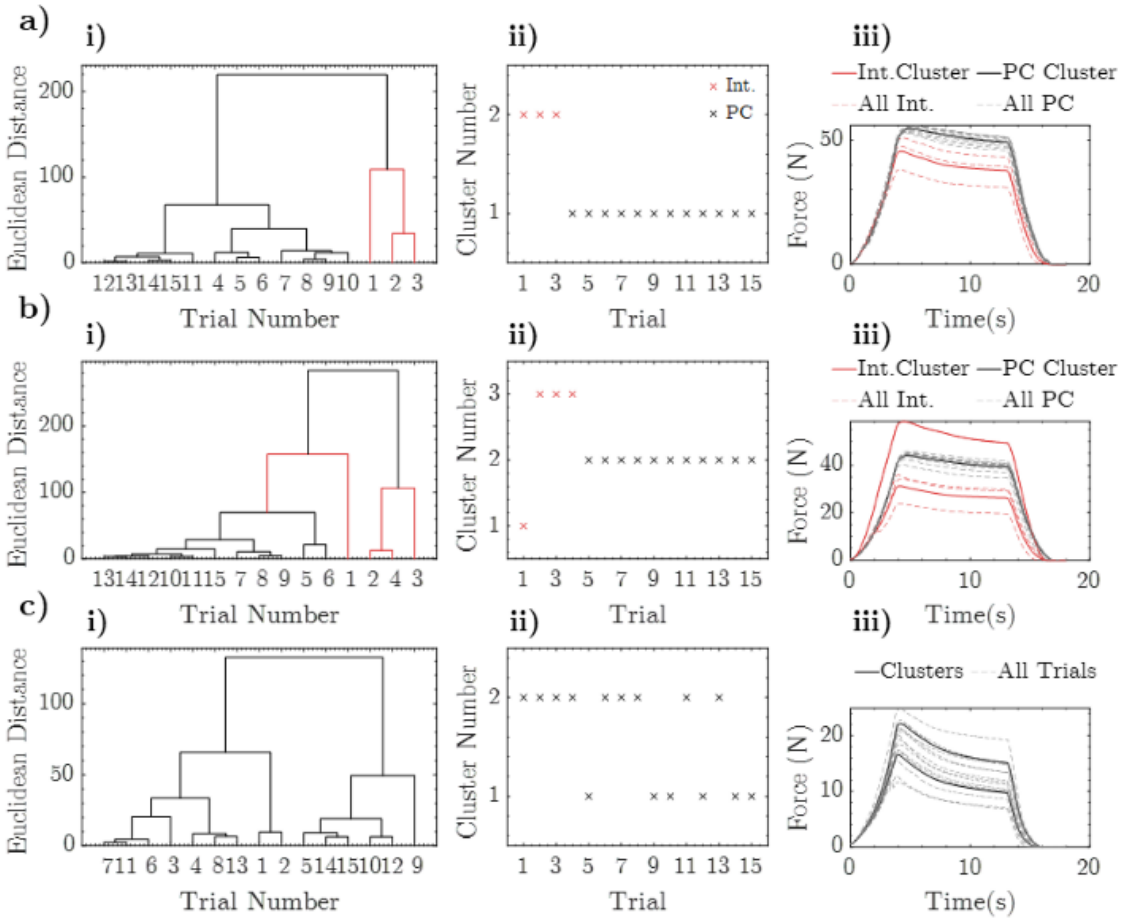

Figure 11 Exemplary visual representation of the data clustering analyses for determination of preconditioning (PC) including i) dendrograms, ii) clusters against the respective trial number, and iii) all force time series with the respective averaged cluster time series. a) The first mandible LPM2 shows a typical output where two clusters were used, b) the first mandible RPM2 shows a case where three clusters were used, and c) from the fourth mandible LPM3 from the fourth mandible shows a case where no preconditioning is evident.

Only 14 trials were completed for the first mandible LPM3. The fourth mandible RPM3 was loaded off-center, displacing the tooth laterally for the first seven trials; these trials are not shown, and 15 subsequent trials were completed. The number of trials in the preload cluster is summarized in Table 1 for each TPBC. Three, two and five were the most common number of preconditioning trials, respectively. Five TPBCs did not indicate a preconditioned state through data clustering; two TPBCs that were hydrated with 2 minutes between trials, and three TPBC that were hydrated with 5 minutes between trials. For these TPBCs, the first trial was used as the preconditioning trial.

Table 1 Repeatability analysis summary including the required preconditioning trials (PC trials), median peak measurements, strain ARMS, force ARMS, and p-values comparing left and right TPBCs. The TPBCs were indicated by dry (D), or hydrated (H), mandible number (1-4), Left (L) or Right (R) side, and the PM2 (2) or PM3 (3).

Tooth	No. of PC trials	Median Peak Strain (25-75%-ile) (με)	Median Peak Force (25%ile-75%-ile) (N)	ARMS Strain (%)	ARMS Force (%)	Strain p-value	Force p-value
D_1_L_2	3	2.84 (2.65-3.26)	55.22 (54.54-55.59)	10.90	2.61	1.000[d]	<0.001[a]
D_1_R_2	4[d]	2.76 (2.49-3.26)	44.23 (42.43-44.96)	30.15	6.74		
D_1_L_3	3	3.58 (2.94-4.19)	48.64 (48.23-48.92)	14.38	1.08	<0.001[a]	<0.001[a]
D_1_R_3	5	8.88 (7.45-9.53)	70.63 (69.62-75.82)	10.02	1.64		
D_2_L_2	1	3.63 (3.19-4.22)	53.71 (51.77-55.31)	24.78	2.93	<0.001[a]	<0.001[a]
D_2_R_2	3	1.07 (0.97-1.13)	78.83 (77.58-79.64)	19.30	2.64		
D_2_L_3	2	2.09 (2.16-2.18)	88.36 (87.82-89.53)	28.49	1.37	0.017[a]	<0.001[a]
D_2_R_3	5	2.70 (2.60-2.76)	121.05 (124.44-121.78)	8.70	1.02		
H_3_L_2	1[c]	3.59 (2.98-3.95)	32.27 (39.81-33.56)	22.27	5.06	<0.001[a]	<0.001[a]
H_3_R_2	1[c]	1.27 (1.11-1.79)	23.73 (21.91-25.41)	30.67	7.43		
H_3_L_3	5	2.62 (2.59-2.82)	40.53 (39.77-41.28)	26.00	3.41	<0.001[a]	<0.001[a]
H_3_R_3	2	1.20 (1.63-1.25)	50.05 (49.32-58.78)	15.84	1.51		
H_4_L_2	1[c]	1.90 (1.76-2.26)	11.35 (10.24-12.41)	26.20	8.10	<0.001[a]	<0.001[a]
H_4_R_2[b]	7[d]	-5.77 (-5.93--5.61)	16.14 (15.22-17.07)	5.62	5.58		
H_4_L_3	1[c]	-1.17 (-2.69--1.25)	18.02 (16.93-27.68)	52.89	14.76	<0.001[a]	0.009[a]
H_4_R_3	1[c]	-0.51 (-0.72--0.13)	16.00 (14.36-16.81)	136.34	5.99		

[a] indicates statistical significance, [b] indicates only 8 trials, [c] indicated no divide evident in clustering, [d] indicates cases where three clusters used),[d] corrected p-value rounded down to upper limit

3.1.2 Intra-TPBC and Inter-TPBC Repeatability

The alignment angle for the PM2 to allow for an intrusive displacement of the mesial root was measured from both camera images and µCT image slices (Table 2). The average angle was 102° ± 5° between the distal edge of the second premolar and the approximate central axis of the mesial root.

Table 2 Alignment angle between distal edge and the approximate central axis of the mesial root of PM2s

	Mean ± SD	Analysis Type
Left-side PM	97° ± 2°	µCT slices
	105° ± 2°	µCT slices
	100° ± 3°	Buccal side image
	105° ± 1°	Buccal side image
	103° ± 2°	Buccal side image
Right-side PM	107° ± 2°	µCT slices
	102° ± 3°	Buccal side image
	104° ± 2°	Buccal side image
Mean Left-side	102° ± 5°	
Mean Right-side	104° ± 4°	
Overall	102° ± 5°	

The peak measurements and ARMS values for strain and force time series data were calculated to quantify the intra-TPBC repeatability (Table 1). The force ARMS values are notably lower than the strain ARMS values. The force ARMS ranged from 1.02% to 14.76%, with an average of 4.49%. The strain ARMS values range from 5.65% to 136.34%, with an average of 28.91%. It should be noted that the fourth mandible RPM3 has the highest strain ARMS value of 136%, which is potentially attributed to the peak strain value being less than 1 µε. The next greatest strain ARMS value is 52.89%. Statistically significant p-values were found for all peak force measurements and seven out of eight peak strain measurements (Table 1), indicating a lack of inter-TPBC repeatability between the left and right side PMs.

From the first mandible, LPM2 trials five and six force and strain data were excluded due to excessive noise in the strain sensor. Similarly, trial 13 was excluded for the second mandible LPM3. A total of 10 trials were still used for the repeatability analysis for these two TPBCs. The

third mandible RPM2 required seven preconditioning trials; therefore, only eight trials could be considered for the repeatability analysis. Representative strain and force time series data are shown in Figure 12.

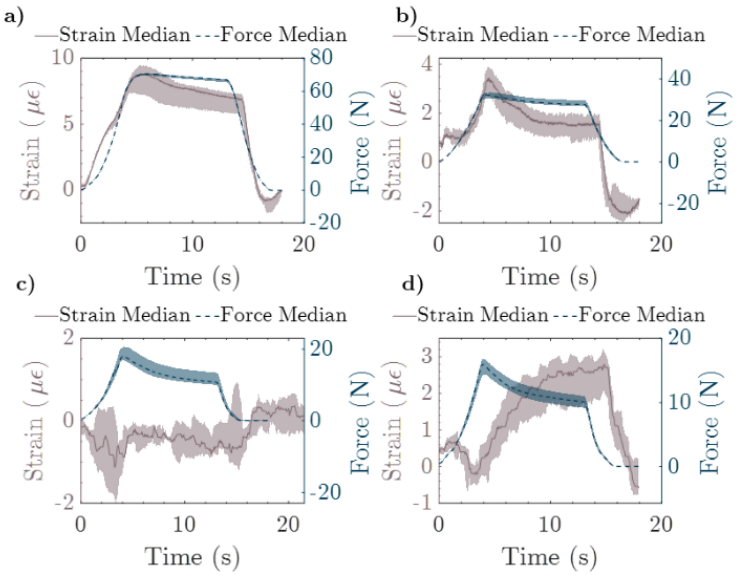

Figure 12 Median time series strain and force measurements indicating the 25th and 75th percentile. Representative TPBC with typical outputs from a) the first mandible RPM3, and b) the third mandible LPM2. Representative TPBC with the largest force ARMS value from the c) fourth mandible LPM3 and the largest strain ARMS value from the d) fourth mandible RPM3.

3.1.3 Long Term Repeatability

The force data were grouped into three clusters to determine if there was a distinguishable change in the mechanical output after repeated trials (Figure 13). An initial chronological divide can be observed for each TPBC, indicating the number of preconditioning trials (Table 3). From the first mandible, no clear chronological divide between the second and third cluster is evident, indicating no significant changes in the system affecting output measurements (Figure 13a and Figure 13b). However, in the second mandible, a chronological divide can be seen at trial 22 and 23, respectively (Figure 13c and Figure 13d). To quantify the intra-TPBC repeatability, the median, 25th, and 75th percentiles for the peak measurements were calculated from all trials after preconditioning was reached (Table 3). The ARMS values for the strain measurements range from 5.62% to 11.68%, and values for the force measurements range from 4.39% to 9.33%.

Table 3 Long term repeatability summary, including required preconditioning trials (PC trials), median peak measurements, strain ARMS, and force ARMS values. The TPBCs are indicated as hydrated (H), with the mandible number (1-2), left (L) or right(R) side and PM2 (2).

	No. of PC trials	Median Peak Strain (25%ile-75%ile) (με)	ARMS Strain (%)	Median Peak Force (25%ile-75%ile) (N)	ARMS Force (%)
H_1_L_2	2	1.94 (1.82-2.36)	8.51	12.55 (12.32-13.77)	4.39
H_1_R_2	3	6.77 (6.37-7.68)	11.68	15.84 (14.94-16.86)	4.73
H_2_L_2	2	6.25 (5.84-6.45)	5.62	18.10 (17.31-19.87)	9.33
H_2_L_2	7	4.42 (3.94-4.95)	8.81	16.56 (14.68-17.82)	8.68

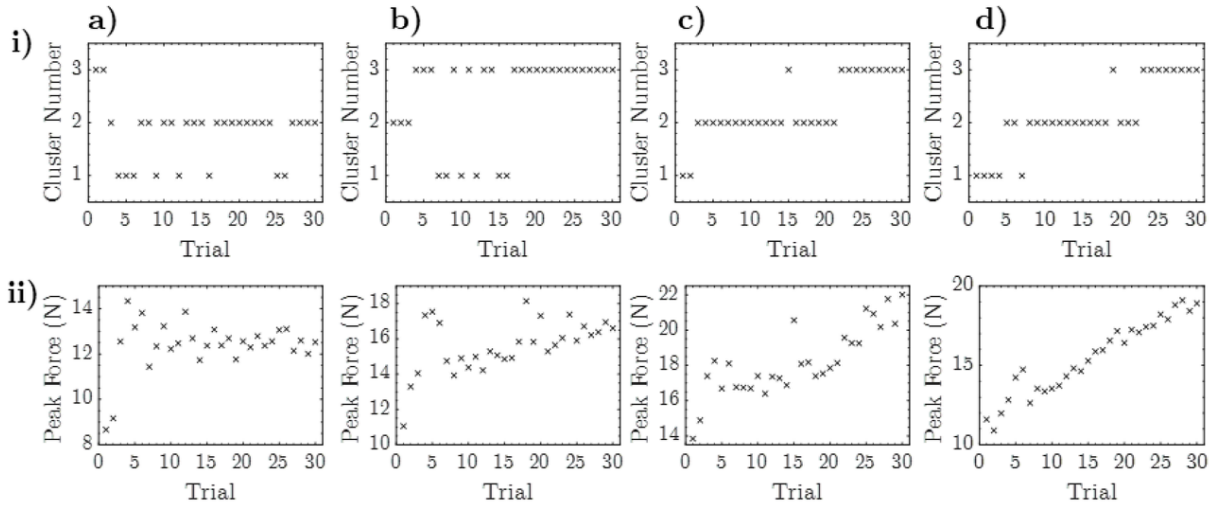

Figure 13 ii) Resultant cluster number plotted against the trial number and ii) peak force plotted against the trial number from the first mandible a) LPM2, b) RPM2 and second mandible c) LPM2, d) RPM2 to determine the stability of the mechanical output

3.2 Experimental Sensitivity

3.2.1 Preloading Sensitivity

To quantify the effect of preload on the peak measurements, the median, 25th, and 75th percentile for the peak measurements were calculated for each preload (Figure 14). Strain data is

missing for the RPM2 due to an FBG breaking during testing. Data from one trial at a 0.5 N and at a 1.0 N preload was not properly exported; therefore, only four trials are reported. The Freidman test showed statistically significant differences between different preloads for the LPM2 strain values ($\chi^2(2)=6.500$, p=0.039), LPM2 force values ($\chi^2(2)=6.500$, p=0.039), and the RPM2 force values ($\chi^2(2)=8.000$, p=0.018). The Dunn multiple pairwise comparison Holm-Bonferroni corrected p-value and calculated SDM were calculated (Table 4). The greatest force SDM values are reported when comparing to the 3.0 N preload case. The LPM2 SDM values range from 6.80 to 8.29 when comparing to a 3.0 N preload as opposed to 1.19 when comparing 0.5 N to 1.0 N. Similarly, SDM values range from 45.49 to 70.03 instead of 19.72 in the RPM2. An increase in peak force was observed at the 3.0 N preload case.

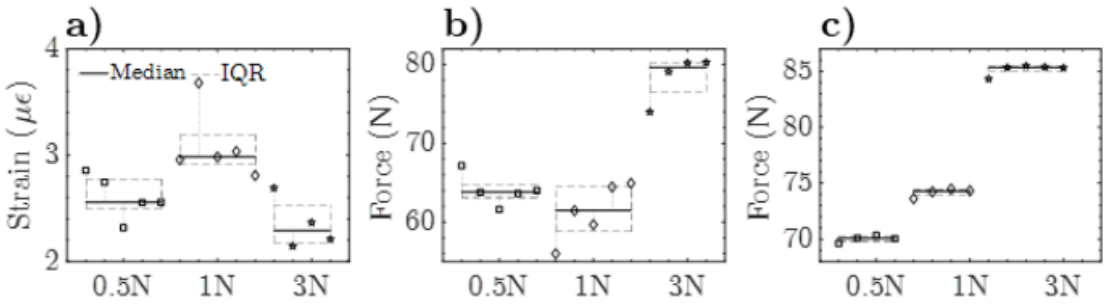

Figure 14 Preload sensitivity peak measurements with respective median, 25th and 75th percentile (IQR) for a) LPM2 strain b) LPM2 force c) RPM2 force

Table 4 Preload sensitivity multiple pairwise output for peak measurements including corrected p-values and the standardized difference in medians (SDM)

Tooth	Preload 1	Preload 2	Strain		Force	
			p-value	SDM	p-value	SDM
Left 2	0.5 N	1.0 N	0.308	2.54	1.000[b]	1.19
	0.5 N	3.0 N	1.000[b]	0.92	0.308	8.29
	1.0 N	3.0 N	0.039[a]	2.70	0.039[a]	6.80
Right 2	0.5 N	1.0 N	-	-	0.630	19.72
	0.5 N	3.0 N	-	-	0.015[a]	70.03
	1.0 N	3.0 N	-	-	0.790	45.49

[a] indicates statistical significance, [b] corrected p-value rounded down to upper limit

3.2.2 Alignment Sensitivity

To quantify the effect of misalignment on the peak measurements, the median, 25^{th}, and 75^{th} percentiles for the peak measurements were calculated for each alignment and plotted for 5° and 10° adjustments, respectively (Figure 15). The Friedman tests found statistically significant differences in peak strain and force measurements between alignments for both the 5° and 10° adjustments (Table 5). The Dunn multiple pairwise comparison Holm-Bonferroni corrected p-values and calculated SDM for the peak measurements are summarized in Table 6 to Table 9. Considering all directions, a ratio of statistically significant to not statistically significant differences and the average SDM magnitude generally increases with the misalignment for both strain and force peak measurements indicating greater changes with greater misalignment.

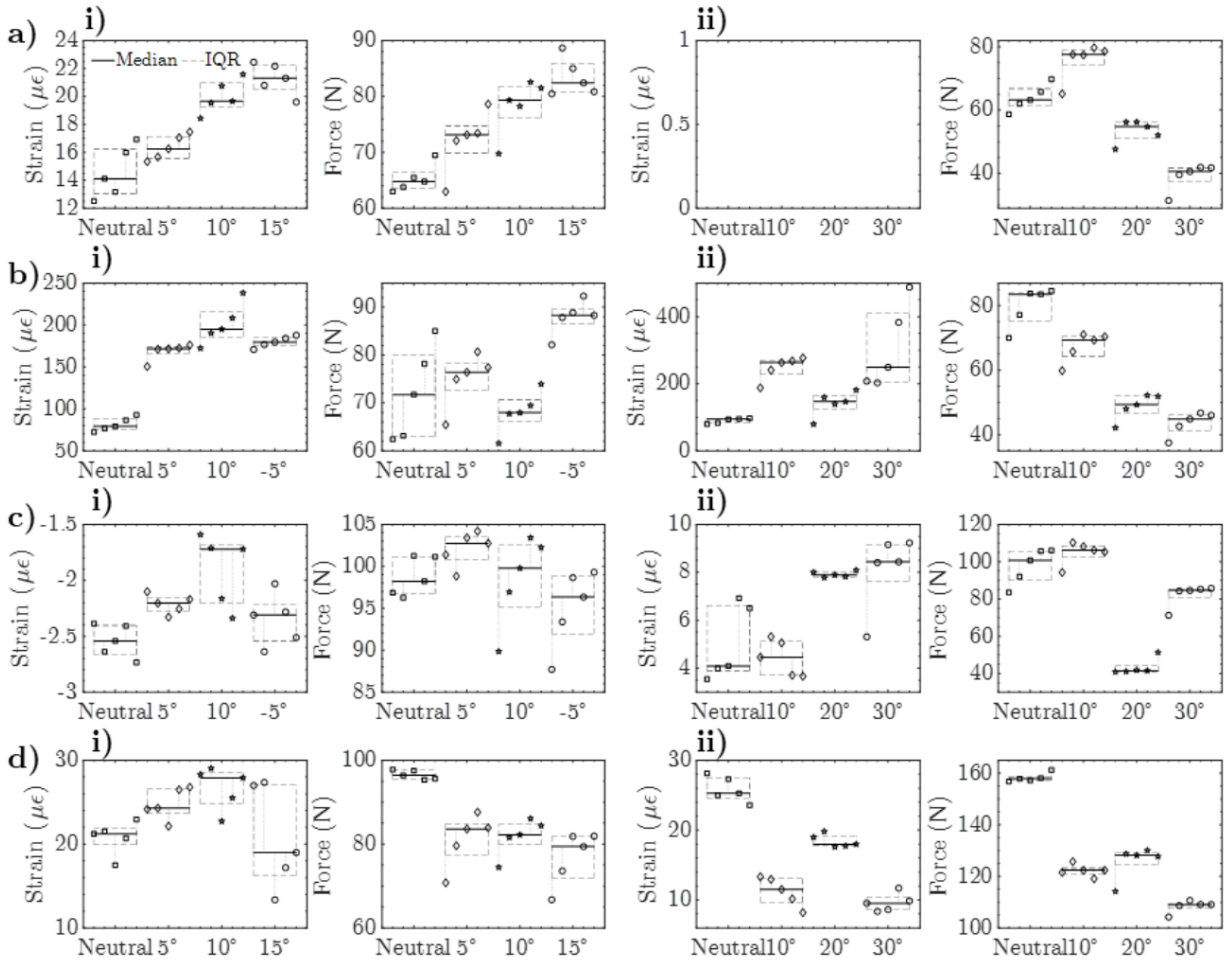

Figure 15 Alignment sensitivity peak measurements with median, 25th, and 75th percentile (IQR) indicated from i) 5° movements and ii) 10° movements for a) LPM2 b) RPM2 c) LPM3 d) RPM3

*Table 5 Position sensitivity Friedman test output (*Note Left 2 lingual 10° data missing due to a broken sensor)*

Tooth	Movement Direction	Test	Strain		Force	
			p-value	Test Statistic	p-value	Test Statistic
Left 2	Lingual	5°	0.003[a]	$\chi^2(3)$=14.040	0.006[a]	$\chi^2(3)$=12.600
		10°	-	-	0.002[a]	$\chi^2(3)$=15.000
Right 2	Buccal	5°	0.002[a]	$\chi^2(3)$=15.000	0.005[a]	$\chi^2(3)$=12.840
		10°	0.006[a]	$\chi^2(3)$=12.600	0.002[a]	$\chi^2(3)$=15.000
Left 3	Distal	5°	0.019[a]	$\chi^2(3)$=9.960	0.004[a]	$\chi^2(3)$=13.560
		10°	0.001[a]	$\chi^2(3)$=12.600	0.003[a]	$\chi^2(3)$=14.040
Right 3	Mesial	5°	0.026[a]	$\chi^2(3)$=9.240	0.004[a]	$\chi^2(3)$=13.560
		10°	0.004[a]	$\chi^2(3)$=13.560	0.003[a]	$\chi^2(3)$=14.040

[a] *indicates statistical significance*

*Table 6 Position sensitivity multiple pairwise comparisons for Lingual movements on the LPM2 including corrected p-values and the standardized difference in medians (SDM) (*Note 10° data missing due to a broken sensor)*

Alignment 1	Alignment 2	Approx. angle change (°)	Strain		Force	
			p-value	SDM	p-value	SDM
0°	5°	5[b]	1.000[c]	0.27	1.000[c]	3.00
5°	10°	5[b]	1.000[c]	4.34	0.450	1.87
10°	15°	5[b]	1.000[c]	1.92	1.000[c]	1.09
0°	10°	10[b]	0.049[a]	3.30	0.049[a]	5.62
5°	15°	10[b]	0.216	6.52	0.216	3.17
0°	10°	10	-	-	1.000[c]	4.70
10°	20°	10	-	-	0.112	8.01
20°	30°	10	-	-	1.000[c]	5.59
0°	15°	15[b]	0.006[a]	4.82	0.018[a]	8.13
0°	20°	20	-	-	1.000[c]	3.06
10°	30°	20	-	-	<0.001[a]	13.03
0°	30°	30	-	-	0.098	8.23

[a] *indicates statistical significance,* [b] *indicates movements from 5° tests,* [c] *corrected p-value rounded down to upper limit*

Table 7 Position sensitivity multiple pairwise comparisons for buccal movements on the RPM2 including corrected p-values and the standardized difference in medians (SDM)

Alignment 1	Alignment 2	Approx. angle change (°)	Strain		Force	
			p-value	SDM	p-value	SDM
0°	-5°	5[b]	0.100	14.90	0.778	2.11
0°	5°	5[b]	1.000[c]	13.05	1.000[c]	0.32
5°	10°	5[b]	0.114	2.10	0.864	2.66
0°	10°	10[b]	0.001[a]	8.89	0.350	2.00
-5°	5°	10[b]	1.000[c]	1.56	0.400	4.13
0°	10°	10	0.049[a]	11.55	1.000[c]	3.85
10°	20°	10	0.450	4.88	1.000[c]	6.69
20°	30°	10	0.216	1.76	1.000[c]	1.69
-5°	10°	15[b]	1.000[c]	1.41	0.001[a]	8.04
0°	20°	20	1.000[c]	3.47	0.112	9.73
10°	30°	20	1.000[c]	0.24	0.098	8.58
0°	30°	30	0.018[a]	11.45	<0.001[a]	11.45

[a] indicates statistical significance, [b] indicates movements from 5° tests, [c] corrected p-value rounded down to upper limit

Table 8 Position sensitivity multiple pairwise comparisons for distal movements on the LPM3 including corrected p-values, and the standardized difference in medians (SDM)

Alignment 1	Alignment 2	Approx. angle change (°)	Strain		Force	
			p-value	SDM	p-value	SDM
0°	-5°	5*[b]	0.400	3.75	0.774	2.71
0°	5°	5[b]	0.098	3.22	0.350	1.13
5°	10°	5[b]	1.000[d]	2.87	0.860	0.96
0°	10°	10[b]	0.018[a]	4.56	0.400	0.55
-5°	5°	10[b,c]	1.000[d]	0.92	<0.001[a]	2.64
0°	10°	10	1.000[d]	0.41	1.000[d]	0.99
10°	20°	10	0.450	9.82	0.006[a]	21.40
20°	30°	10	1.000[d]	1.05	1.000[d]	16.13
-5°	10°	15[b,c]	1.000[d]	1.60	1.000[d]	0.72
0°	20°	20	0.216	5.95	0.049[a]	12.45
10°	30°	20	0.049[a]	5.20	0.216	6.28
0°	30°	30	0.018[a]	4.12	1.000[d]	3.12

[a] indicates statistical significance, [b] indicates movements from 5° tests, [c] indicates movements in the negative direction, [d] corrected p-value rounded down to upper limit

Table 9 Position sensitivity multiple pairwise comparisons for mesial movements on the RPM3 including corrected p-values and the standardized difference in medians (SDM)

Alignment 1	Alignment 2	Approx. angle change (°)	Strain		Force	
			p-value	SDM	p-value	SDM
0°	5°	5[b,c]	1.000[d]	2.33	0.350	5.01
5°	10°	5[b]	1.000[d]	2.24	1.000[d]	0.39
10°	15°	5[b]	0.100	2.70	0.400	0.74
0°	10°	10[b]	0.042[a]	4.33	0.778	7.53
5°	15°	10[b,c]	1.000[d]	1.72	0.864	0.94
0°	10°	10	0.021[a]	9.31	0.216	27.45
10°	20°	10	0.774	5.68	1.000[d]	2.38
20°	30°	10	0.400	10.49	0.189	8.06
0°	15°	15[b,c]	1.000[d]	0.74	0.001[a]	6.11
0°	20°	20	1.000[d]	7.08	1.000[d]	13.36
10°	30°	20	1.000[d]	1.57	1.000[d]	9.25
0°	30°	30	0.006[a]	13.75	<0.001[a]	39.60

[a] *indicates statistical significance,* [b] *indicates movements from 5° tests,* [c] *indicates movements in the negative direction,* [d] corrected p-value rounded down to upper limit

3.2.3 Sensor Depth Sensitivity

To quantify the effect of sensor depth on peak measurements, the median, 25th, and 75th percentiles for the peak measurements were calculated for each sensor depth (Figure 16). Peak strain measurements between sensor depths for the LPM2 ($\chi^2(2)=10.000$, $p=0.007$), and the RPM2 ($\chi^2(2)=7.600$, $p=0.022$) had statistically significant differences. The peak force measurements for the LPM2 ($\chi^2(2)=4.800$, $p=0.091$), and the RPM2 ($\chi^2(2)=1.600$, $p=0.449$) did not have statistically significant differences. The resulting Dunn pairwise comparison corrected p-values and SDM for the peak strain measurements were calculated (Table 10). Although only two of the six cases are statistically significant, five of the six cases had SDM values greater than 1, ranging from 6.16 to 20.19.

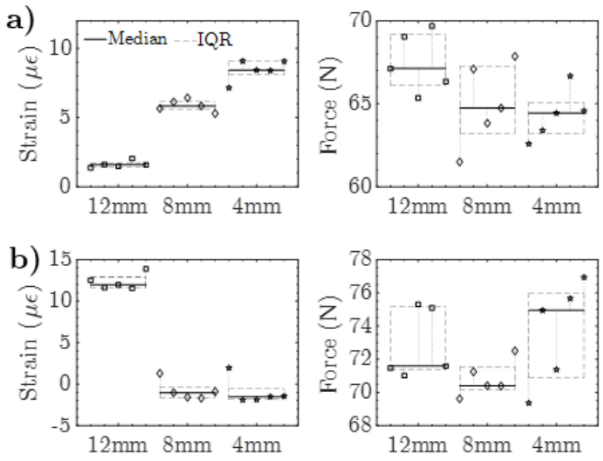

Figure 16 Sensor depth peak measurements with respective median, 25th, and 75th percentile (IQR) for the a) LPM2 and b) RPM2

Table 10 Sensor depth multiple pairwise comparisons for peak measurements including corrected p-values and the standardized difference in medians (SDM)

Tooth	Depth 1	Depth 2	Strain	
			p-value	SDM
Left 2	12 mm	8 mm	0.456	17.74
	12 mm	4 mm	0.005[a]	20.19
	8 mm	4 mm	0.570	6.16
Right 2	12 mm	8 mm	0.108	18.93
	12 mm	4 mm	0.033[a]	18.01
	8 mm	4 mm	1.000[b]	0.63

[a] indicates statistical significance, [b] corrected p-value rounded down to upper limit

3.3 Experimental Reproducibility

The median, 25th, and 75th percentiles for the peak measurements were calculated for each position in which the FBG and TPBC were replaced onto the testing stage to determine the reproducibility of the peak measurements (Figure 17). Friedman tests found statistically significant differences for two of four TPBCs concerning the peak strain measurements and all four TPBCs concerning peak force measurements. Specifically, statistically significant differences

in the peak strain values for the LPM2 ($\chi^2(2)$=9.960, p=0.018) and the RPM2 ($\chi2(2)$=9.240, p=0.026). The LPM3 ($\chi^2(2)$=6.120, p=0.106) and the RPM3 ($\chi^2(2)$=7.320, p=0.062) peak strain values did not have statistically significant differences. Peak force values had statistically significant differences for the LPM2 ($\chi^2(2)$=9.720, p=0.021), RPM2 ($\chi^2(2)$=13.560, p=0.004), LPM3 ($\chi^2(2)$=14.040, p=0.003), and the RPM3 ($\chi^2(2)$=12.840, p=0.005). The resulting Dunn pairwise comparison Holms-Bonferroni corrected p-values and SDM for the peak measurements are summarized in Table 11. The greatest difference in median peak measurements for LPM2 was 1.24 με between position 2 and position 3 for strain and 13.82 N between position 3 and position 4 for force. For the RPM2 the greatest difference in strain measurements was 1.25 με between position 1 and position 3, and 8.75 N between position 1 and position 3 for force. For the LPM3 the greatest difference in strain measurements was 1.24 με between position 2 and position 4, and 18.37 N between position 2 and position 3 for force. Finally, for the RPM3 the greatest difference in strain measurements was 1.15 με between position 1 and position 4 and 30.06 N between position 2 and position 4 for force.

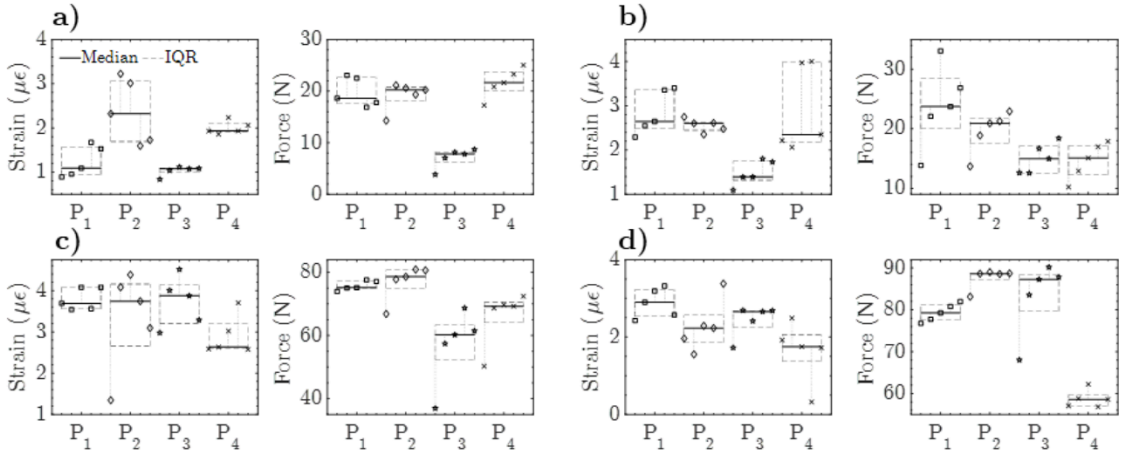

Figure 17 Experimental reproducibility peak measurements with respective median, 25th, and 75th percentile (IQR) for the a) LPM2, b) RPM2, c) LPM3, d) RPM3. Position one to four indicated on the x-axis by P_1 to P_4, respectively

Table 11 Experimental reproducibility multiple pairwise output for peak strain and peak force measurements including corrected p-values and standardized difference in medians (SDM)

Tooth	Position 1	Position 2	Strain		Force	
			p-value	SDM	p-value	SDM
Left 2	P1	P2	0.400	2.88	1.000[b]	1.61
	P1	P3	1.000[b]	0.08	0.042[a]	10.82
	P1	P4	0.450	4.51	1.000[b]	3.00
	P2	P3	0.084	3.84	0.400	12.42
	P2	P4	1.000[b]	1.13	1.000[b]	1.39
	P3	P4	0.098	10.19	0.049[a]	13.82
Right 2	P1	P2	1.000[b]	0.17	1.000[b]	2.81
	P1	P3	0.042[a]	4.23	0.021	8.75
	P1	P4	1.000[b]	0.53	0.006[a]	8.64
	P2	P3	0.098	7.70	0.774	5.94
	P2	P4	1.000[b]	0.30	0.400	5.83
	P3	P4	0.216	2.02	1.000[b]	0.11
Left 3	P1	P2	-	-	1.000[b]	3.46
	P1	P3	-	-	0.049[a]	14.91
	P1	P4	-	-	1.000[b]	5.88
	P2	P3	-	-	0.006[a]	18.37
	P2	P4	-	-	0.216	9.34
	P3	P4	-	-	1.000[b]	9.04
Right 3	P1	P2	-	-	0.400	9.37
	P1	P3	-	-	1.000[b]	8.02
	P1	P4	-	-	1.000[b]	20.69
	P2	P3	-	-	1.000[b]	1.35
	P2	P4	-	-	0.006[a]	30.06
	P3	P4	-	-	0.098	28.71

[a] indicates statistical significance, [b] corrected p-value rounded down to upper limit

4 Discussion

The data presented are intended to define the repeatability, reproducibility and sensitivity of the proposed experimental method and determine the importance of experimental variables to aid in outlining a more robust and comparable standard testing method for PDL mechanics

research. While many studies in the literature study PDL mechanics using intact TPBCs, a rigorous evaluation of how controlled experimental variables can affect measurements is lacking.

4.1 Experimental Repeatability

4.1.1 Preconditioning

It is understood that a parallel fibre tissue has a degree of plasticity, and preconditioning should be used to achieve a repeatable or stationary phase prior to testing [102]. The method for determining when the PDL is preconditioned is not well defined and, in most cases, is vague. Using data clustering to group the trials into initial and preconditioned states provided a more objective method to determine when the PDL is preconditioned than previously reported. Further, this method considers the uniqueness of each PDL, determining when each PDL is preconditioned individually. The required number of trials ranged from one to five for the dry condition and two to seven for the hydrated condition. Previously, dynamic cyclic tests such as Bergomi *et al.* [104] cited approximately 1000 cycles required for preconditioning of *in vitro* bovine samples; the PDL was considered preconditioned when the variability between the peak compressive and tensile stresses during cyclic loading reached less than 10%. Oskui and Hashemi [46] defined 10 preconditioning cycles for *in vitro* swine PDL samples before the results became repeatable during cyclic experiments. Dorow *et al.* [40] reported up to 16 trials required for preconditioning of *in vitro* swine PDL samples and considered them preconditioned when the hysteresis curve reached a limit. Most *ex vivo* studies such as Papadopoulou *et al.* [72], Knaup *et al.* [76] and Romanyk *et al.*[15] do not reference any preconditioning trials. In this study, the average peak force between the initial and preconditioned state clusters had a percent difference of 13% for dry and 36% for hydrated conditions, indicating the necessity for preconditioning trials when using an intact TPBC.

The hydrated condition only showed a chronological divide in data clustering for three of the eight TPBCs tested, and the TPBCs where no chronological divide was found had larger force ARMS values than the other hydrated TPBCs. This suggests that reaching a stationary phase in the hydrated environment may not always be possible, arguably due to the fluid being replaced in the PDL. When the TPBC is in a dry state, it is expected that the fluid in the PDL will be pushed out of the space, and the stationary phase mechanical response of the PDL will be a dry

response. Conversely, when the TPBC is hydrated, it is expected that some of the fluid in the PDL space is replenished after each trial, and therefore, less plasticity is expected across all trials. Two of four and one of four TPBCs demonstrated preconditioning patterns when the TPBC was unloaded for two and five minutes between trials, respectively. It could be argued that there is less fluid movement into the PDL during the two-minute wait time to replenish what was expelled, and therefore, more plasticity is evident. Based on the results, preconditioning was shown to be a controlled variable that should be considered prior to beginning an experimental study and not left to arbitrary or anecdotal decisions. The mechanical response of the PDL will vary between different loading regimes and environments, and the number of preconditioning trials will likely not be transferable. However, the method for determining when the PDL is at a stationary phase should be objective and more thoroughly defined. Indeed, the difference between dry and hydrated samples here points to how differences in the experimental protocol may impact the need for preconditioning.

4.1.2 Intra-TPBC Repeatability

Intra-TPBC analysis indicated time series repeatability based on the calculated ARMS values and repeatability in peak output measurements based on the median, 25^{th} and 75^{th} percentiles for both force and strain. The strain and force time series data demonstrated a detectable loading, hold, and offloading pattern that was expected with the displacement-controlled experimental protocol. In general, the ARMS values from both strain and force measurements are greater for hydrated cases than dry conditions; this could be attributed to the PDL not reaching a stationary preconditioned state.

The intra-TPBC repeatability from the previous work using an FBG sensing method within the PDL reported average coefficient of variation (CV) values for the strain time series between 20% and 1000%. The CV value is calculated by dividing the standard deviation by the mean value. It can be argued that the time series CV value was amplified by the small mean strain magnitudes during the early stages of loading and late stages of unloading (i.e., the denominator approaches zero). To avoid such amplification, the minimum CV value was also reported for each TPBC and ranged from 4% to 45% [15]. The peak strain measurement reported

for a similar displacement rate and displacement was 4.770 ± 2.237 με, which is within the range of peak strain measurements reported in this study for the dry condition (1.71 με to 6.64 με).

4.1.3 Inter-TPBC Repeatability

Inter-TPBC analysis did not indicate repeatable peak strain or force measurements between the left and right side PMs. With a similar experimental procedure, Romanyk *et al.* [15] reported statistically significant differences in three of the six right and left side TPBC comparisons and suggested that sensor placement was a likely cause of the differences. In this work, considerable efforts were made to control the experimental setup between trials, including the alignment angle of the TPBC and the location of the sensor. Inter-TPBC geometry differences and high sensitivity to experimental inputs arguably make sensor placement and TPBC alignment too difficult to control between TPBCs without more sophisticated imaging techniques. The magnitude of peak output measures within each TPBC should be considered independently, and, likely, comparisons between the left and right sides of the mandible for the same tooth may not be possible.

4.1.4 Long-term Repeatability

Long-term repeatability analysis demonstrated similar repeatability to the inter-TPBC repeatability, based on comparable calculated ARMS values for both strain and force. Data clustering methods indicated preconditioning trials for all four TPBCs, ranging from two to four trials. As the number of preconditioning trials is comparable to those found with TPBCs tested with only 15 trials, it can be suggested that the data clustering method is not dependent on the number of trials. Two of the four TPBCs did not indicate a clear second chronological divide indicating a change in the PDL mechanical output. Two TPBCs demonstrated a divide at 22 and 23 trials. The peak measurements plotted by trial indicate stable measurements for all but one case where the peak measurements appear to increase with trial number (Figure 13). There were no notable jumps or changes observed in the trends seen for each TPBC. The peak measurements' stability can hold up to 30 trials. However, care must be taken if an increasing peak measurement trend is seen. This result demonstrates the possibility of collecting two complete data sets from a single TPBC for future studies; this is significant as it was concluded above that left and right side TPBC magnitudes cannot be confidently compared.

4.2 Experimental Sensitivity

4.2.1 Preloading Sensitivity

Due to the non-linear properties of the PDL, it is essential that the TPBC is tested with a consistent initial condition. In this study, the initial condition was controlled with a preload. A change in preload led to a statistically significant difference in the peak force measurements that demonstrated a general increase with preload. The preload does not appear to affect the repeatability of the system. It can be noted there was a smaller difference in peak force measurements between a 0.5 N and a 1.0 N preload than a 3.0 N preload. It was concluded that the preload should be controlled within at least 0.5 N between trials.

4.2.2 Alignment Sensitivity

In the present study, strain and force output measures were sensitive to the TPBC alignment conveying the importance of controlling the input displacement vector between trials. Changing the angular alignment of the TPBC will change the input displacement vector and the angle at which the root moves into the alveolus. As the tooth is displaced axially within the alveolus, the collagen fibres will stretch to accommodate the movement. If the force is not directed along the axis of the root, the tooth may rotate within the alveolus, causing the collagen fibres to both stretch and compress differently along the root. Additionally, as the displacement vector becomes increasingly misaligned, the interaction between the tooth, PDL, and alveolar bone will also change. The axis of rotation of the tooth has been shown to change with a change in force [4]. As the misalignment led to a change in the force magnitudes, the axis of rotation of the tooth between alignments arguably changed and, therefore, the mechanical response of the TPBC. The FBG sensor was kept at the same placement during the different alignments, measuring the strain at a consistent location. The observed changes in the peak strain measurements suggest that different alignments affect how the PDL responds. Specifically, greater misalignments have a greater effect on the PDL's response. It can be concluded that the force and strain output measurements are sensitive to the alignment angle of the TPBC and need to be controlled as precisely as possible, practically within 5°. An alignment angle of 102° ± 5° across multiple PM2 with varying morphology was found. Using this alignment angle across multiple TPBC was deemed acceptable as the standard deviation was 5°.

4.2.3 Sensor Depth Sensitivity

When varying the sensor depth, there were no statistically significant differences observed in the peak force measurements. This is expected as the input displacement vector (i.e., TPBC alignment) was not changed between trials. Statistically significant differences were observed in the peak strain measurements in both TPBCs. The lowest SDM value was 0.63 between an 8 mm and a 4 mm sensor depth in the RPM2; the next lowest value was 6.16 between an 8 mm and a 4 mm sensor depth in the LPM2 (Table 10). The RPM2 peak strain values compared were both negative (i.e. tension strains), likely caused by the sensor moving too far out of the PDL space and measuring within the gingiva due to poor sensor placement or a low alveolar crest. Experimentally, it has been reported that the mechanical properties of the PDL change with depth along the root [37], [112]. Similarly, multiple FE models have demonstrated the varying stress/strain state along the length of the root [61], [66]. It has been suggested this variation is caused by the complex PDL geometry and collagen fibre orientation [61], [112]. It is clear that the FBG sensor is sensitive to the changes in the PDL mechanics along the root and must be controlled to less than 4 mm.

4.3 Experimental Reproducibility

It was shown above that the peak measurements cannot be compared across different TPBCs. However, it was found that with caution, the peak measurements can be reproduced within the same TPBC. Although two of the four TPBCs demonstrated statistically significant differences in peak strain measurements between positions, the absolute differences in magnitude were small and comparable across TPBCs with no obvious discrepancies between positions (Figure 17). All four TPBC had a statistically significant difference in peak force across the positions. For the most part, the SDM values were low (0.11 to 9.37), with the exception of position 3 within the LPM2, position 3 in the LPM3, and position 4 in the RPM3, where noticeable jumps occurred and the SDM values ranged from 9.04 to 30.06. Although general reproducibility is shown, the TPBC alignment angle, sensor location, sensor depth, and sensor angle must be rigorously controlled between positions.

4.4 Limitations and Future Works

Caution must be taken when considering the results presented as this preliminary study has a small sample size. A sample size of n=10 was chosen for the repeatability analysis based on previously reported work [15], a sample size of n=5 trials per variation was selected for the sensitivity analysis to limit the effect of potential fatigue of the ligament driving the changes between each variation. The experimental procedure proposed has potential future applications with *ex vivo* and *in vivo* studies due to the non-destructive nature of the sensing technique. Future work should focus on identifying the location of the FBG within the PDL using µCT imaging techniques and investigation into the accuracy of the strain measurements. Although results are repeatable and comparable to previously reported values with a similar sensing mechanism [15], measurements are much smaller than those reported in the literature. Using a similar tooth, displacement direction, final displacement, and measuring a peak force of approximately 15 N, Qian *et al.* [66] reported maximum principal strains on the order of 100,000 µε, suggesting the FBG is not measuring actual PDL strains. Likely, as the FBG is not intimately adhered to the PDL, strain measurements presented are a proxy measure for the strain field within the PDL, and only a subset of strains are detected at the specific location. More work must be done to identify how the strains measured from the FBG compare to the physical PDL strain and how the strain measurements are affected by the presence of physical aspects, such as collagen fibres, to define what the FBG is truly measuring.

5 Conclusion

It has been suggested that a significant factor leading to the variation ranging six orders of magnitude in reported PDL Young's Modulus is the inconsistencies in experimental protocols [13]. Therefore, this work aimed to define the influence of various parameters on the output and repeatability of the strain and force measurements with a consistent displacement regime. It was concluded that:

1) Outlining and controlling the preload, alignment, sensor depth, and objectively defining the number of preconditioning trials for each TPBC allowed for repeatable intra-TPBC peak and time series output measures. However, inter-TPBC repeatability was not

possible. Stability in the peak measurements over 30 trials indicated long-term repeatability with no obvious damage to the PDL.

2) The peak strain and force measurements are extremely sensitive to confounding variables, specifically preload, alignment, and sensor depth.
3) As inter-TPBC repeatability was not achieved in this study, it is important to be able to achieve similar measurements from within a single TPBC. In general, peak strain and force measurements were reproducible within a single TPBC when input parameters were thoroughly controlled.

Rigorous control of the starting conditions, alignment, and sensor depth both between and within studies may help to decrease the variability in reported mechanical properties in future *ex vivo* studies. Although there are limitations to the use of FBG sensors, this remains a promising method to obtain proxy measures of strains within an intact TPBC, which was previously not possible due to the small size and complex geometry of the PDL.

Chapter 4: Using an In-Fiber Bragg Grating Sensor to Measure strain within the Periodontal Ligament Space in an Intact Swine Premolar

The following manuscript is under preparation for submission to a peer-reviewed forum at a later date upon publication of the manuscript presented in Chapter 3. The first author of this manuscript is also the author of this thesis.

1 Introduction

The Periodontal Ligament (PDL) is a connective tissue that occupies the narrow space between the tooth and surrounding alveolar bone. In healthy humans, the width ranges from 0.15 mm to 0.35 mm along the root [26], [113]. It provides support, proprioception, nutrition, and protection within the Tooth-PDL-Bone complex (TPBC) [3], [4], [113]. Fluid systems within the PDL, including vascular and extracellular fluids, will resist rapid high magnitude loads due to the fluid's incompressibility, acting as a shock absorber to loads such as mastication and bruxism [4], [12], [113], [114]. Collagen fibres makeup 53% to 74% of the PDL's volume [27], [28] and form a hammock-like support structure around the tooth [4]. The fibres, resting in a crimped state, will begin to stretch to resist forces as the extracellular fluid seeps out of the PDL when a load is held [4], [114]. The PDL can trigger a cellular biological response leading to permanent tooth movement when a low magnitude load is held, as seen in orthodontics [3], [4], [113]. The mechanical properties of the PDL can be affected by various factors such as external loading [3], disease (periodontitis) [4], and injury [7]. As such, the PDL's mechanical properties are essential in characterizing the response of the TPBC to mechanical forces [3], [4], [7], [8], [30].

Due to the small and variable geometry, direct mechanical measurements of an intact TPBC are challenging. In general, the mechanical properties of the PDL are estimated through uniaxial testing of isolated PDL sections [36], [43], [103], through Finite Element (FE) Analysis [13], [61],

[115], or through a combination of experimental and numerical techniques [13], [52], [66], [67], [69], [71], [75]. Isolating the PDL allows for a direct isolated material measurement, but disrupts the PDL's three-dimensional collagen fibre support [13], [40]. An FE model can be useful in simulating the PDL's response within an intact TPBC. However, the accuracy is heavily reliant on user-defined geometry, material properties, and assumptions [14], [75]. Various PDL numerical models with ranging complexity have been implemented [61], [66], [67], [69], [75]. However, as there are no direct mechanical measurements from an intact TPBC, these models cannot be directly validated and are instead implicitly validated based on the structural response (i.e., force/displacement outputs).

A fibre optic sensing method, specifically an in-Fibre Bragg grating (FBG) sensor, has previously been used to obtain strain measurements from within the PDL space of an intact swine premolar [15], [20]. An FBG is small and flexible, which allows for insertion into an intact PDL space. Briefly, an FBG consists of periodic changes of the refractive index within the core of a silica fibre. A broad spectrum of light is passed through the fibre core, and the FBG reflects a narrow wavelength. The shift in the reflected wavelength can then be related to the axial mechanical strain on the sensor[87]. Peak FBG strain measurements from within the PDL space have previously been reported on the order of microstrain (με) [15]. Conversely, PDL strain predictions from previously reported FE models were on the order of magnitude of 10,000 με [61], [66], [72], [75], [76]. As there is an apparent discrepancy of at least four orders of magnitude between FBG strain and reported FE model estimates of physical strain, it was argued that, as the FBG is not adhered to the PDL, the output strain measure is only a proxy of the PDL's physical strain.

A rigorous investigation into the repeatability and sensitivity of the FBG output strain measurements was completed in Chapter 3 [15]. However, it lacked investigation into the FBG location, as well as predictability and accuracy of the strain measures. For a measurement technique to be useful, it should be repeatable, have predictable outcomes compared to other approaches, and be accurate. This study focused on the predictability of the FBG strain measurements through a cross-verification method to determine if (1) FBG strain magnitudes were relatable to FE strains, and (2) if a change in FBG strain could be related to a change in

FE strain when altering tooth displacement applied to an intact swine TPBC. Direct FBG strain measurements from an intact TPBC, if predictive of the physical PDL strain, would allow for stronger verification of FE models which, for example, could improve the functionality as a tool to optimize orthodontic treatments. Additionally, FBGs could be used to monitor the PDL's mechanical properties over time without having to sacrifice the specimen for *ex vivo* mechanical tests, improving research regarding characterization and treatments in applications such as the progression of periodontitis [4], [8], [9], repair and regeneration of an injured PDL [7], [116], or age [51].

2 Materials and Methods

2.1 Experimental Procedure

Swine mandibles (n=14) were retrieved from 12-14 week Duroc X (Large White X Landrace) from the Surgical Medical Research Institute at the University of Alberta. Prior to euthanization, the animals were used for purposes outside of this study. Ethical approval for this study was granted by exemption from the University of Alberta Animal Care and Use Committee. Each mandible was stored at -24°C immediately after euthanization and was thawed at 0°C over 24 hours prior to testing. The distal (posterior) portion of the mandible was sectioned into left and right segments to include the second premolars. The base of each segment was cast in dental stone and secured onto a custom-designed testing stage that interfaced with a universal testing machine (Instron Electroplus E3000, Instron, Norwood, MA), as seen in Chapter 3. The testing stage was designed to allow for the angular alignment of the TPBC relative to the probe and free translation in the buccal (cheek)/lingual (tongue) and distal/mesial (anterior) directions to ensure a purely compressive load was applied to the TPBC. The second premolars were aligned with approximately 102° between the distal edge of the tooth and probe as defined in Chapter 3. Alignment at this angle was in an attempt to displace the mesial (anterior) root intrusively (i.e., towards the apex of the root) (Figure 18a). Each TPBC was submerged in 0.9% NaCl during testing. The gingiva around the tooth crown was removed to the level of the alveolar bone, and the TPBC was completely unloaded for approximately five minutes between each trial to allow for fluid recovery. Each TPBC was preloaded to 0.5 N and then subjected to a displacement-controlled test with a loading and unloading rate of 0.05 mm/s. Specified displacements were held

for 10 seconds prior to unloading and ranged from 0.08 mm to 0.30 mm (Table 12). Each TPBC was subjected to two different displacements, and a total of 15 trials were completed for each displacement.

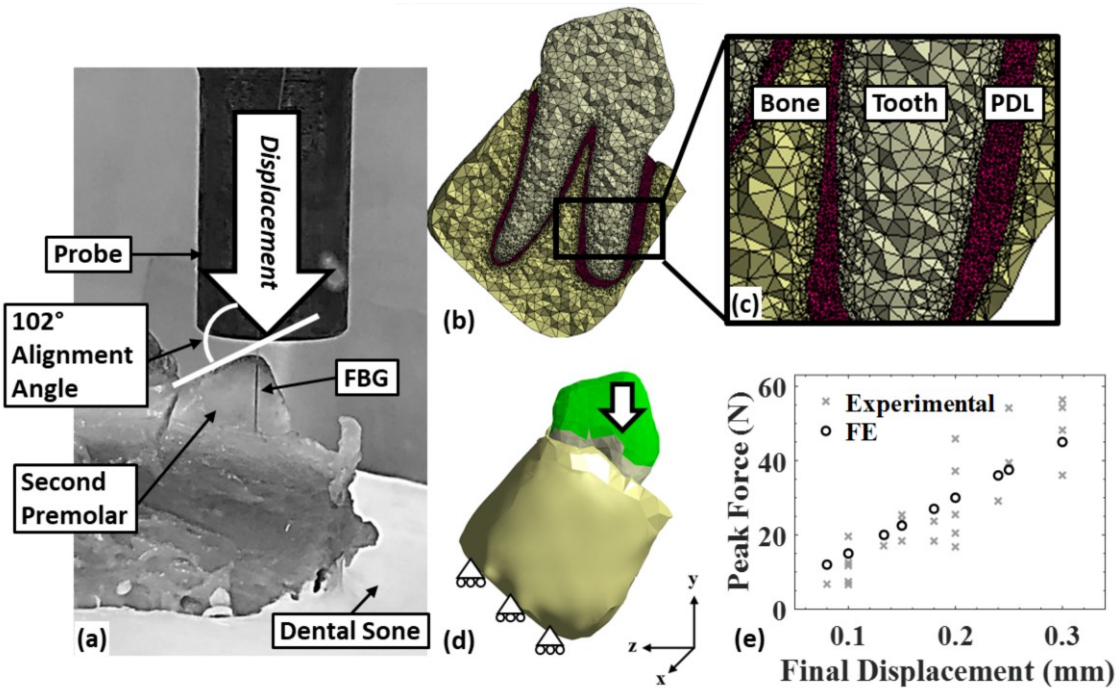

Figure 18 (a) Experimental set up for a right second premolar TPBC, indicating the direction of displacement of the tooth crown. (b) Cross-section of the mesh used for FE analysis of a representative TPBC and (c) a close up of the mesh in the bone, tooth and PDL to demonstrate the element size. (d) Illustration of the boundary conditions applied to the FE analysis, including the compressive displacement of the crown and the constraint of the bone in the y-axis. (e) Experimental and FE peak force for each displacement to confirm the FE model output is comparable to experimental data.

The number of preconditioning trials for each displacement within a TPBC was determined by exploratory hierarchical data clustering using Ward's Method on MATLAB (MathWorks, Natick, MA) as described in Chapter 3. Briefly, the force time-series data from each displacement were split into two clusters based on similarity. When a chronological divide was determined between the two clusters, the trials within the first cluster were considered preconditioning trials and the ten subsequent trials were used for analysis. However, if more than five preconditioning trials were identified, all subsequent trials were used. When no chronological divide was

determined, three preconditioning trials were used; representing the average number of preconditioning trials found in Chapter 3 (Table 12). A preconditioned state is only valid for the loading regime used for preconditioning and should be reconsidered when the loading regime is changed [102]. Therefore, a preconditioning analysis was completed for both displacements.

An FBG (0.125 mm major diameter, Technica SA, Beijing CN) with a 1 mm gauge length at the tip was inserted using a 27 1 ¼ gauge needle into the PDL space on the buccal side of the mesial root. The FBG was inserted to approximately align with the mesial root's long axis to an approximate depth of 14 mm below the tooth cusp, controlled by markings on the FBG. A MicronOptics Interrogator (SM130 Optical Sensing Interrogator, Micron Optics, Atlanta, USA) was used as a light source and collected the peak reflected wavelength at 200 Hz. The shift in wavelength was converted to strain using a gauge factor of -1.21 pm/με [15]. A negative gauge factor converted compressive strains to a positive value for ease of interpretation. The strain data were filtered using a 4^{th} order Butterworth filter with a cutoff frequency of 100 Hz and 1000 averages in MATLAB. The maximum magnitude of strain and force measurements prior to unloading were found for each trial, and the average and standard deviation were calculated for each displacement.

2.2 Finite Element Analysis

A representative second premolar geometry was created from microcomputed tomography (μCT) scans (SkyScan 1076; Bruker-MicroCT, Kontich, Belgium, current 110 μA, voltage 100 kV, voxel size of 17.2 micron) (Figure 18b-d). The bone and tooth geometries were created using imaging software (Mimics 22.0.0.524, Materialise, Leuven, Belgium). The PDL was created in the space between the bone and tooth using additional imaging software (3-matic, Materialise, Leuven, Belgium; ANSYS Discovery SpaceClaim 2020 R1) and had a variable thickness between 0.04 mm and 1.05 mm, with an average thickness of 0.36 mm. The mesh and FE analysis were completed using ANSYS Workbench (ANSYS Academic Research Mechanical, Release 2020 R1, Canonsburg, PA, USA). The tooth, PDL, and bone were assumed to be homogeneous, linear elastic, isotropic materials. A mesh density analysis was completed to ensure the reaction force was independent of the mesh density, the reaction force converged within 0.34% over seven mesh iterations (Appendix B). A sensitivity analysis was completed to ensure the reaction force was not greatly affected by

the tooth and bone's material properties. The reaction force varied by 1.8% when the tooth's Young's Modulus was adjusted between 10,000 MPa and 25,000 MPa, and 2.4% when the bone's Young's Modulus was adjusted between 2,000 MPa and 20,000 MPa (Appendix B). The PDL's Young's Modulus was varied between 0.10 MPa and 0.80 MPa, which were expected Young's Moduli values from a comparable study [66]. To find the best fit with the experimental force/displacement data, the force/displacement data from the FE model was calculated at each Young's Modulus. A root mean square between the experimental and numerical results was calculated for each iteration to find the best fit between experimental and numerical results (Figure 18e) (Appendix B). The tooth had a Young's Modulus of 20,000 MPa, Poisson's ratio of 0.30 [66], [75], an element edge length of 1 mm, and 155,883 elements. The bone had a Young's Modulus of 13,000 MPa, Poisson's ratio of 0.30 [75], [117], an element edge length of 1 mm, and 241,853 elements. The PDL had a Young's Modulus of 0.46 MPa, Poisson's ratio of 0.30, an element edge length of 0.12 mm, and 430,924 elements. The contact between the PDL and bone, and PDL and tooth, were modelled as a perfectly bonded contact with an element edge length of 0.12 mm. Ten-node tetrahedral elements (SOLID187) and eight-node contact elements (CONTA174) were used.

To reproduce the experimental setup, the TPBC was aligned so the y-axis ran through the long axis of the mesial root, and the base of the alveolar bone was constrained to prevent displacement in the y-axis. A compressive displacement of 0.30 mm was applied to the tooth crown (Figure 18d).

2.2.1 Sensor Location

To determine the location of the FBG within the PDL space, the FBG was left in place for three of the final four tested TPBCs that were then scanned using µCT (SkyScan 1076; Bruker-MicroCT, Kontich, Belgium, current 278 µA, voltage 90 kV, voxel size of 8.9 micron). The tooth crowns were partially removed by cutting excess crown along the approximate transverse plane prior to imaging due to size constraints within the µCT scanner. The tooth and FBG geometries were reconstructed (Mimics 22.0.0.524, Materialise, Leuven, Belgium). Each tooth was manually aligned so that the y-axis was along the mesial root and the origin was at the root's approximate apex. The FBG tip location relative to the origin was recorded (ANSYS Discovery SpaceClaim

2020 R1)(Figure 19a). This process was completed three times, and the coordinates were averaged. Three regions of interest were defined from the average FBG tip location using approximate dimensions of the FBG (0.125 mm x 1 mm x 0.125 mm). The average strain in the y-axis, representing the axial strain recorded by the FBG, for each region of interest was recorded from the FE model at the appropriate tooth displacements. As there were variations in size and shape between the TPBCs used to determine the FBG region of interest and the representative FE model, the three regions of interest were translated within the representative geometry to ensure the entire volume of the FBG was included. Specifically, the first region of interest was translated -0.906 mm along the z-axis, the second region of interest was translated 0.614 mm along the y-axis, and the third region of interest was translated 1.329 mm along the y-axis.

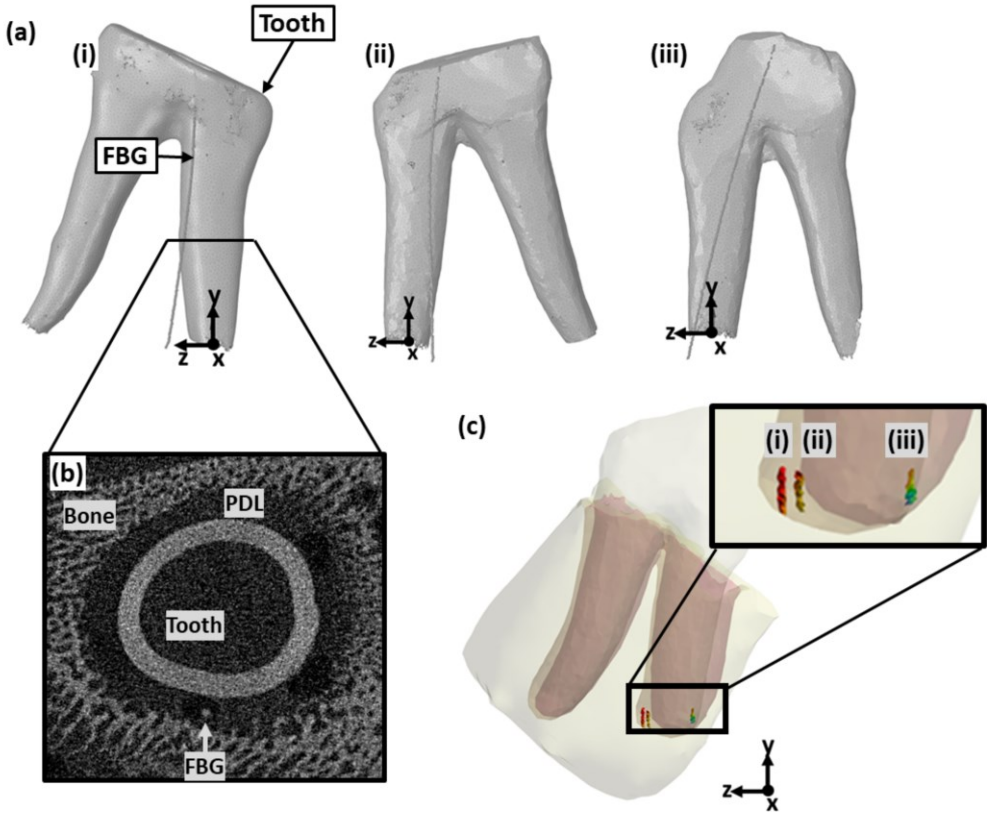

Figure 19 (a) Three-dimensional model of the tooth and FBG for three representative TPBCs from (i) the left side of the sixth mandible, (ii) the right side of the sixth mandible, and (iii) the right side of the seventh mandible. (b) A μCT slice showing the alveolar bone, mesial root and FBG fiber, note the contrast of this image has been altered for ease of interpretation. (c) Region of interest from three FBG sensors within the representative FE model.

2.3 Linear Regression

An experimental ratio was calculated for each TPBC to quantify the change in output strain and force measurements. The experimental ratio is the average peak measurements from the first displacement divided by the average peak measurements from the second displacement. A corresponding FE ratio was calculated to quantify the expected change in FE strain and force outputs. From the FE model, the reaction force at the base of the TPBC for each displacement was recorded. Using the third sensor's region of interest as a representative sensor location (Figure 19a), the average y-axis strain was recorded for each tooth displacement. The FE ratio, for both force and strain, was found by dividing the FE output from each first displacement by the second. A simple linear regression between the experimental and FE ratio was completed for both strain and force outputs. The R^2, F-Statistic, and p-value for each regression were calculated using MATLAB. A sample size power calculation was not possible due to the lack of related historical data. Instead, a minimum sample size of 10 for simple linear regression was fulfilled [118].

3 Results

3.1 Force and Strain Output Measures

Average peak experimental strain and force measurements are summarized in Table 12. Of the 14 second premolars tested, two were not suitable for analysis, and therefore, not included. The first was not properly cast in dental stone, and the second had an oscillating sensor output indicating the sensor was not placed within the PDL. Exemplar strain and force outputs are shown in Figure 20. The peak strain and force measurements at similar displacements vary. For example, five TPBCs were subjected to a displacement of 0.10 mm, peak strain measures ranged from -2.71 με to 7.55 με, and peak force measures ranged from 6.64 N to 19.60 N. Overall, there was a general increase in peak measurements with an increase in displacement. Peak strain values ranged from -5.00 με to 13.59 με at 0.20 mm and 0.30 mm, respectively. Peak force values ranged from 6.64 N to 56.35 N at 0.10 mm and 0.30 mm, respectively.

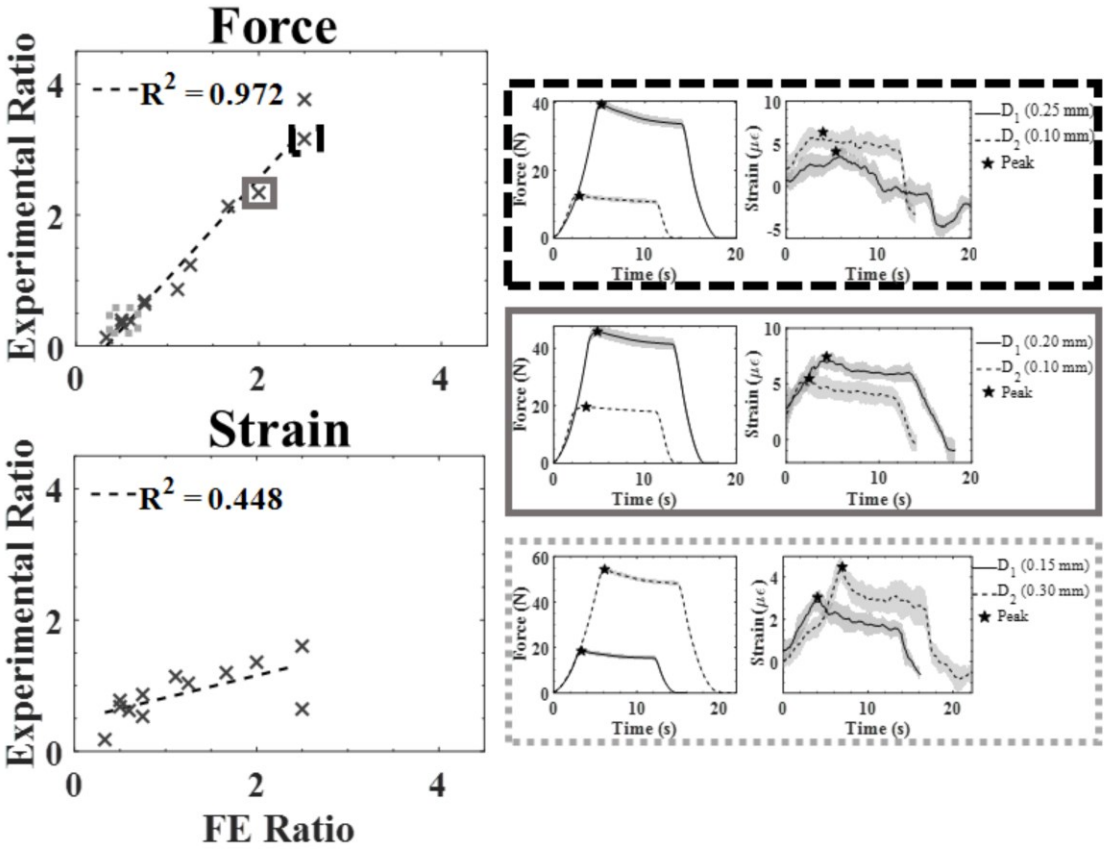

Figure 20 Left side, linear regression for the force and strain experimental to FE ratios. Right side, three representative time series data for force and strain at the first and second tooth displacements (D_1 and D_2, respectively)

Table 12 Summary of the experimental protocol including the number of preconditioning trials (PC) and the displacements for each TPBC. The average and standard deviation (SD) of the peak output measures from the experimental and the FE model are summarized. Each mandible section is indicated by a number (M#) and an indication of the left (L2) or the right side (R2).

	PC Trials	Displacement (mm)	Mean Strain (SD) (με)	Mean Force (SD) (N)	FE Strain (με)	FE Force (N)
M2_L2	1	0.10	2.13 (0.64)	7.41 (0.73)	138,010	15.00
	7	0.30	11.98 (2.41)	56.35 (1.32)	414,020	45.01
M1_L2	3[a]	0.15	3.04 (0.50)	18.39 (1.02)	207,010	22.51
	3[a]	0.30	4.47 (0.53)	54.31 (1.27)	414,020	45.01
M1_R2	7	0.10	7.55 (2.85)	6.64 (0.28)	138,010	15.00
	3[a]	0.20	9.73 (2.06)	16.79 (1.09)	276,010	30.01
M3_R2	3[a]	0.18	8.45 (2.95)	18.35 (2.20)	248,410	27.01
	8	0.30	13.59 (2.08)	48.21 (1.69)	414,020	45.01
M2_R2	3	0.15	-2.66 (4.12)	23.86 (1.15)	207,010	22.51
	3[a]	0.20	-5.00 (1.50)	37.19 (1.53)	276,010	30.01
M7_R2	1	0.10	-2.71 (0.58)	11.76 (1.06)	138,010	15.00
	3[a]	0.13	-3.13 (0.45)	17.10 (0.63)	183,960	20.00
M5_R2	6	0.20	9.75 (2.15)	20.49 (1.17)	276,010	30.01
	1	0.18	8.56 (2.90)	23.69 (4.48)	248,410	27.01
M6_R2	7	0.30	4.48 (0.55)	36.07 (1.65)	414,020	45.01
	3[a]	0.24	4.33 (0.22)	29.12 (3.35)	331,220	36.01
M6_L2	3[a]	0.25	4.16 (1.13)	54.16 (1.21)	345,020	37.51
	3	0.15	3.47 (2.34)	25.39 (1.38)	207,010	22.51
M4_R2	2	0.20	7.44 (0.86)	45.87 (1.96)	276,010	30.01
	8	0.10	5.48 (0.87)	19.60 (0.10)	138,010	15.00
M5_L2	3	0.25	4.09 (1.05)	39.42 (1.10)	345,020	37.51
	6	0.10	6.36 (1.14)	12.47 (0.73)	138,010	15.00
M7_L2	2	0.20	8.88 (1.55)	25.48 (1.83)	276,010	30.01
	3[a]	0.08	5.54 (0.48)	6.77 (0.77)	110,410	12.00

[a] *indictes trials where a preconditioned state was not identified through data clustering*

Table 13 summarizes the three regions of interest representing FBG locations within the FE model, respective peak experimental force and strain output measures, and corresponding strain and force outputs from the FE model. Corresponding FBG and FE strain magnitudes

differed on average by 200%, suggesting a one-to-one comparison between experimental and numerical models is not advisable.

Table 13 Summary of the peak strain and force outputs from the experimental results and FE model for three representative TPBCs. The translated region of interest for the approximate location of the FBG sensor relative to the apex of the mesial root from the scanned TPBC to ensure the volume of the FBG would be within the FE PDL geometry are defined. A similar coordinate system was used for all regions of interest, the positive x-axis was towards the buccal direction, the positive y-axis was towards the occlusal plane, and the positive z-axis was towards the distal direction. Each mandible section is indicated by a number (M#) and an indication of the left (L2) or the right side (R2).

		Experimental		FE Analysis		
	Displacement (mm)	Strain (SD) (με)	Force (SD) (N)	Strain (με)	Force (N)	Region of Interest [x,y,z] - [x,y,z]
M6_L2	0.25	4.16 (1.13)	54.16 (1.21)	34,419	37.51	[-0.895, -0.268, 1.250] – [-0.770, 0.732, 1.375]
	0.15	3.47 (2.34)	25.39 (1.38)	20,651	22.51	
M6_R2	0.30	4.48 (0.55)	36.07 (1.65)	155,300	45.01	[0.158, -0.200, 1.095] – [0.283, 0.800, 1.220]
	0.24	4.33 (0.22)	29.12 (3.35)	124,240	36.01	
M7_R2	0.10	-2.71 (0.58)	11.76 (1.06)	138,010	15.00	[0.962, 0.100, -1.198] – [1.087, 1.100, -1.073]
	0.13	-3.13 (0.45)	17.10 (0.63)	183,960	20.00	

3.2 Linear regression

A statistically significant linear relationship between the experimental and FE strain ratio can explain 44.8% of the variation in the experimental strain ratio ($F(1,10)=8.12$, $p=0.017$, $R^2=0.448$) (Figure 20). The strain experimental ratio was 0.477 when the FE ratio was 0.00 and increased by 0.339 for every unit increase of the FE ratio. Similarly, a statistically significant linear relationship between the experimental and FE force ratios can explain 97.2% of the variation in experimental force ratio ($F(1,10)=344.97$, $p<0.001$, $R^2=0.972$) (Figure 20). The force experimental ratio was -0.504 when the FE ratio was 0.00 and increased by 1.530 for every unit increase of the FE ratio.

4 Discussion

The aim of this work was to provide preliminary data to determine if FBG strain measures were related to expected PDL strain values determine through FE strain outputs. It was shown that the FBG and FE strain magnitudes do not match. However, a statistically significant linear relationship between the FE and experimental ratio suggests that the FBG is capable of predicting the change in strain calculated in the FE model due to a change in tooth displacement.

The experimental output strain measures varied between TPBCs, ranging from -5.00 to 13.59 με with tooth displacements ranging from 0.08 mm to 0.30 mm. It was suggested in Chapter 3 that the difference in peak measurements between TPBCs may be partially attributed to sensor placement [15]. The location of the FBG sensor was identified on μCT scans from three TPBCs. From the limited sample size, it was observed that the location of the terminal end of the FBG was not consistent (Figure 19a). Although the general insertion location and angle appear to be relatable, the further down the root, the more a deviation in fibre location is evident. It is speculated that this was due to the narrow and variable geometry of the PDL space. Arguably, during insertion, the needle, and therefore the FBG, will be partially guided by the unique shape of the PDL space. This could partially explain why it was found in Chapter 3 that the FBG is able to measure similar peak strains when replaced within the same TPBC, but not between them. Although the depth, angle, and location of insertion can be controlled, ultimately, using the current insertion method, the location of the FBG tip cannot be controlled between TPBCs.

The FE output force/displacement values lay within the bounds of the experimental force/displacement outputs, providing confidence that the model is adequate for comparison to the experimental data (Figure 18e). An apparent discrepancy was observed between the peak experimental and the respective FE strain measurements. Experimental strains ranged from -3.13 με to 4.48 με, and FE strains ranged from 20,651 με to 183,960 με. In Chapter 3, the reported experimental FBG strain measures, with a similar experimental setup, were comparable to the experimental peak values found in this work, ranging from -5.77 με to 11.68 με with a tooth displacement of 0.20 mm. Comparing exact strain magnitudes between different FE models is not practical, as a wide range of material properties for the PDL have been reported, and the properties

are dependent on species, age, location along the root, displacement rate, and environment [13]. However, multiple FE studies using a swine model have reported strains with a similar order of magnitude as that of the FE strain output of this study (i.e., 10,000 με) [61], [66], [69], [75]. Due to the apparent discrepancy, it is argued that the FBG strain magnitudes do not represent the magnitudes of physical strains in PDL material; this is likely attributed to the FBG not being adhered to the PDL. It can be argued that the complex interaction between the sensor and the PDL is likely a function of factors such as friction, the interaction between the bone/tooth/FBG, and fluid movement.

It can be speculated from the ability of the FBG to predict a change in FE strain, that the FBG strain measures can be used to monitor a change in physical strain over time within the PDL, which has potential applications in *in vivo* studies. For example, inflammation within the PDL from periodontitis can lead to degradation of collagen fibers and detachment from the cementum, affecting the PDL's mechanical properties [4], [9]. Injury to the PDL, such as luxations and avulsions, will alter the mechanical properties of the PDL as collagen fibres are severed [7], [116]. A potential method to track the progression of periodontitis or repair and regeneration from injury within the PDL is to monitor PDL material properties [7], [9], [116]. FBG strain measurements from an intact *in vivo* TPBC would allow for temporal monitoring of the material properties without having to sacrifice the animals for *ex vivo* testing. Similarly, strain measurements from an intact TPBC could lead to better validation of PDL FE models. Advancement of PDL FE models could be used for optimization and predictive purposes within orthodontics as FE models consider the complex TPBC geometry and can be adjusted to incorporate anatomical and physiological variation between patients [11].

It should be noted that the presented FE model was validated using force/displacement data (Figure 18e). Although frequently used to validate PDL FE models [66], [72], [76], this level of validation is not as strong as if strain measurements from within the PDL were available. This work is limited by the linear elastic model assumed for the PDL. Implementing an FE model with hyperelastic or viscoelastic material properties could improve the linear relationship between the experimental and FE ratio, as the FE ratios calculated would better approximate the complex response of the PDL to mechanical loads. Although the PDL is known to be a nonlinear,

viscoelastic, anisotropic, heterogeneous material, linear elastic models are frequently implemented and have been reported to approximate the PDL's stress/strain state under appropriate loading conditions (i.e., quasi-static loading rates) [14], [61], [119]. In this work, to minimize the viscoelastic effects so the PDL could be approximated as a linear elastic material, a constant and quasi-static displacement rate was used. The strong linear relationship between the FE and experimental force ratios provides confidence the linear elastic assumption was appropriate. The FBG was identified on µCT images (Figure 19b). However, the density of the FBG fibre was similar to the bone. Therefore, limitations arise as the location of the fibre was identified manually as opposed to utilizing thresholding techniques. Future works should focus on more sophisticated methods for distinguishing the bone from the fibre, such as decalcification of the TPBC prior to µCT imaging. This study induced a change in strain within the PDL by way of a change in tooth displacement. To better characterize the relationship between the PDL and FBG output, future works should focus on defining the FBG strain change in relation to different mechanical parameters such as loading direction and loading rate, or material parameters such as altering fluid content and fibre attachment. This is a vital step towards using the FBG to monitor changes in strain *in vivo*, as some parameters may have a greater or lesser effect on the FBG measurement and may bias the output.

Using cross-verification between FBG and FE strain outputs, it was determined that the FBG can predict the change in strain within the FE model. Therefore, it was speculated that the FBG is capable of detecting a change in physical strain within the TPBC. This study provides a first step in characterizing the predictability of the FBG sensor compared to an FE model.

Chapter 5: Conclusion, Limitations, and Future Work

This chapter details the conclusions of this study and the contributions to the literature. The limitations and future works are detailed.

1 Conclusions

The objectives of this thesis were to expand upon previous work presented by Romanyk *et al.* [15] on the use of in-fibre Bragg grating (FBG) sensors within an intact periodontal ligament (PDL) space. A displacement-controlled experimental protocol was designed to obtain force, displacement, and FBG strain measurements from an intact tooth-PDL-bone complex (TPBC). A rigorous investigation demonstrated the repeatability of the output measures, sensitivity of the output measures to experimental input parameters, and reproducibility of the output measures. Using the defined experimental protocol, the relationship between FBG strain measurements and respective finite element (FE) strain outputs was assessed.

A custom-testing stage was introduced for more sophisticated testing of TPBC sections. It was an advancement upon previous works as output force measurements were possible, potential reaction forces from the testing stage were reduced due to the translating base, and more precise control of the TPBC alignment was possible. It was found that output strain and force time series data within a single TPBC were repeatable. However, the peak output measures were not repeatable between the corresponding left and right side TPBCs. A rigorous investigation of the experimental protocol input parameters had a significant effect on the output peak strain and force measurements. Consideration and control of the preload, alignment, and sensor depth are essential for meaningful output measures from an intact TPBC. In addition, a data clustering method was proposed as an objective method for determining a preconditioned state in the PDL. Although the mechanical properties of the PDL are frequently studied, there is a wide range of reported material properties, Young's Moduli ranging from 0.01 MPa to 1750 MPa [13]. It has

been suggested that inconsistencies in testing procedures may attribute to this variation [13]. To the authors knowledge, this study provides novel work in quantifying the effect of various experimental input parameters of strain and force outputs from a TPBC. Therefore, demonstrating the importance of definition and control of experimental protocols including alignment, starting position, and preconditioning *a priori* for more reliable and comparable output measures.

It was determined that when an FBG was replaced within the same TPBC output peak strain and force measures were reproducible. Further, it was shown that a TPBC could be tested repeatedly with no apparent damage or fatigue present in the PDL, suggesting at least 30 trials could be collected from a single TPBC. This was essential for future, practical use of the sensing method for comparison between time points, as it was concluded that the peak measurements were not comparable across TPBCs. To detect a change in strain within the TPBC, each TPBC was subjected to two tooth displacements. Using a cross-verification technique between FBG strains and corresponding FE strains it was concluded that a one-to-one comparison of strain magnitudes is not advisable. However, the FBG sensor was capable of measuring a predictable ratio of change in strain with respect to FE measurements. Therefore, it was speculated that an FBG sensor is capable of measuring a representative change in strain within the PDL space.

It was concluded that the FBG sensor can be replaced within the same TPBC and, with control of the input loading regime, produce reproducible peak measurements at various iterations. Additionally, it was speculated that the FBG is capable of measuring representative changes in strain from within an intact TPBC. This contributes to current literature by defining a new sensing method to detect representative direct strain measurement from within an intact TPBC that can be used within *in vivo* applications for temporal monitoring of the PDL mechanical response. Direct measurement can allow for stronger validation of FE models, which, for example, could be used to optimize orthodontic treatments. FE models can be adapted to mimic the anatomy and physiology of a patient, and once validated, can be used to apply various loading regimes. The FE model could therefore be used as a predictive tool for orthodontic outcomes and to ensure applied forces are high enough to initiate tooth movement while minimizing negative side effects, such as root resorption [3], [11], [12]. Temporal monitoring of the PDL, without having to sacrifice a specimen to isolate the PDL for direct mechanical measurement or histology, would

allow for monitoring the repair and regeneration of a PDL effected by disease or injury. Historically, techniques such as clinical probing, radiographs, and histology were used to determine the extent of regeneration within the PDL, biomechanical function of the PDL was not considered [4], [7]. FBG sensors provide the ability to monitor the mechanical output during regeneration, which could be implemented to improve the characterization of the PDL injury, the healing process, and treatment protocols.

2 Limitations and Future Works

There are various opportunities for this work to be expanded and improved. As with many *ex vivo* studies, the sample size and variability between and within specimens limits the presented results. Inconsistencies in root geometry, crown geometry, and PDL width are believed to have an effect on the input displacement vector acting on the mesial root and the relative position of the FBG. As it was demonstrated that the output peak strain and force measures were sensitive to the alignment of the TPBC, and therefore the input displacement vector, consistent alignment between TPBCs is essential. This study utilized landmarks on the crown to align the TPBC in the mesial/distal directions. However, in the buccal/lingual directions, the TPBC was aligned by eye. Future works should focus on more sophisticated techniques for consistent alignment. It is possible that landmarks on the crown are not sufficient for alignment, and imaging of the root geometry is required to align the TPBCs consistently.

The location of three FBGs was identified, and it was observed that although the angle of insertion close to the crown appears to be consistent between TPBCs, the FBG tip is not in a consistent location at the root apex. It is suggested the root and alveolus geometry and the size and rigidity of the needle used to place the FBG are potentially guiding the needle resulting in the inconsistencies between TPBCs. As the output peak strain measurements were not comparable across TPBCs, it could be postulated that these differences may be attributed to the variation in FBG location. Various FE studies, including the model presented here, have demonstrated the variability in the strain state throughout the PDL [61], [66]. In order to compare the output strain measures between TPBCs, measurements must be from a comparable location within the PDL. Future work could investigate different FBG insertion locations and techniques to guide the FBG

to a consistent point. The FBG was located after experiments using microcomputed tomography (µCT). The presented FBG locations were limited by manual identification within the µCT scan. As the density of the bone and FBG were similar, thresholding techniques could not be used. Advancement in imaging and location of the sensor could provide for more accurate FBG identification within the µCT scan. It is speculated that identifying individual sensor locations and using them to find the corresponding strains from an FE model may allow for comparison of measurement magnitudes between TPBCs as this would take into consideration the variable TPBC geometry and sensor location. This would allow for a true comparison between exact geometries and FBG locations and could be beneficial for the advancement of FBG sensing techniques for use in validation of FE models.

Experimentally, a quasi-static loading rate was implemented so that the PDL could be approximated as a linear elastic material. Within the FE model, the force peak measures were shown to fit within the experimental measures, and a strong linear relationship (R^2=0.972) between the FE and experimental force ratios provided confidence this assumption was appropriate. However, this work did not consider the relaxation behaviour or time dependent response of the PDL, such as loading rate, which are vital to tooth movement [39]. Future works should consider the introduction of time dependent properties within the FE model and assessment of how these properties effect FBG measurements. Similarly, the implementation of hyperelastic material properties may allow for a stronger linear relationship between the FE and experimental ratios as the FE ratio would capture the toe region in the time series.

The simple linear regression presented is limited by the sample size and range of ratio values. In the present study, a change in strain within the PDL was induced by a change in tooth displacement. Although this gives an indication of how the FBG measures change with an altered mechanical loading state, the effect of parameters such as different final loads, loading direction, time dependence, or alteration of the material properties on the FBG output measures is still not known and should be considered in future works.

The presented sensing technique has potential *in vivo* applications. As more work is completed to characterize how the FBG reacts to different mechanical and material changes to

the TPBC, the FBG has the potential to be used to monitor changes within an intact, *in vivo* TPBC. Although the FBG was shown to be sensitive to experimental inputs, and the magnitudes are not comparable across TPBCs, the FBG can be replaced within the same TPBC and measure reproducible outputs. Further, it was shown the FBG is capable of measuring a predictable change in strain. This suggests that an FBG can be placed *in vivo* at various time points, and the change in output magnitudes can be compared to a FE ratio of change. This has potential applications for monitoring how the PDL's mechanical properties progress through regeneration, disease, or age without having to sacrifice specimens at various time points to dissect and mechanically test the PDL.

References

[1] "National Health Expenditure Trends, 1975 to 2019," p. 47.

[2] "Canadian Dental Association." https://www.cda-adc.ca/en/oral_health/specialties/ (accessed Nov. 22, 2020).

[3] W. R. Proffit, H. W. Fields, and D. M. Sarver, *Contemporary orthodontics*, 5th ed. Elsevier, 2013.

[4] M. G. Newman, H. H. Takei, and F. A. Caranza, *Caranza's clinical periodontology*, 9th ed. Saunders, 2002.

[5] P. I. Eke, B. A. Dye, L. Wei, G. O. Thornton-Evans, and R. J. Genco, "Prevalence of periodontitis in adults in the United States: 2009 and 2010," *J. Dent. Res.*, vol. 91, no. 10, pp. 914–920, Oct. 2012, doi: 10.1177/0022034512457373.

[6] M. Nishihira, K. Yamamoto, Y. Sato, H. Ishikawa, and A. Natali, "Mechanics of periodontal ligament," in *Dental Biomechanics*, Taylor & Francis, New York, 2003, pp. 20–34.

[7] U. Mandel and A. Viidik, "Effect of splinting on the mechanical and histological properties of the healing periodontal ligament in the vervet monkey (Cercopithecus aethiops)," *Arch. Oral Biol.*, vol. 34, no. 3, pp. 209–217, Jan. 1989, doi: 10.1016/0003-9969(89)90010-1.

[8] Y. Yamazaki, "Effects of destructive periodontitis, induced by diet, on the mechanical properties of the periodontal ligament of the mandibular first molar in golden hamsters," *J. Periodontal Res.*, vol. 27, no. 2, pp. 149–158, 1992, doi: 10.1111/j.1600-0765.1992.tb01817.x.

[9] S. S. Chukkapalli and T. P. Lele, "Periodontal cell mechanotransduction," *Open Biol.*, vol. 8, no. 9, p. 180053, 2018, doi: 10.1098/rsob.180053.

[10] V. Zaleckiene, V. Peciuliene, V. Brukiene, and S. Drukteinis, "Traumatic dental injuries: Etiology, prevalence and possible outcomes," *Stomatologija*, vol. 16, no. 1, pp. 7–14, 2014.

[11] J. Chen, W. Li, M. V. Swain, M. Ali Darendeliler, and Q. Li, "A periodontal ligament driven remodeling algorithm for orthodontic tooth movement," *J. Biomech.*, vol. 47, no. 7, pp. 1689–1695, May 2014, doi: 10.1016/j.jbiomech.2014.02.030.

[12] D. Cardaropoli and L. Gaveglio, "The influence of orthodontic movement on periodontal tissues level," *Semin. Orthod.*, vol. 13, no. 4, pp. 234–245, Dec. 2007, doi: 10.1053/j.sodo.2007.08.005.

[13] T. S. Fill, J. P. Carey, R. W. Toogood, and P. W. Major, "Experimentally determined mechanical oroperties of, and models for, the periodontal ligament: Critical review of current literature," *J. Dent. Biomech.*, vol. 2011, Apr. 2011, doi: 10.4061/2011/312980.

[14] T. S. Fill, R. W. Toogood, P. W. Major, and J. P. Carey, "Analytically determined mechanical properties of, and models for the periodontal ligament: Critical review of literature," *J. Biomech.*, vol. 45, no. 1, pp. 9–16, Jan. 2012, doi: 10.1016/j.jbiomech.2011.09.020.

[15] D. L. Romanyk, R. Guan, P. W. Major, and C. R. Dennison, "Repeatability of strain magnitude and strain rate measurements in the periodontal ligament using fibre Bragg gratings: An ex vivo study in a swine model," *J. Biomech.*, vol. 54, pp. 117–122, Mar. 2017, doi: 10.1016/j.jbiomech.2017.01.047.

[16] E. Al-Fakih, N. A. A. Osman, and F. R. M. Adikan, "The use of fiber Bragg grating sensors in biomechanics and rehabilitation applications: The state-of-the-art and ongoing research topics," *Sensors*, vol. 12, no. 10, pp. 12890–12926, Sep. 2012, doi: 10.3390/s121012890.

[17] A. D. Kersey, "Fiber grating sensors," *IEEE J. Light. Technol.*, vol. 15, no. 8, pp. 1442–1463, Aug. 1997, doi: 10.1109/50.618377.

[18] B. Lee, "Review of the present status of optical fiber sensors," *Opt. Fiber Technol.*, vol. 9, no. 2, pp. 57–79, Apr. 2003, doi: 10.1016/S1068-5200(02)00527-8.

[19] G. Rajan, *Optical fiber sensors : Advanced techniques and applications*. CRC Press, 2017.

[20] L. Zen Karam, M. Scandelari Milczewski, and H. Jose Kalinowski, "Strain monitoring of the periodontal ligament in pig's mandibles," Oct. 2012, vol. 8421, pp. 84215W-84215W, doi: 10.1117/12.975270.

[21] R. L. Drake, A. W. Vogl, and A. W. M. Mitchell, "Head and neck," in *Gray's Anatomy for Students*, 4th ed., Philadelphia, PA, 2020, pp. 823-1121.e4.

[22] H. Amold and H. Werner, *Foundations of dental technology*. Hanover Park, IL: Quintessence Publishing Co. Inc, 2014.

[23] J. C. Türp and K. W. Alt, "Anatomy and morphology of human teeth," in *Dental anthropology: fundamentals, limits and prospects*, K. W. Alt, F. W. Rösing, and M. Teschler-Nicola, Eds. Vienna: Springer, 1998, pp. 71–94.

[24] W. Beertsen, C. A. G. McCulloch, and J. Sodek, "The periodontal ligament: a unique, multifunctional connective tissue," *Periodontol. 2000*, vol. 13, no. 1, pp. 20–40, Feb. 1997, doi: 10.1111/j.1600-0757.1997.tb00094.x.

[25] C. a. G. Mcculloch, P. Lekic, and M. D. Mckee, "Role of physical forces in regulating the form and function of the periodontal ligament," *Periodontol. 2000*, vol. 24, no. 1, pp. 56–72, 2000, doi: 10.1034/j.1600-0757.2000.2240104.x.

[26] A. Nanci and D. D. Bosshardt, "Structure of periodontal tissues in health and disease*," *Periodontol. 2000*, vol. 40, no. 1, pp. 11–28, 2006, doi: 10.1111/j.1600-0757.2005.00141.x.

[27] H. R. Mühlemann, "Tooth mobility: A review of clinical aspects and research findings," *J. Periodontol.*, vol. 38, no. 6, p. Suppl:686-713, Dec. 1967, doi: 10.1902/jop.1967.38.6_part2.686.

[28] K. Komatsu, "Mechanical Strength and Viscoelastic Response of the Periodontal Ligament in Relation to Structure," *J. Dent. Biomech.*, vol. 2010, Dec. 2009, doi: 10.4061/2010/502318.

[29] Y. Liang, Z. Hu, B. Chang, and X. Liu, "Quantitative characterizations of the Sharpey's fibers of rat molars," *J. Periodontal Res.*, vol. 55, no. 2, pp. 307–314, 2020, doi: 10.1111/jre.12716.

[30] B. K. Berkovitz, "The structure of the periodontal ligament: an update," *Eur. J. Orthod.*, vol. 12, no. 1, pp. 51–76, Feb. 1990, doi: 10.1093/ejo/12.1.51.

[31] M. Kaku and M. Yamauchi, "Mechano-regulation of collagen biosynthesis in periodontal ligament," *J. Prosthodont. Res.*, vol. 58, no. 4, pp. 193–207, Oct. 2014, doi: 10.1016/j.jpor.2014.08.003.

[32] T. de Jong, A. D. Bakker, V. Everts, and T. H. Smit, "The intricate anatomy of the periodontal ligament and its development: Lessons for periodontal regeneration," *J. Periodontal Res.*, vol. 52, no. 6, pp. 965–974, 2017, doi: 10.1111/jre.12477.

[33] B. Owen, G. Gullion, G. Heo, J. P. Carey, P. W. Major, and D. L. Romanyk, "Measurement of forces and moments around the maxillary arch for treatment of a simulated lingual incisor and high canine malocclusion using straight and mushroom archwires in fixed lingual appliances," *Eur. J. Orthod.*, vol. 39, no. 6, pp. 665–672, Nov. 2017, doi: 10.1093/ejo/cjx028.

[34] J. A. Yee, T. Türk, S. Elekdağ-Türk, L. L. Cheng, and M. A. Darendeliler, "Rate of tooth movement under heavy and light continuous orthodontic forces," *Am. J. Orthod. Dentofacial Orthop.*, vol. 136, no. 2, p. 150.e1-150.e9, Aug. 2009, doi: 10.1016/j.ajodo.2008.06.027.

[35] C. Gonzales, H. Hotokezaka, M. Yoshimatsu, J. H. Yozgatian, M. A. Darendeliler, and N. Yoshida, "Force magnitude and duration effects on amount of tooth movement and root resorption in the rat molar," *Angle Orthod.*, vol. 78, no. 3, pp. 502–509, May 2008, doi: 10.2319/052007-240.1.

[36] S. R. Toms, J. E. Lemons, A. A. Bartolucci, and A. W. Eberhardt, "Nonlinear stress-strain behavior of periodontal ligament under orthodontic loading," *Am. J. Orthod. Dentofacial Orthop.*, vol. 122, no. 2, pp. 174–179, Aug. 2002, doi: 10.1067/mod.2002.124997.

[37] U. Mandel, P. Dalgaard, and A. Viidik, "A biomechanical study of the human periodontal ligament," *J. Biomech.*, vol. 19, no. 8, pp. 637–645, Jan. 1986, doi: 10.1016/0021-9290(86)90169-7.

[38] W. J. Ralph, "Tensile behaviour of the periodontal ligament," *J. Periodontal Res.*, vol. 17, no. 4, pp. 423–426, Jul. 1982, doi: 10.1111/j.1600-0765.1982.tb01172.x.

[39] W. D. van Driel, E. J. van Leeuwen, J. W. Von den Hoff, J. C. Maltha, and A. M. Kuijpers-Jagtman, "Time-dependent mechanical behaviour of the periodontal ligament," *Proc. Inst. Mech. Eng. [H]*, vol. 214, no. 5, pp. 497–504, 2000, doi: 10.1243/0954411001535525.

[40] C. Dorow, N. Krstin, and F.-G. Sander, "Experiments to determine the material properties of the periodontal ligament," *J. Orofac. Orthop. Fortschritte Kieferorthopädie*, vol. 63, no. 2, pp. 94–104, Mar. 2002, doi: 10.1007/s00056-002-0107-4.

[41] F. Genna, L. Annovazzi, C. Bonesi, P. Fogazzi, and C. Paganelli, "On the experimental determination of some mechanical properties of porcine periodontal ligament," *Meccanica*, vol. 43, no. 1, pp. 55–73, Feb. 2008, doi: 10.1007/s11012-007-9094-2.

[42] H. F. Atkinson and W. J. Ralph, "In vitro strength of the human periodontal ligament," *J. Dent. Res.*, vol. 56, no. 1, pp. 48–52, Jan. 1977, doi: 10.1177/00220345770560011001.

[43] C. Dorow, N. Krstin, and F.-G. Sander, "Determination of the mechanical properties of the periodontal ligament in a uniaxial tensional experiment," *J. Orofac. Orthop. Fortschritte Kieferorthopädie*, vol. 64, no. 2, pp. 100–107, Feb. 2003, doi: 10.1007/s00056-003-0225-7.

[44] C. S. Sanctuary, H. W. A. Wiskott, J. Justiz, J. Botsis, and U. C. Belser, "In vitro time-dependent response of periodontal ligament to mechanical loading," *J. Appl. Physiol. Bethesda Md 1985*, vol. 99, no. 6, pp. 2369–2378, Dec. 2005, doi: 10.1152/japplphysiol.00486.2005.

[45] E. Tanaka *et al.*, "Dynamic shear properties of the porcine molar periodontal ligament," *J. Biomech.*, vol. 40, no. 7, pp. 1477–1483, Jan. 2007, doi: 10.1016/j.jbiomech.2006.06.022.

[46] I. Z. Oskui and A. Hashemi, "Dynamic tensile properties of bovine periodontal ligament: A nonlinear viscoelastic model," *J. Biomech.*, vol. 49, no. 5, pp. 756–764, Mar. 2016, doi: 10.1016/j.jbiomech.2016.02.020.

[47] B. Wu *et al.*, "Viscoelastic properties of human periodontal ligament: Effects of the loading frequency and location," *Angle Orthod.*, vol. 89, no. 3, pp. 480–487, 2019, doi: 10.2319/062818-481.1.

[48] M. Najafidoust, A. Hashemi, and I. Z. Oskui, "Dynamic viscoelastic behavior of bovine periodontal ligament in compression," *J. Periodontal Res.*, vol. 55, no. 5, pp. 651–659, 2020, doi: 10.1111/jre.12751.

[49] B. Wu *et al.*, "Frequency-related viscoelastic properties of the human incisor periodontal ligament under dynamic compressive loading," *PLoS ONE*, vol. 15, no. 7 July, 2020, doi: 10.1371/journal.pone.0235822.

[50] K. Komatsu, Y. Yamazaki, S. Yamaguchi, and M. Chiba, "Comparison of biomechanical properties of the incisor periodontal ligament among different species," *Anat. Rec.*, vol. 250,

no. 4, pp. 408–417, 1998, doi: 10.1002/(SICI)1097-0185(199804)250:4<408::AID-AR3>3.0.CO;2-T.

[51] K. Komatsu, T. Shibata, A. Shimada, A. Viidik, and M. Chiba, "Age-related and regional differences in the stress-strain and stress-relaxation behaviours of the rat incisor periodontal ligament," *J. Biomech.*, vol. 37, no. 7, pp. 1097–1106, Jul. 2004, doi: 10.1016/j.jbiomech.2003.11.013.

[52] S. R. Toms, G. J. Dakin, J. E. Lemons, and A. W. Eberhardt, "Quasi-linear viscoelastic behavior of the human periodontal ligament," *J. Biomech.*, vol. 35, no. 10, pp. 1411–1415, Oct. 2002, doi: 10.1016/S0021-9290(02)00166-5.

[53] K. Komatsu, C. Sanctuary, T. Shibata, A. Shimada, and J. Botsis, "Stress–relaxation and microscopic dynamics of rabbit periodontal ligament," *J. Biomech.*, vol. 40, no. 3, pp. 634–644, Jan. 2007, doi: 10.1016/j.jbiomech.2006.01.026.

[54] D. L. Romanyk, G. W. Melenka, and J. P. Carey, "Modeling stress-relaxation behavior of the periodontal ligament during the initial phase of orthodontic treatment," *J. Biomech. Eng.*, vol. 135, no. 9, pp. 091007-091007–8, Jul. 2013, doi: 10.1115/1.4024631.

[55] A. N. Natali, P. G. Pavan, E. L. Carniel, and C. Dorow, "Viscoelastic response of the periodontal ligament: An experimental–numerical analysis," *Connect. Tissue Res.*, vol. 45, no. 4–5, pp. 222–230, Jan. 2004, doi: 10.1080/03008200490885742.

[56] A. I. Zhurov, G. Limbert, D. P. Aeschlimann, and J. Middleton, "A constitutive model for the periodontal ligament as a compressible transversely isotropic visco-hyperelastic tissue," *Comput. Methods Biomech. Biomed. Engin.*, vol. 10, no. 3, pp. 223–235, Jun. 2007, doi: 10.1080/13639080701314894.

[57] A. N. Natali, E. L. Carniel, P. G. Pavan, F. G. Sander, C. Dorow, and M. Geiger, "A visco-hyperelastic-damage constitutive model for the analysis of the biomechanical response of the periodontal ligament," *J. Biomech. Eng.*, vol. 130, no. 3, Jun. 2008, doi: 10.1115/1.2900415.

[58] I. Z. Oskui, A. Hashemi, and H. Jafarzadeh, "Biomechanical behavior of bovine periodontal ligament: Experimental tests and constitutive model," *J. Mech. Behav. Biomed. Mater.*, vol. 62, pp. 599–606, Sep. 2016, doi: 10.1016/j.jmbbm.2016.05.036.

[59] R. Uhlir *et al.*, "Biomechanical characterization of the periodontal ligament: Orthodontic tooth movement," *Angle Orthod.*, vol. 87, no. 2, pp. 183–192, Mar. 2017, doi: 10.2319/092615-651.1.

[60] M. Bergomi, J. Cugnoni, M. Galli, J. Botsis, U. C. Belser, and H. W. A. Wiskott, "Hydro-mechanical coupling in the periodontal ligament: A porohyperelastic finite element model," *J. Biomech.*, vol. 44, no. 1, pp. 34–38, Jan. 2011, doi: 10.1016/j.jbiomech.2010.08.019.

[61] J. Ortún-Terrazas, J. Cegoñino, U. Santana-Penín, U. Santana-Mora, and A. Pérez del Palomar, "Approach towards the porous fibrous structure of the periodontal ligament using micro-computerized tomography and finite element analysis," *J. Mech. Behav. Biomed. Mater.*, vol. 79, pp. 135–149, Mar. 2018, doi: 10.1016/j.jmbbm.2017.12.022.

[62] Y. Yang and W. Tang, "Analysis of mechanical properties at different levels of the periodontal ligament," *Biomed. Res.*, vol. 28, no. 20, 2017, Accessed: Sep. 18, 2019. [Online]. Available: http://www.alliedacademies.org/abstract/analysis-of-mechanical-properties-at-different-levels-of-the-periodontal-ligament-8734.html.

[63] H. Huang, W. Tang, B. Yan, B. Wu, and D. Cao, "Mechanical responses of the periodontal ligament based on an exponential hyperelastic model: a combined experimental and finite element method," *Comput. Methods Biomech. Biomed. Engin.*, vol. 19, no. 2, pp. 188–198, Jan. 2016, doi: 10.1080/10255842.2015.1006207.

[64] H. Huang, W. Tang, Q. Tan, and B. Yan, "Development and parameter identification of a visco-hyperelastic model for the periodontal ligament," *J. Mech. Behav. Biomed. Mater.*, vol. 68, pp. 210–215, Apr. 2017, doi: 10.1016/j.jmbbm.2017.01.035.

[65] B. K. Connizzo and G. R. S. Naveh, "In situ AFM-based nanoscale rheology reveals regional non-uniformity in viscoporoelastic mechanical behavior of the murine periodontal ligament," *J. Biomech.*, vol. 111, p. 109996, Oct. 2020, doi: 10.1016/j.jbiomech.2020.109996.

[66] L. Qian, M. Todo, Y. Morita, Y. Matsushita, and K. Koyano, "Deformation analysis of the periodontium considering the viscoelasticity of the periodontal ligament," *Dent. Mater.*, vol. 25, no. 10, pp. 1285–1292, Oct. 2009, doi: 10.1016/j.dental.2009.03.014.

[67] K. L. Andersen, E. H. Pedersen, and B. Melsen, "Material parameters and stress profiles within the periodontal ligament," *Am. J. Orthod. Dentofacial Orthop.*, vol. 99, no. 5, pp. 427–440, 1991, doi: 10.1016/S0889-5406(05)81576-8.

[68] A. Ziegler, L. Keilig, A. Kawarizadeh, A. Jäger, and C. Bourauel, "Numerical simulation of the biomechanical behaviour of multi-rooted teeth," *Eur. J. Orthod.*, vol. 27, no. 4, pp. 333–339, Aug. 2005, doi: 10.1093/ejo/cji020.

[69] A. N. Natali, E. L. Carniel, P. G. Pavan, C. Bourauel, A. Ziegler, and L. Keilig, "Experimental–numerical analysis of minipig's multi-rooted teeth," *J. Biomech.*, vol. 40, no. 8, pp. 1701–1708, Jan. 2007, doi: 10.1016/j.jbiomech.2006.08.011.

[70] L. Dong-Xu, W. Hong-Ning, W. Chun-Ling, L. Hong, S. Ping, and Y. Xiao, "Modulus of elasticity of human periodontal ligament by optical measurement and numerical simulation," *Angle Orthod.*, vol. 81, no. 2, pp. 229–236, Mar. 2011, doi: 10.2319/060710-311.1.

[71] K. Papadopoulou, L. Keilig, T. Eliades, R. Krause, A. Jäger, and C. Bourauel, "The time-dependent biomechanical behaviour of the periodontal ligament - An in vitro experimental

study in minipig mandibular two-rooted premolars," *Eur. J. Orthod.*, vol. 36, Nov. 2011, doi: 10.1093/ejo/cjr134.

[72] K. Papadopoulou *et al.*, "Biomechanical time dependency of the periodontal ligament: A combined experimental and numerical approach," *Eur. J. Orthod.*, vol. 35, no. 6, pp. 811–818, Dec. 2013, doi: 10.1093/ejo/cjs103.

[73] C.-H. Chang, Y.-N. Lei, Y.-H. Ho, Y.-H. Sung, and T.-S. Lin, "Predicting the holistic force-displacement relation of the periodontal ligament: In-vitro experiments and finite element analysis," *Biomed. Eng. OnLine*, vol. 13, no. 1, p. 107, Jul. 2014, doi: 10.1186/1475-925X-13-107.

[74] L. Keilig *et al.*, "In vivo measurements and numerical analysis of the biomechanical characteristics of the human periodontal ligament," *Ann. Anat. - Anat. Anz.*, vol. 206, pp. 80–88, Jul. 2016, doi: 10.1016/j.aanat.2015.08.004.

[75] A. Nikolaus, J. D. Currey, T. Lindtner, C. Fleck, and P. Zaslansky, "Importance of the variable periodontal ligament geometry for whole tooth mechanical function: A validated numerical study," *J. Mech. Behav. Biomed. Mater.*, vol. 67, pp. 61–73, Mar. 2017, doi: 10.1016/j.jmbbm.2016.11.020.

[76] T. J. Knaup *et al.*, "Time-dependent behavior of porcine periodontal ligament: A combined experimental, numeric in-vitro study," *Am. J. Orthod. Dentofacial Orthop.*, vol. 153, no. 1, pp. 97–107, Jan. 2018, doi: 10.1016/j.ajodo.2017.05.034.

[77] D. C. A. Picton, "Tooth mobility—an update," *Eur. J. Orthod.*, vol. 12, no. 1, pp. 109–115, Feb. 1990, doi: 10.1093/ejo/12.1.109.

[78] D. J. Wills, D. C. A. Picton, and W. I. R. Davies, "An investigation of the viscoelastic properties of the periodontium in monkeys," *J. Periodontal Res.*, vol. 7, no. 1, pp. 42–51, 1972, doi: 10.1111/j.1600-0765.1972.tb00630.x.

[79] D. C. Picton and D. J. Wills, "Viscoelastic properties of the periodontal ligament and mucous membrane," *J. Prosthet. Dent.*, vol. 40, no. 3, pp. 263–272, Sep. 1978, doi: 10.1016/0022-3913(78)90031-8.

[80] G. G. Ross, C. S. Lear, and R. DeCou, "Modeling the lateral movement of teeth," *J. Biomech.*, vol. 9, no. 11, pp. 723–734, Jan. 1976, doi: 10.1016/0021-9290(76)90174-3.

[81] K. Tanne, T. Nagataki, Y. Inoue, M. Sakuda, and C. J. Burstone, "Patterns of initial tooth displacements associated with various root lengths and alveolar bone heights," *Am. J. Orthod. Dentofac. Orthop. Off. Publ. Am. Assoc. Orthod. Its Const. Soc. Am. Board Orthod.*, vol. 100, no. 1, pp. 66–71, Jul. 1991, doi: 10.1016/0889-5406(91)70051-W.

[82] A. Hohmann *et al.*, "Influence of different modeling strategies for the periodontal ligament on finite element simulation results," *Am. J. Orthod. Dentofacial Orthop.*, vol. 139, no. 6, pp. 775–783, Jun. 2011, doi: 10.1016/j.ajodo.2009.11.014.

[83] P. Shokrani, A. Hashemi, M. B. Shirin, and I. Z. Oskui, "Effect of geometric dimensions and material models of the periodontal ligament in orthodontic tooth movement," *Orthod. Craniofac. Res.*, vol. n/a, no. n/a, doi: 10.1111/ocr.12381.

[84] Y.-N. Lei, C.-Y. Chen, Y.-C. Chen, and T.-S. Lin, "Holistic force-displacement behavior of porcine periodontal ligament-numerical simulation and in-vitro experiment," *J. Biomech. Sci. Eng.*, vol. 12, no. 1, 2017, doi: 10.1299/jbse.16-00604.

[85] K. O. Hill, Y. Fujii, D. C. Johnson, and B. S. Kawasaki, "Photosensitivity in optical fiber waveguides: Application to reflection filter fabrication," *Appl. Phys. Lett.*, vol. 32, no. 10, pp. 647–649, May 1978, doi: 10.1063/1.89881.

[86] G. Meltz, W. W. Morey, and W. H. Glenn, "Formation of Bragg gratings in optical fibers by a transverse holographic method," *Opt. Lett.*, vol. 14, no. 15, p. 823, Aug. 1989, doi: 10.1364/OL.14.000823.

[87] K. O. Hill and G. Meltz, "Fiber Bragg grating technology fundamentals and overview," *J. Light. Technol.*, vol. 15, no. 8, pp. 1263–1276, Aug. 1997, doi: 10.1109/50.618320.

[88] S. C. Tjin, Y. K. Tan, M. Yow, Y.-Z. Lam, and J. Hao, "Recording compliance of dental splint use in obstructive sleep apnoea patients by force and temperature modelling," *Med. Biol. Eng. Comput.*, vol. 39, no. 2, pp. 182–184, Mar. 2001, doi: 10.1007/BF02344801.

[89] L. Carvalho, J. C. C. Silva, R. N. Nogueira, J. L. Pinto, H. J. Kalinowski, and J. A. Simúes, "Application of Bragg grating sensors in dental biomechanics," *J. Strain Anal. Eng. Des.*, vol. 41, no. 6, pp. 411–416, Aug. 2006, doi: 10.1243/03093247JSA191.

[90] S. Padma, S. Umesh, S. Asokan, and T. Srinivas, "Bite force measurement based on fiber Bragg grating sensor," *J. Biomed. Opt.*, vol. 22, no. 10, p. 107002, Oct. 2017, doi: 10.1117/1.JBO.22.10.107002.

[91] S. Umesh, S. Padma, S. Asokan, and T. Srinivas, "Fiber Bragg Grating based bite force measurement," *J. Biomech.*, vol. 49, no. 13, pp. 2877–2881, Sep. 2016, doi: 10.1016/j.jbiomech.2016.06.036.

[92] M. S. Milczewski, J. C. C. Da Silva, C. Martelli, L. Grabarski, I. Abe, and H. J. Kalinowski, "Force monitoring in a maxilla model and dentition using optical fiber Bragg gratings," *Sensors*, vol. 12, no. 9, Art. no. 9, Sep. 2012, doi: 10.3390/s120911957.

[93] M. S. Milczewski, H. J. Kalinowski, J. C. C. da Silva, I. Abe, J. A. Simões, and A. Saga, "Stress monitoring in a maxilla model and dentition," in *21st International Conference on Optical Fiber Sensors*, May 2011, vol. 7753, p. 77534V, doi: 10.1117/12.886071.

[94] L. Ren, G. Song, M. Conditt, P. C. Noble, and H. Li, "Fiber Bragg grating displacement sensor for movement measurement of tendons and ligaments," *Appl. Opt.*, vol. 46, no. 28, pp. 6867–6871, Oct. 2007, doi: 10.1364/AO.46.006867.

[95] C. R. Dennison *et al.*, "Ex vivo measurement of lumbar intervertebral disc pressure using fibre-Bragg gratings," *J. Biomech.*, vol. 41, no. 1, pp. 221–225, Jan. 2008, doi: 10.1016/j.jbiomech.2007.07.015.

[96] C. R. Dennison, P. M. Wild, D. R. Wilson, and P. A. Cripton, "A minimally invasive in-fiber Bragg grating sensor for intervertebral disc pressure measurements," *Meas. Sci. Technol.*, vol. 19, no. 8, p. 085201, Aug. 2008, doi: 10.1088/0957-0233/19/8/085201.

[97] C. R. Dennison, P. M. Wild, M. F. Dvorak, D. R. Wilson, and P. A. Cripton, "Validation of a novel minimally invasive intervertebral disc pressure sensor utilizing in-fiber Bragg gratings in a porcine model: An ex vivo study," *Spine*, vol. 33, no. 17, p. E589, Aug. 2008, doi: 10.1097/BRS.0b013e31817c55e2.

[98] P. Vakiel *et al.*, "Stress measurements on the articular cartilage surface using fiber optic technology and in-vivo gait kinematics," *Ann. Biomed. Eng.*, vol. 48, no. 12, pp. 2836–2845, Dec. 2020, doi: 10.1007/s10439-020-02516-x.

[99] P. Vakiel, C. R. Dennison, M. Shekarforoush, M. Scott, D. A. Hart, and N. G. Shrive, "Measuring the internal stress in ovine meniscus during simulated in vivo gait kKinematics: A novel method ssing fibre optic technology," *Ann. Biomed. Eng.*, Oct. 2020, doi: 10.1007/s10439-020-02652-4.

[100] P. Vakiel *et al.*, "Mapping Stresses on the Tibial Plateau Cartilage in an Ovine Model Using In-Vivo Gait Kinematics," *Ann. Biomed. Eng.*, Oct. 2020, doi: 10.1007/s10439-020-02650-6.

[101] C. R. Dennison, P. M. Wild, D. R. Wilson, and M. K. Gilbart, "An in-fiber Bragg grating sensor for contact force and stress measurements in articular joints," *Meas. Sci. Technol.*, vol. 21, p. 115803, 2010.

[102] A. Viidik, "Mechanical properties of parallel-fibred collagenous tissues," in *Biology of collagen*, Academic Press, 1980, pp. 237–255.

[103] F. Genna, L. Annovazzi, C. Bonesi, P. Fogazzi, and C. Paganelli, "On the experimental determination of some mechanical properties of porcine periodontal ligament," *Meccanica*, vol. 43, no. 1, pp. 55–73, Feb. 2008, doi: 10.1007/s11012-007-9094-2.

[104] M. Bergomi, H. W. Anselm Wiskott, J. Botsis, T. Shibata, and U. C. Belser, "Mechanical response of periodontal ligament: Effects of specimen geometry, preconditioning cycles and time lapse," *J. Biomech.*, vol. 42, no. 14, pp. 2410–2414, Oct. 2009, doi: 10.1016/j.jbiomech.2009.06.031.

[105] M. E. Weaver, F. M. Sorenson, and E. B. Jump, "The miniature pig as an experimental animal in dental research," *Arch. Oral Biol.*, vol. 7, no. 1, pp. 17-IN6, Jan. 1962, doi: 10.1016/0003-9969(62)90044-4.

[106] J. H. Ward Jr, "Hierarchical grouping to optimize an objective function," *J. Am. Stat. Assoc.*, vol. 58, no. 301, pp. 236–244, Mar. 1963, doi: 10.1080/01621459.1963.10500845.

[107] R. S. King, *Cluster analysis and data mining: An introduction.* Dulles, Virginia: Mercury Learning & Information, 2015.

[108] C. J. Willmott, "Some comments on the evaluation of model performance," *Bull. Am. Meteorol. Soc.*, vol. 63, no. 11, pp. 1309–1313, Nov. 1982, doi: 10.1175/1520-0477(1982)063<1309:SCOTEO>2.0.CO;2.

[109] M. Friedman, "The use of ranks to avoid the assumption of normality implicit in the analysis of variance," *J. Am. Stat. Assoc.*, vol. 32, no. 200, pp. 675–701, 1937, doi: 10.2307/2279372.

[110] O. J. Dunn, "Multiple comparisons using rank sums," *Technometrics*, vol. 6, no. 3, pp. 241–252, Aug. 1964, doi: 10.1080/00401706.1964.10490181.

[111] S. Holm, "A simple sequentially rejective multiple test procedure," *Scand. J. Stat.*, vol. 6, no. 2, pp. 65–70, 1979.

[112] M. Pini, P. Zysset, J. Botsis, and R. Contro, "Tensile and compressive behaviour of the bovine periodontal ligament," *J. Biomech.*, vol. 37, no. 1, pp. 111–119, Jan. 2004, doi: 10.1016/s0021-9290(03)00234-3.

[113] W. Beertsen, C. A. McCulloch, and J. Sodek, "The periodontal ligament: a unique, multifunctional connective tissue," *Periodontol. 2000*, vol. 13, pp. 20–40, Feb. 1997, doi: 10.1111/j.1600-0757.1997.tb00094.x.

[114] S. M. Bien, "Hydrodynamic damping of tooth movement," *J. Dent. Res.*, vol. 45, no. 3, pp. 907–914, May 1966, doi: 10.1177/00220345660450036701.

[115] P. M. Cattaneo, M. Dalstra, and B. Melsen, "The finite element method: A tool to study orthodontic tooth movement," *J. Dent. Res.*, vol. 84, no. 5, pp. 428–433, May 2005, doi: 10.1177/154405910508400506.

[116] J. Shinohara, T. Shibata, A. Shimada, and K. Komatsu, "The biomechanical properties of the healing periodontium of replanted rat mandibular incisors," *Dent. Traumatol.*, vol. 20, no. 4, pp. 212–221, 2004, doi: 10.1111/j.1600-9657.2004.00244.x.

[117] N. M. B. K. Willems *et al.*, "Determination of the relationship between collagen cross-links and the bone–tissue stiffness in the porcine mandibular condyle," *J. Biomech.*, vol. 44, no. 6, pp. 1132–1136, Apr. 2011, doi: 10.1016/j.jbiomech.2011.01.023.

[118] S. Milton, "A sample size formula for multiple regression studies," *Public Opin. Q.*, vol. 50, no. 1, pp. 112–118, 1986.

[119] K. Tanne, M. Sakuda, and C. J. Burstone, "Three-dimensional finite element analysis for stress in the periodontal tissue by orthodontic forces," *Am. J. Orthod. Dentofac. Orthop. Off. Publ. Am. Assoc. Orthod. Its Const. Soc. Am. Board Orthod.*, vol. 92, no. 6, pp. 499–505, Dec. 1987, doi: 10.1016/0889-5406(87)90232-0.

[120] M. Bergomi, H. W. A. Wiskott, J. Botsis, A. Mellal, and U. C. Belser, "Load response of periodontal ligament: Assessment of fluid flow, compressibility, and effect of pore pressure," *J. Biomech. Eng.*, vol. 132, no. 1, p. 014504, Jan. 2010, doi: 10.1115/1.4000154.

[121] C. Persson, S. Evans, R. Marsh, J. L. Summers, and R. M. Hall, "Poisson's ratio and strain rate dependency of the constitutive behavior of spinal dura mater," *Ann. Biomed. Eng.*, vol. 3, no. 38, pp. 975–983, 2010, doi: 10.1007/s10439-010-9924-6.

[122] M. Poppe, C. Bourauel, and A. Jäger, "Determination of the elasticity parameters of the human periodontal ligament and the location of the center of resistance of single-rooted teeth: A study of autopsy specimens and their conversion into finite element models," *J. Orofac. Orthop. Fortschritte Kieferorthopädie*, vol. 63, no. 5, pp. 358–370, Sep. 2002, doi: 10.1007/s00056-002-0067-8.

Appendix A: Relevant MATLAB code

Data analysis in the presented work was completed using MATLAB unless otherwise specified. This appendix includes relevant MATLAB code to the data analysis for filtering the strain data, averaging data, calculating the root mean square, calculating the standardized difference in medians, finding the peak measurements, and completing data clustering.

1 Data Filter and Conversion of Wavelength

```
%% After Strain data is opened, start times are aligned, and each trial is
organized into a single array. Due to equipment availability, two
interrogators were used for the collection of data. Therefore, slight
differences are evident in sample rate and filtering of the data

%% Define sample rate

% SmartScan interrogator filter parameters
filt=50; % cut off frequency
acqrate_s=2500;%Average Sampling rate for Smart Scan interrogator

%Micro Optic interrogator filter parameters
acqrate_s= 1453.6 % Average Sampling rate for Micron Optics interrogator
filt=100; %cutoff frequency

%Convert wavelength data to strain data. During experiments, there was a 2
%second delay between the interrogator and in Instron starting. Therefore,
%there was 2 seconds of wavelength data collected prior to loading. The
%average wavelength over these 2 seconds was found and used as the starting
%wavelength to convert wavelength data

% "wavelength_this_experiment" includes the raw wavelength data

% average starting wavelength (nm)
start_wavelength=mean(wavelength_this_experiment(1:acqrate_s*2,:));
% Conversion of wavelength to strain (με)
strain_this_experiment_1=(wavelength_this_experiment(:)-
start_wavelength).*1000./1.21;

% The strain data was then filtered
      % *only for the Micron Optics interrogator*, 1D median 1000 average
filter
      strain_this_experiment_1=medfilt1(strain_this_experiment_1,1000);
% Define the 4th order butterworth filter
      [B,A] = butter(4,filt/acqrate_s);
% Filter wavelength data
    strain_this_experiment= filtfilt(B,A,strain_this_experiment_1);
% create an array of all trials after preconditioning including time

% strain array
% "PC" Preconditioning Trial
```

```
% "trial" number of trials
% "time_strain" time array for strain data
% "time_force" time array for strain data

  strain(:,1)=time_strain;
  strain(:,2:trial+1)= strain_all_experiments(PC+1:PC+trial,:)';

  force(:,1)=time_force;
  force(:,2:trial+1)= force_all_experiments(PC+1:PC+trial,:)';
```

2 Average Time Series

```
% Average and standard deviation strain and force data
 for a=1:length(strain)
    aveStrain(a,1)=strain(a,1);
    aveStrain(a,2)=mean(strain(a,2:trial+1));
    aveStrain(a,3)=std(strain(a,2:trial+1));
 end

 for a=1:length(force)
    aveForce(a,1)=force(a,1);
    aveForce(a,2)=mean(force(a,2:trial+1));
    aveForce(a,3)=std(force(a,2:trial+1));
 end

 % median, 25th, and 75th percentile calculation

for a=1:length(time_strain)
    aveStrain(a,1)=time_strain(a);
    aveStrain(a,2)=median(strain(a,:));
    aveStrain(a,3)=prctile(strain(a,:),25);
    aveStrain(a,4)=prctile(strain(a,:),75);
end
for b=1:length(time_force)
    aveForce(b,1)=time_force(b);
    aveForce(b,2)=median(force(b,:));
    aveForce(b,3)=prctile(force(b,:),25);
    aveForce(b,4)=prctile(force(b,:),75);
end
```

3 Peak Time Values

```
% Find the peak measurements and times for force and strain
% "holdd" is a defined as the time after the loading period to search data
% for the peak measurement, this is less than 10 in some cases where a spike
is observed during unload

for c=1:trial

    [peak_strainn,
peak_strain_point]=max(abs((strain_1(1:(displacement/0.05+holdd)*acqrate_s,c+
1)))); % Find maximum absolute value of strain
```

```
    peak_strain_time(c,1)=time_strain(peak_strain_point); % Find the time of
the peak measurement of strain
    peak_strain(c,1)=strain(peak_strain_point,c+1); %Find peak value of
strain
    peak_strain_point=0;

    [peak_force(c,1), peak_force_point]=max(force(:,c+1)); % Find peak force
measurement
    peak_force_time(c,1)=time_force(peak_force_point); % Find corresponding
peak force time
    peak_force_point=0;
end
```

4 Standardize Difference in Medians and Adjusted Root Mean Square Calculations

```
%% Find the root mean square "RMSE" for strain and force for adjusted root
mean square (ARMS) calculation
RMSE_s=0;
RMSE_f=0;
count=0;
    for bb=1:length(time_strain)
    for aa=1:10
    RMSE_s=RMSE_s+(aveStrain(bb,2)-strain(bb,aa))^2;
    count=count+1;
    end
    end
    RMSE_s=(RMSE_s/(count))^0.5; % Root Mean square for strain time series

    count=0;
    for bb=1:length(time_force)
    for aa=1:10
    RMSE_f=RMSE_f+(aveForce(bb,2)-force(bb,aa))^2;
    count=count+1;
    end
    end
    RMSE_f=(RMSE_f/(count))^0.5; % Root Mean square for force time series

%For sensitivity analysis, all trials were grouped by iteration
%compile all strain values
strain_PC=strain(:,2:PCtrial+1); % preconditioning trials
strain_P1=strain(:,PCtrial+2:PCtrial+6); % First Iteration
strain_P2=strain(:,PCtrial+7:PCtrial+11); % Second Iteration
strain_P3=strain (:,PCtrial+12:PCtrial+16); % Third Iteration
strain_P4=strain (:,PCtrial+17:PCtrial+21); % Forth Iteration

%compile all force values
force_PC=force(:,2:PCtrial+1);
force_P1=force(:,PCtrial+2:PCtrial+6);
force_P2=force(:,PCtrial+7:PCtrial+11);
force_P3=force(:,PCtrial+12:PCtrial+16);
force_P4=force(:,PCtrial+17:PCtrial+21);
```

```
% Organize all peak values, Note peak values were found using same method as
above and separated by iteration

     For_stat=zeros(10,5);
     For_stat(1:PCtrial,1)=Peak_strain_PC';
     For_stat(1:5,2)=Peak_strain_P1';
     For_stat(1:5,3)=Peak_strain_P2';
     For_stat(1:5,4)=Peak_strain_P3';
     For_stat(1:5,5)=Peak_strain_P4';
         % For_stat(6:8,1)=Peak_force_PC';
     For_stat(6:10,2)=Peak_force_P1';
     For_stat(6:10,3)=Peak_force_P2';
     For_stat(6:10,4)=Peak_force_P3';
     For_stat(6:10,5)=Peak_force_P4';

 % Find the median peak force and strain values
     for aa= 1:4 % 4iterations
     peak_med_strain(1,aa)=median(For_stat(1:5,aa+1));
     peak_med_force(1,aa)=median(For_stat(6:10,aa+1));
     end

%% Find the average deviation from median for force and strain
     ME_s_all=0;
     ME_f_all=0;
for bb=1:4
     ME_s_all=0;
     ME_f_all=0;
for aa=1:5 % 5 trials
ME_s_all=ME_s_all+abs(For_stat(aa,bb+1)-peak_med_strain(1,bb));
ME_f_all=ME_f_all+abs(For_stat(aa+5,bb+1)-peak_med_force(1,bb));
end
ME_s(bb,1)=(ME_s_all/(5)); % Average deviation from the median for strain
     ME_f(bb,1)=(ME_f_all/(5)); % Average deviation from the median for orce
end


%% Find the standardized difference in median values (example form alignment
data) Note that "x" is a defined array that was previously "output" above
where x(:,3) is "peak_med_strain" for all iterations, x(:,13) is "ME_s" for
all iterations. Similarly, x(:,8) is "peak_med_force" for all iterations,
x(:,16) is "ME_f" for all iterations.
i=1;
bb=2;
aa=1;
for aa=1:3
for bb=2:4
    if bb>aa&& bb<5
      % Find the difference in the medians for strain
        diff(i,1)=abs(x(aa,3)-x(bb,3));
      % Find the average deviation for the median for both trials for strain
        diff(i,2)=((x(aa,13)+x(bb,13))/2);
      % Find the standardized difference in medians for strain
        diff(i,3)=diff(i,1)/diff(i,2);

       % Find the difference in the medians for force
        diff(i,4)=abs(x(aa,8)-x(bb,8));
      % Find the average deviation for the median for both trials for force
```

```
        diff(i,5)=((x(aa,16)+x(bb,16))/2);
      % Find the standardized difference in medians for force
        diff(i,6)=diff(i,4)/diff(i,5);

       i=i+1;
    else
        bb=bb+1;
    end
end
end
```

5 Data Clustering

```
Z=linkage(force_all_experiments,'ward','euclidean'); %Cluster force data for
all experiments
c=cluster(Z,'maxclust',num_clusters); %c tells the cluster number of each
experiment
```

Appendix B: Finite Element Model Setup

A finite element (FE) model of a tooth-periodontal ligament (PDL)-bone complex (TPBC) representing a swine second premolar was created to estimate the expected strain output from an in-Fibre Bragg grating (FBG) sensor placed within the PDL space. Various input parameters were investigated to ensure the FE model was appropriate, including the width of the PDL, appropriate PDL material properties, mesh convergence, and the sensitivity of the reaction force to the tooth and bone material properties. For each simulation, the crown of the tooth was displaced to a maximum displacement of 0.3 mm in the y-axis, and the base of the bone was constrained in the y-axis (Figure 21). Solid ten-node tetrahedral elements (SOLID187), and eight-node contact element (CONTA174) were used.

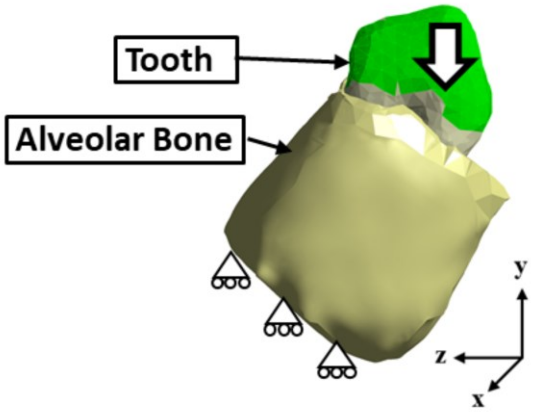

Figure 21 Basic FE model setup illustrating the displacement of the crown and the constraint of the base of the bone in the y-axis

1 Periodontal Ligament Size

A single, representative geometry was used for the FE analysis. The model was created using microcomputed tomography (µCT) scans of a right premolar (SkyScan 1076; Bruker-MicroCT, Kontich, Belgium, current 110 µA, voltage 100 kV, voxel size of 17.2 micron). The bone and tooth were segmented using imaging software (Mimics 22.0.0.524, Materialise, Leuven, Belgium, 3-matic, Materialise, Leuven, Belgium; ANSYS Discovery SpaceClaim 2020 R1). The PDL was created in the space between the bone and the tooth (3-matic, Materialise, Leuven, Belgium; ANSYS

Discovery SpaceClaim 2020 R1). The width of the FE model PDL varied from 0.04 mm to 1.05 mm, with an average thickness of 0.36 mm.

The FE PDL geometry was compared to six µCT scans of right and left second premolars to ensure the geometry was representative of a swine premolar. One of the scans was used to create the FE geometry, and three scans were scanned at a higher resolution (SkyScan 1076; Bruker-MicroCT, Kontich, Belgium, current 278 µA, voltage 90 kV, voxel size of 8.9 micron), indicated in Table 14. Each scan was first aligned so the y-axis ran through the mesial root and the z-axis ran through the center of the mesial and distal roots (DataViewer Software, SkyScan). The width of the mesial root PDL was measured at three locations along the root (Figure 22a), (CTAn, SkyScan). The first location was approximately 0.17 mm to 0.34 mm above the root apex, the second was halfway between the last µCT slice enamel was visible and the root apex, and the third was 0.17 mm to 0.34 mm below the slice where the alveolar bone fully surrounded both roots. At each location, the PDL width was measured in the mesial, buccal, distal, and lingual directions (Figure 22b). Each measurement was repeated three times on three different evenly spaced slices, for a total of 36 measurements per location. The width of the FE PDL geometry was measured at the same approximate three locations, three measurements in each of the four directions were taken for a total of 12 measurements per location (ANSYS Discovery SpaceClaim 2020 R1). The average and standard deviation at each location and the average and standard deviation for each tooth were calculated (Table 14).

Table 14 Average PDL width within the mesial root at the approximate apex, middle, and top of the root

Tooth	Apex (SD) (mm)	Middle (SD) (mm)	Top (SD) (mm)	Overall (SD) (mm)
Right[a,c]	0.46 (0.19)	0.46 (0.20)	0.42 (0.20)	0.45 (0.20)
Right[b]	0.55 (0.22)	0.42 (0.11)	0.50 (0.11)	0.49 (0.16)
Right[b]	0.56 (0.26)	0.50 (0.10)	0.50 (0.09)	0.52 (0.17)
Left[a]	0.50 (0.23)	0.47 (0.21)	0.46 (0.19)	0.48 (0.21)
Left[a]	0.47 (0.26)	0.43 (0.19)	0.48 (0.23)	0.46 (0.23)
Left[b]	0.60 (0.12)	0.43 (0.09)	0.45 (0.10)	0.49 (0.13)
ALL	0.52 (0.22)	0.45 (0.16)	0.47 (0.16)	0.48 (0.19)
Model	0.76 (0.44)	0.44 (0.22)	0.40 (0.28)	0.53 (0.36)

[a] scans taken with 17.2 micron resolution, [b] scans taken with 8.9 micron resolution, [c] geometry used for FE model

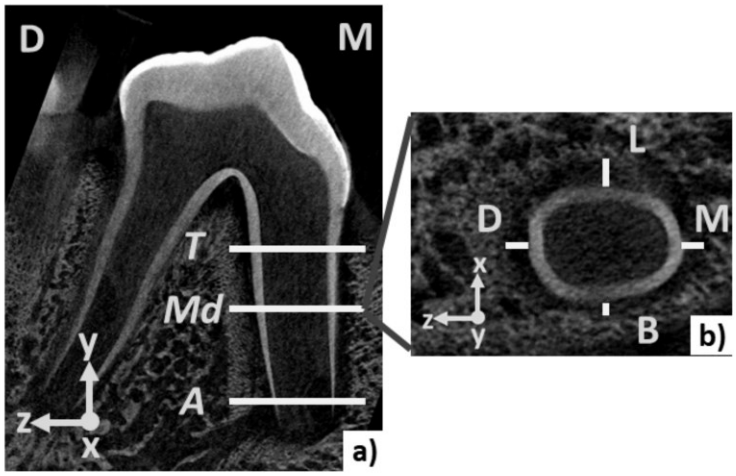

Figure 22 a) Representative μCT scan slice of a left second premolar indicating the Apex (A), Middle (Md), and Top (T) levels of the root where measurements were taken. b) Coronal slice indicating the Lingual (L), Mesial (M), Buccal (B), and Distal (D) direction where measurements were taken.

It was concluded that the FE PDL geometry was comparable to the scanned PDLs, and it was appropriate to use as a representative geometry. The greatest variation between the scans and FE model occurred at the root apex; this is likely due to the variable geometry of the PDL. It can be seen in Figure 23 the width of the PDL depends on the direction. It is likely that the alignment of the μCT scans and the location of the measurements led to the variation observed between the μCT scans and the FE geometry.

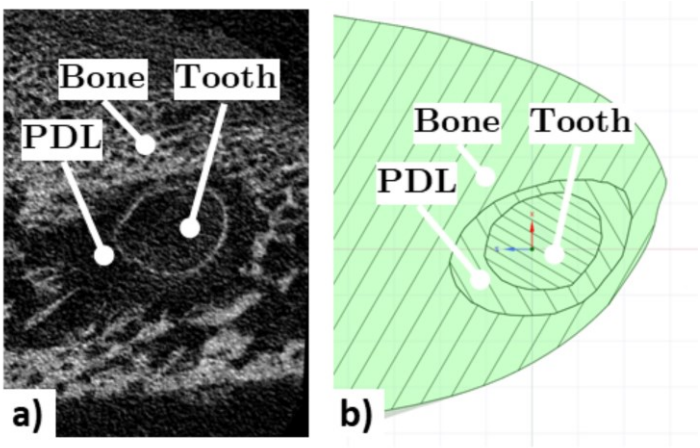

Figure 23 Image demonstrating the apical PDL shape in the mesial root in a) μCT images and b) the FE geometry

2 Periodontal Ligament Parameter Selection

The PDL Young's Modulus and Poisson's ratio have been reported to range between 0.01 MPa to 1750 MPa and 0.30 to 0.49, respectively [1]. To ensure the appropriate material properties were implemented for the presented experimental protocol, the FE force/displacement output was compared to the experimental peak force/displacement output. The PDL is understood to act as an incompressible fluid during rapid, high magnitude loading and be more compressible during quasi-static loading as the extracellular fluid will begin to be expelled from the PDL [2]–[5]. As a quasi-static loading rate was applied experimentally, a Poisson's ratio of 0.30 was assumed [6]–[8]. The Young's Modulus of the PDL was varied between 0.10 and 0.80 MPa [9] in intervals of 0.10 MPa. As the PDL Young's Modulus was varied, the tooth and bone had a Young's Modulus of 20,000 MPa [9], [10] and 13,000 MPa [10], [11], respectively. The Poisson's ratio for the tooth and bone was 0.30. The geometry had 106,510 nodes and 62,415 elements. The force/displacement output for each Young's Modulus was compared to the experimental data by Equation *(6)*:

$$error = \sqrt{\frac{\sum(experimental - FE)^2}{n}} \tag{6}$$

where n is the total number of experimental data points. The lowest error was found between 0.40 MPa and 0.50 MPa. The Young's Modulus was then increased from 0.40 MPa to 0.50 MPa in intervals of 0.01 MPa to find the lowest error. The error calculated at each PDL Young's modulus are displayed in Figure 24. The lowest error was found at 0.46 MPa, the corresponding experimental and FE force/displacement data are shown in Figure 24.

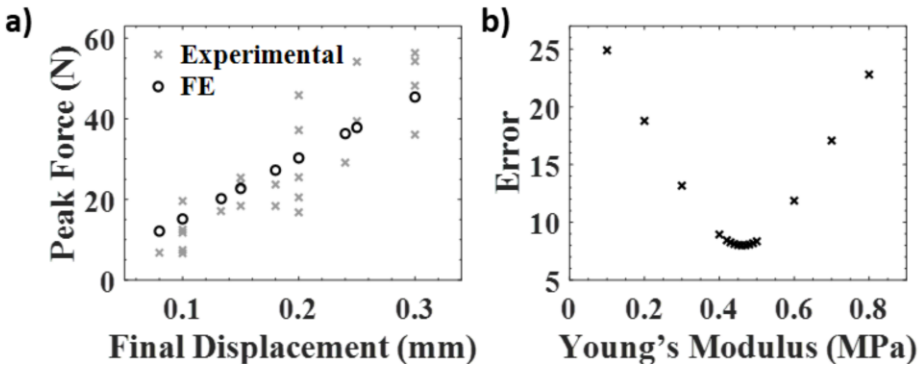

Figure 24 a) Experimental and FE force/displacement data demonstrating the comparable output. b) Error calculated between the experimental and FE output force/displacement data for different Young's Moduli of the PDL.

3 Mesh Convergence

A mesh convergence analysis was completed to ensure the output of the FE analysis was independent of the mesh density. The Young's Modulus of the tooth, bone, and PDL were 20,000 MPa [9], [10], 13,000 MPa [10], [11], and 0.46 MPa, respectively. The Poisson's ratio was 0.30 for the tooth, bone, and PDL. Three parameters were used to check for mesh convergence (Figure 25). The reaction force at the base of the TPBC was chosen as this was an output parameter used for analysis and for comparison with the experimental data. Strain measurements were also used for analysis; therefore, two strain outputs were also considered for the mesh convergence analysis. A directional strain in the y-axis within the PDL at the mesial root apex was close to the regions of interest used for analysis. The average maximum principal strain in the PDL in a location halfway up the mesial root was used to ensure the mesh convergence held at a point removed from the region of interest used for analysis. The region of interest at the root's apex was defined as the PDL within a 1 mm cube that lay between the three FBG locations used for analysis, [-0.36, -1.00, 0.25] to [0.64, 0.00, 1.25]. The second region of interest was defined as the PDL within a 0.5 mm x 1 mm x 1mm cube that was 4 mm above the root apex, [1.50, 4.00, 0.50] to [2.00, 5.00, 0.50]. The origin (i.e., [0.00 ,0.00 ,0.00]) was defined at the center of the mesial root apex.

The mesh refinement consisted of decreasing the element size of the PDL, tooth, bone and contact regions. The element sizes and the number of elements within each mesh are summarized in Table 15 and Table 16, respectively. It should be noted that the maximum element size is dictated by the edge length of the triangles that form the geometry as it was created with an ".stl"

file format. The reaction force, peak strain in the y-axis, and maximum principal strain for each mesh are summarized in Table 17, and Figure 25. The parameters selected for mesh convergence approached an asymptotic solution within the first three meshes tested. Mesh 5 was deemed acceptable as there were multiple elements through the thickness of the PDL, the element size at the contact regions were similar to the PDL, and there were not excess elements in the portions of the tooth and bone away from the PDL slowing computational time. A representative visualization of the mesh refinement is shown through cross-sections of the TPBC for Mesh 1, 5, and 7 (Figure 26).

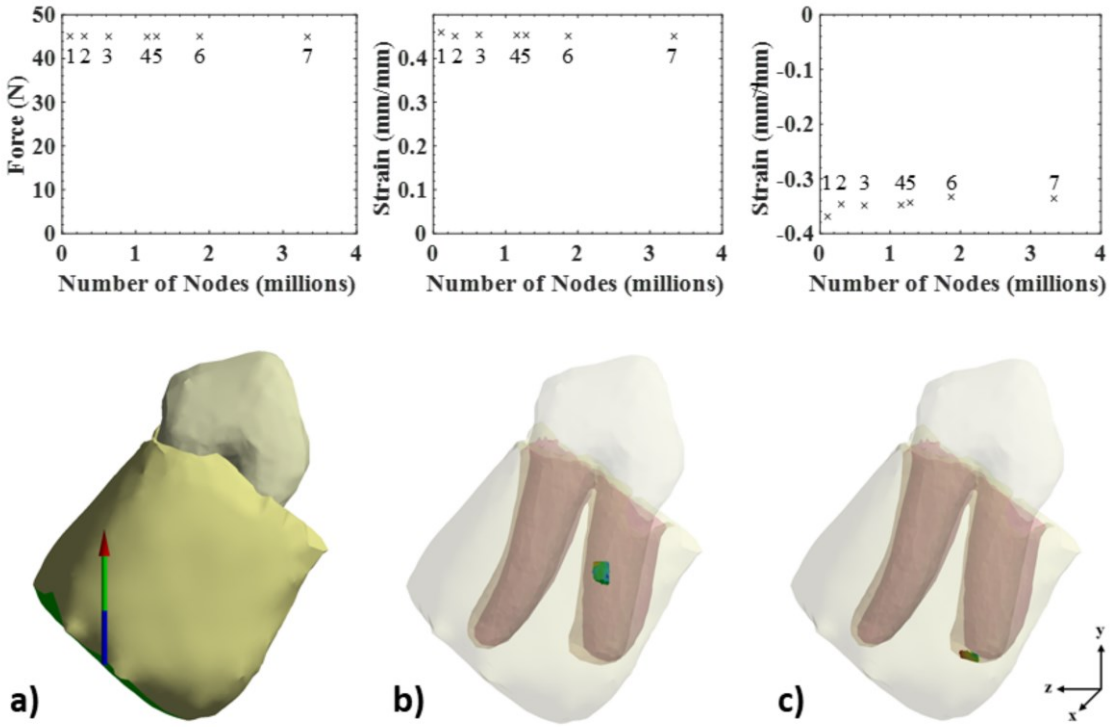

Figure 25 Visual representation of three parameters used for mesh density, a) reaction force, b) maximum principal strain halfway along the root, and c) directional strain along the y-axis along the root apex. Along the top are the peak measures for the respective nodes within the geometry, along the bottom show where the output measures are within the geometry.

Table 15 Element sizes for the PDL, bone, and tooth used for each mesh during the mesh convergence analysis

	Element size (mm)						
Mesh No.	1	2	3	4	5	6	7
PDL	1	0.2	0.1	0.1	0.12	0.1	0.075
Bone	1	1	1	1	1	0.1	0.075
Tooth	1	1	1	1	1	0.1	0.075
Contact	-	0.3	0.3	0.225	0.12	-	-

Table 16 Number of elements and nodes in each mesh defined in Table 15

	Total		PDL		Tooth		Bone	
Mesh No.	Nodes	Elements	Nodes	Elements	Nodes	Elements	Nodes	Elements
1	107978	63222	41047	22155	41363	25596	25568	15471
2	302254	184791	210322	126289	60544	39180	31388	19322
3	631921	422421	540210	364089	60323	39010	31388	19322
4	1155274	781095	927184	634068	142120	92868	85970	54159
5	1283835	829822	666262	432182	370722	241497	246851	156143
6	1868892	1200510	508164	309425	914586	602927	446142	288158
7	3331952	2178923	830240	512051	1700186	1138702	801526	528170

Table 17 Peak reaction force, average maximum principal strain and average directional strain in the y-axis output values for each mesh defined for mesh convergence analysis

Mesh No.	Reaction Force(N)	Maximum Principal Strain (mm/mm)	Directional Strain (y-axis) (mm/mm)
1	45.072	0.456	-0.369
2	45.089	0.451	-0.347
3	45.009	0.454	-0.349
4	44.955	0.453	-0.348
5	45.013	0.453	-0.344
6	45.007	0.451	-0.333
7	44.936	0.451	-0.336

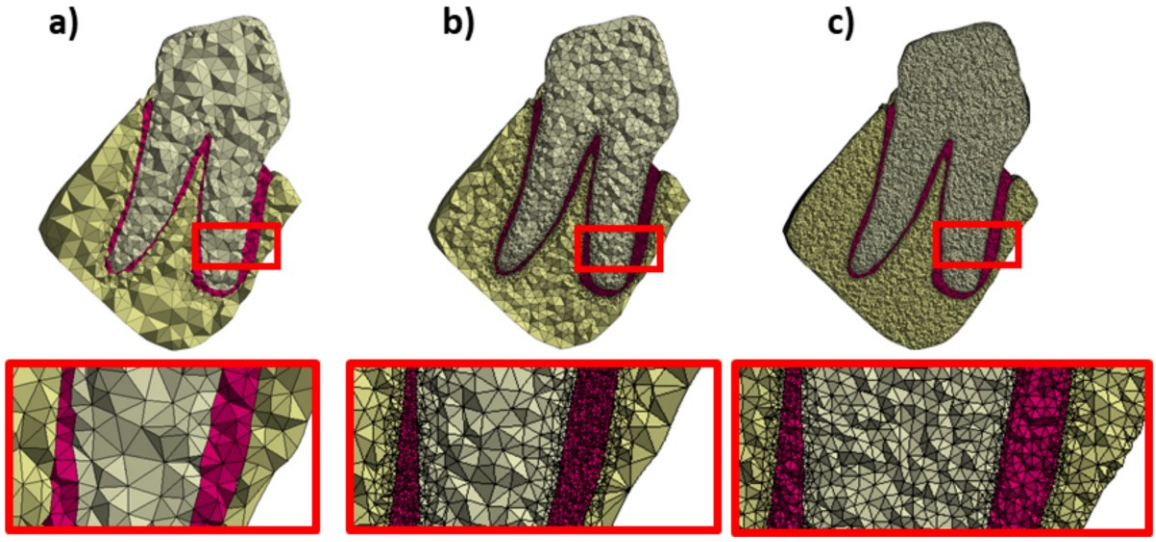

Figure 26 Representative mesh densities shown with a cross-section of the TPBC. A close up section of the PDL for each mesh is shown. a) Mesh 1, b) Mesh 5, c) Mesh 7

4 Bone and Tooth Parameter Selections

The PDL is much softer than the tooth and bone, and initial tooth displacement resulting from an externally applied load is mostly affected by the material properties of the PDL [10]. The tooth and bone were assumed to be homogeneous and linear elastic. The material parameters selected for the FE model were based on parameters used by Nikolaus *et al.* [10], which were selected to fit within a range of previously reported material properties for the bone and tooth. A sensitivity analysis was conducted to ensure the tooth and bone material properties did not greatly affect the output reaction force in the FE model. The PDL's Young's modulus was 0.46 MPa, and the Poisson's ratio was 0.30. The Poisson's ratio for the tooth and bone was assumed to be 0.3. The tooth's Young's Modulus ranged from 10,000 MPa to 25,000 MPa. When the tooth's Young's Modulus was adjusted, the bone had a Young's modulus of 13,000 MPa. Similarly, the bone's Young's Modulus was ranged from 2,000 MPa to 20,000 MPa. When the bone's Young's Modulus was adjusted, the tooth had a Young's Modulus of 20,000 MPa. The geometry had 1,282,366 nodes and 828,660 elements. The material properties and the respective peak force values are plotted in Figure 27.

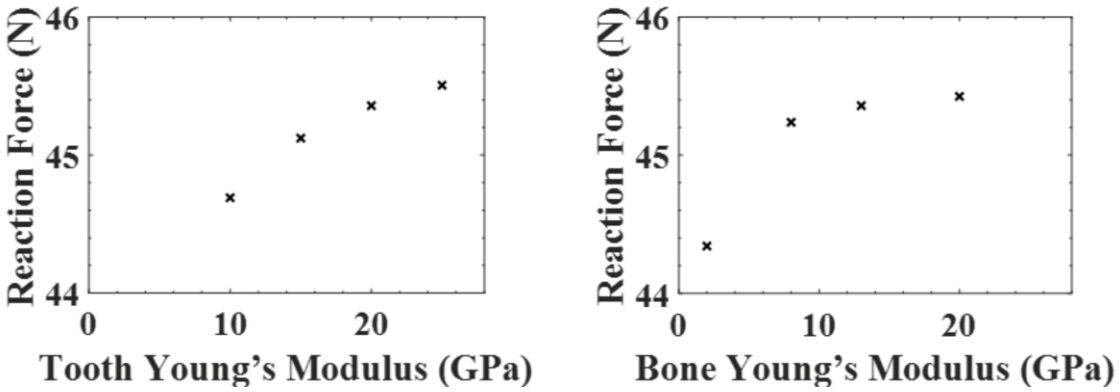

Figure 27 Output reaction force as an output of changing the tooth (left) and bone (right) Young's Modulus.

Understandably, with a lower Young's Modulus of the tooth and the bone, the reaction force was lower. The variation in reaction force was 1.8 % and 2.4 % between the lowest and highest Young's Modulus investigated for the tooth and bone, respectively, suggesting within the range investigated, the tooth and bones Young's Modulus do not have a great effect on the reaction force. A Yong's Modulus of 20,000 MPa [9], [10], 13,000 MPa [10], [11], for the tooth and bone, respectively, was deemed acceptable an did not greatly affect the output force.

5 References

[1] T. S. Fill, J. P. Carey, R. W. Toogood, and P. W. Major, "Experimentally determined mechanical oroperties of, and models for, the periodontal ligament: Critical review of current literature," *J. Dent. Biomech.*, vol. 2011, Apr. 2011, doi: 10.4061/2011/312980.

[2] W. R. Proffit, H. W. Fields, and D. M. Sarver, *Contemporary orthodontics*, 5th ed. Elsevier, 2013.

[3] D. Cardaropoli and L. Gaveglio, "The influence of orthodontic movement on periodontal tissues level," *Semin. Orthod.*, vol. 13, no. 4, pp. 234–245, Dec. 2007, doi: 10.1053/j.sodo.2007.08.005.

[4] M. Bergomi, H. W. A. Wiskott, J. Botsis, A. Mellal, and U. C. Belser, "Load response of periodontal ligament: Assessment of fluid flow, compressibility, and effect of pore pressure," *J. Biomech. Eng.*, vol. 132, no. 1, p. 014504, Jan. 2010, doi: 10.1115/1.4000154.

[5] C. Persson, S. Evans, R. Marsh, J. L. Summers, and R. M. Hall, "Poisson's ratio and strain rate dependency of the constitutive behavior of spinal dura mater," *Ann. Biomed. Eng.*, vol. 3, no. 38, pp. 975–983, 2010, doi: 10.1007/s10439-010-9924-6.

[6] K. Papadopoulou *et al.*, "Biomechanical time dependency of the periodontal ligament: A combined experimental and numerical approach," *Eur. J. Orthod.*, vol. 35, no. 6, pp. 811–818, Dec. 2013, doi: 10.1093/ejo/cjs103.

[7] M. Poppe, C. Bourauel, and A. Jäger, "Determination of the elasticity parameters of the human periodontal ligament and the location of the center of resistance of single-rooted teeth: A study of autopsy specimens and their conversion into finite element models," *J. Orofac. Orthop. Fortschritte Kieferorthopädie*, vol. 63, no. 5, pp. 358–370, Sep. 2002, doi: 10.1007/s00056-002-0067-8.

[8] T. J. Knaup *et al.*, "Time-dependent behavior of porcine periodontal ligament: A combined experimental, numeric in-vitro study," *Am. J. Orthod. Dentofacial Orthop.*, vol. 153, no. 1, pp. 97–107, Jan. 2018, doi: 10.1016/j.ajodo.2017.05.034.

[9] L. Qian, M. Todo, Y. Morita, Y. Matsushita, and K. Koyano, "Deformation analysis of the periodontium considering the viscoelasticity of the periodontal ligament," *Dent. Mater.*, vol. 25, no. 10, pp. 1285–1292, Oct. 2009, doi: 10.1016/j.dental.2009.03.014.

[10] A. Nikolaus, J. D. Currey, T. Lindtner, C. Fleck, and P. Zaslansky, "Importance of the variable periodontal ligament geometry for whole tooth mechanical function: A validated numerical study," *J. Mech. Behav. Biomed. Mater.*, vol. 67, pp. 61–73, Mar. 2017, doi: 10.1016/j.jmbbm.2016.11.020.

[11] N. M. B. K. Willems *et al.*, "Determination of the relationship between collagen cross-links and the bone–tissue stiffness in the porcine mandibular condyle," *J. Biomech.*, vol. 44, no. 6, pp. 1132–1136, Apr. 2011, doi: 10.1016/j.jbiomech.2011.01.023.